AD-A058 630 ARMY COMMUNICATIONS RESEARCH AND DEVELOPMENT COMMAND --ETC F/G 4/1
TIME-SERIES MODELING AND ANALYSIS OF HIGH FREQUENCY (HF) VERTIC--ETC(U)
JUL 78 R J D'ACCARDI

UNCLASSIFIED CORADCOM-78-7 NL

1 OF 2
AD
A058630

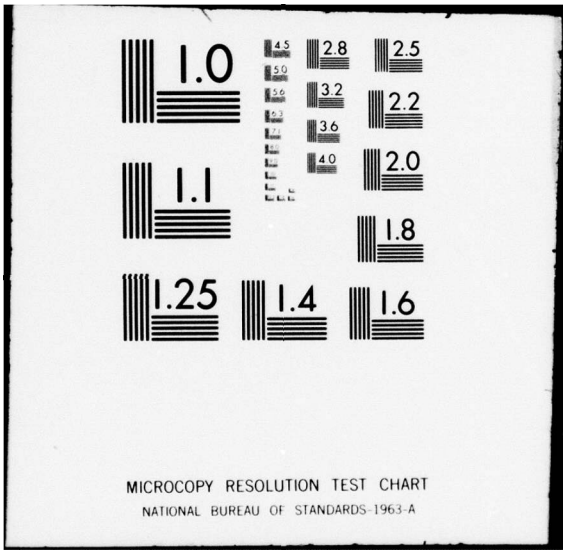
1.0
1.1
1.25
1.4
1.6
1.8
2.0
2.2
2.5
2.8
3.2
3.6
4.0
4.5
5.0
5.6
6.3
MICROCOPY RESOLUTION TEST CHART
NATIONAL BUREAU OF STANDARDS-1963-A

LEVEL II

12

RESEARCH AND DEVELOPMENT TECHNICAL REPORT
CORADCOM- 78-7

TIME-SERIES MODELING AND ANALYSIS OF HIGH FREQUENCY (HF) VERTICAL AND SHORT-PATH OBLIQUE INCIDENCE IONOSPHERIC SOUNDINGS

Richard J. D'Accardi

CENTER FOR COMMUNICATIONS SYSTEMS

July 1978

CORADCOM
US ARMY COMMUNICATION RESEARCH & DEVELOPMENT COMMAND
FORT MONMOUTH, NEW JERSEY 07703

NOTICES

Disclaimers

The citation of trade names and names of manufacturers in this report is not to be construed as official Government indorsement or approval of commercial products or services referenced herein.

Disposition

Destroy this report when it is no longer needed. Do not return it to the originator.

UNCLASSIFIED

SECURITY CLASSIFICATION OF THIS PAGE (When Data Entered)

(14)

REPORT DOCUMENTATION PAGE

READ INSTRUCTIONS BEFORE COMPLETING FORM

1. REPORT NUMBER: CORADCOM-78-7	2. GOVT ACCESSION NO.
3. RECIPIENT'S CATALOG NUMBER	
4. TITLE (and Subtitle): (6) TIME-SERIES MODELING AND ANALYSIS OF HIGH FREQUENCY (HF) VERTICAL AND SHORT-PATH OBLIQUE INCIDENCE IONOSPHERIC SOUNDINGS.	5. TYPE OF REPORT & PERIOD COVERED: (9) FINAL TECHNICAL REPORT.
6. PERFORMING ORG. REPORT NUMBER	
7. AUTHOR(s): (10) Richard J. D'Accardi	8. CONTRACT OR GRANT NUMBER(s)
9. PERFORMING ORGANIZATION NAME AND ADDRESS: Center for Communications Systems, ATTN: DRDCO-COM-RQ, US Army Communications R&D Command, Fort Monmouth, New Jersey 07703	10. PROGRAM ELEMENT, PROJECT, TASK AREA & WORK UNIT NUMBERS: 611101.91A.34.11.04
11. CONTROLLING OFFICE NAME AND ADDRESS: Center for Communications Systems, ATTN: DRDCO-COM-RQ, US Army Communications R&D Command, Fort Monmouth, New Jersey 07703	12. (11) REPORT DATE: July 1978
	13. NUMBER OF PAGES: 140
14. MONITORING AGENCY NAME & ADDRESS (if different from Controlling Office): (12) 153p.	15. SECURITY CLASS. (of this report): UNCLASSIFIED
	15a. DECLASSIFICATION/DOWNGRADING SCHEDULE

16. DISTRIBUTION STATEMENT (of this Report)

(A) Approved for Public Release
Distribution Unlimited

17. DISTRIBUTION STATEMENT (of the abstract entered in Block 20, if different from Report)

18. SUPPLEMENTARY NOTES

19. KEY WORDS (Continue on reverse side if necessary and identify by block number)

Ionospheric forecasting, ionospheric analysis, time-series modeling, spectral analysis, design of experiments, HF Communications, ionosphere, communications, ionosondes

20. ABSTRACT (Continue on reverse side if necessary and identify by block number)

One example of a non-stationary physical process that influences communications systems can be derived from a millimeter wave link operating over a stable line-of-sight path. Such a system would encounter a rapid change in its propagation path if a heavy rainstorm suddenly disturbed the link. Another example is derived from the adverse effects on high frequency radio communications caused by sudden variations in the ionosphere. Due to the random nature of these phenomena, and due to the time-dependence of experimental information, a

→ next page

DD FORM 1 JAN 73 1473 EDITION OF 1 NOV 65 IS OBSOLETE

UNCLASSIFIED

SECURITY CLASSIFICATION OF THIS PAGE (When Data Entered)

410489 78 09 08 017 LB

20. ABSTRACT (cont)

logical approach to forecasting these phenomena and interpreting the results seems to lie within the realm of non-stationary time-series modeling. Considering the premise that communications operational effectiveness is dependent on environmental effects, a procedural approach is recommended for characterizing ionospheric effects on High Frequency (HF) Communications utilizing time-series modeling. The recommended technique stresses the structuring of the appropriate difference equations through the criterion of minimum residual variance.

The main objectives of this study are as follows:

(i) The design of a statistical experiment is presented for pulsing the ionosphere for the purpose of obtaining both vertical incidence and oblique incidence ionospheric information. The design includes the collection and coding of the data for time-dependent modeling and analysis.

(ii) Development of a procedure for structuring forecasting models from non-stationary stochastic realizations. This specifically covers the identification and fitting of Autoregressive (AR), Moving-Average (MA), and mixed Autoregressive-Moving Averages models (ARMA).

(iii) It is shown that the widely accepted Ames-Egan method is not very realistic or useful in the near-real-time analysis and prediction of ionospheric soundings. An alternative approach is recommended, which utilizes repeated information observed within the same time intervals.

(iv) A spectral analysis of the non-stationary ionospheric information is performed. This includes the selection of the most appropriate lag window. Considered were those of Bartlett, Tukey, Parzen and the rectangular lag window.

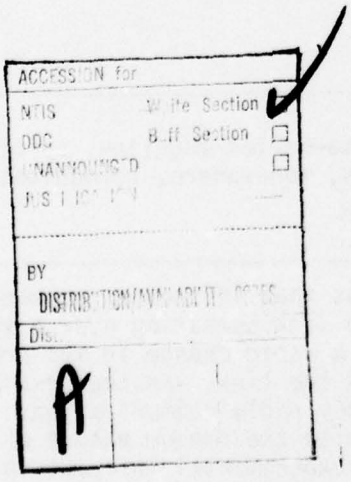

TABLE OF CONTENTS

TABLE OF CONTENTS (Continued)

TABLE OF CONTENTS (Continued)

LIST OF FIGURES

LIST OF FIGURES (Continued)

LIST OF FIGURES (Continued)

LIST OF FIGURES (Continued)

LIST OF TABLES

LIST OF TABLES (Continued)

1. INTRODUCTION

In communications systems analysis, one deals with the characterization of data for which the underlying process occurs naturally. The development of natural phenomena is usually monitored with the passage of time. For example, the surface temperature of the ocean is measured by a ship traveling in a straight line; rainfall density is monitored as a function of rate/hour; ionospheric effects in communications are mapped as a function of time of day. Therefore, in analyzing and modeling such systems, one must regard data in the form of a time series. A time series is a random or non-deterministic function, x, of an independent variable, t. In most situations, t will represent time or some other physical parameter such as space. The characteristic feature of time series is that future behavior can be closely estimated, but cannot be predicted exactly as would be the case for purely deterministic functions. In many applications of analysis and modeling, it is convenient to assume that certain physical processes can be described by deterministic functions. However, if the underlying process is "stochastic", then the deterministic point of view may give misleading information with respect to the independent variables.

The field of statistical analysis as applied to communications is premised in the fact that classical functional analysis is not adequate in dealing with a random process. A great deal can be deduced from those random processes that are stationary, i. e., a process which is in statistical equilibrium. However, for those physical processes which are non-stationary, analysis may be untenable and the "randomness" or non-stationarities must be dealt with in order to bring the process into statistical equilibrium prior to analysis. If this randomness is not properly approached, then meaningful results of analysis would be very difficult to obtain. One example of a non-stationary process is the adverse effects on High Frequency (HF) radio communications caused by sudden variations in the ionosphere.

The question of characterizing the ionosphere for HF radio communications has been approached from many points of view, [1], [2]. Primarily, information gathered over twenty or so years is analyzed by the National Bureau of Standards, [2], and monthly and yearly summaries in the form of

world contours are published. Ionospheric forecasts are considered to be either long-term, short-term [2], or real-time. Long-term forecasts usually predict undisturbed monthly median conditions at a particular hour for some specified month. They may be prepared to cover a long period of time in the future, i.e., one year, or even an entire solar cycle (22 years). Long-term forecasts are most useful in planning and management of the HF spectrum. Short-term forecasts usually predict ionospheric conditions in the near future. They are prepared by modifying long-term predictions by using values of local magnetic activity to account for disturbances caused by changes in the geomagnetic field. A true real-time prediction scheme would probably require that forecasts be available concurrently with ionosonde observations.

It should be noted that the ionosphere is composed of definable layers of differing electron density, namely, the D, E, F_1 and F_2 layers. These are subject to violent and random changes in altitude and density due to sunspot activity, diurnal (daily) effects of the sun's radiation, magnetic storms, sudden ionospheric disturbances, and other natural phenomena. These changes may either occur suddenly with little warning, or they may take place in a cyclical manner due to combination of these layers into a single F layer during night-time (diurnal effects) hours. This activity of the layers directly affects the reliability of HF communications to the extent that they may cause outages for extended periods of time. Due to the random nature of this phenomenon, and due to the time dependence of the information, a logical approach to forecasting and interpreting the results with respect to systems performance seems to lie within the realm of non-stationary time-series modeling. Therefore, the aim of this report is to develop statistical models to forecast in near real-time and to characterize the underlying stochastic process of short-path oblique incidence (OI) and vertical incidence (VI) high frequency (HF) information up to sixty minutes in advance.

In Section 2, a systematic presentation is given of the essential theory, philosophy, and modeling, utilizing the time-series methodology. Section 3 is a presentation of the modeling and analysis of 500 Km path ionospheric data acquired between Fort Monmouth, New Jersey, and Fort Drum, New York. A Spectral Analysis of the ionospheric information is presented in Section 4.

2. BASIC CONCEPTS IN TIME SERIES AND SPECTRAL ANALYSIS

In this section the basic concepts in time series and spectral analysis are presented. We explain how a time series can be thought of as a realization from a stationary stochastic process and, hence, be described by certain statistical functions. The conditions that insure the stability of a linear system are developed, and the stationary stochastic models, i.e., the autoregressive, the moving average, and the mixed autoregressive-moving average, are introduced. We also develop a "backward filter" whereby these stationary stochastic models can be used to describe non-stationary time series, and we introduce a procedural approach to fit the models to non-stationary time series.

With regard to spectral analysis, a brief and basic description of some of the concepts that will be utilized in the analysis of climatological, ionospheric, and man/machine interface data, will be given. In section 2.5 we shall be concerned with the *spectrum* in general, with respect to the aforementioned linear stochastic models. In section 2.6 we shall deal with spectral estimators and illustrate the manner in which the concept of the *window* enters the scope of the analysis. The *cross spectrum* is defined in section 2.7 along with its properties and a brief discussion of the role it plays in spectral analysis. Finally, more complete treatment of the *window* (types and properties) will be given in sections 2.8, 2.9 and 2.10.

2.1 TIME SERIES AND STOCHASTIC PROCESSES

A time series can be thought of as a sequence of highly correlated successive measurements (serially correlated) representing some aspect of a physical phenomena. Each of the measurements is associated with a moment of time and, in some cases, some other physical parameter. A time series can either be continuous or discrete, depending upon whether the observations are continuous or discrete. In this study we shall be concerned with only finite discrete time series which are measured at equidistant time intervals, or those continuous time series that have been digitized to form finite discrete series. We shall denote such a time series by x_t.

Time series can also be generally classified as being either a deterministic function or a non-deterministic function of time. A deterministic time series is one that can be described by an explicit mathematical relationship; hence, the future values of the series can be forecasted exactly. Many physical phenomena occurring in practice produce deterministic data, such as the increase in water pressure as one descends into the oceans, or the path of a spaceship to the moon. However, in most cases, time series occurring in practice are non-deterministic; that is, they exhibit random or fluctuating properties. Unlike the deterministic time series, there does not exist any explicit mathematical relationship with which to forecast exact values in the future. Hence, for those time series which are random in nature, we must describe them in terms of probability statements and statistical averages rather than by explicit relationships. The prime area of interest in this study will be in *non-deterministic* time series; hence, it will not be possible for us to precisely forecast future values of the time series.

To describe these non-deterministic time series, we use the concept of a stochastic process; that is, we consider an observed non-deterministic time series as a realization of a stochastic process. To explain the relationship between non-deterministic, or statistical, time series and stochastic processes, consider the following. A given time series $\{x_t, t = 1, 2, \ldots, n\}$ representing an ordered random phenomenon is assumed to be a single sample from a particular generating process $\{X_t, t = -\infty, \ldots, -1, 0, 1, \ldots, \infty\}$. This collection, or ensemble, of all possible sample time series which the random phenomenon might have produced and its associated probability distribution is called a stochastic process. Thus, a given time series x_t from a random phenomenon may be regarded as one physical realization of the doubly infinite set of functions which might have been generated by the stochastic process. The set is doubly infinite because an infinite set of values is possible at any given time and because there are an infinite number of time points.

A stochastic process is said to be *strongly stationary,* or *stationary* in the strict sense, if the joint probability distribution of any set of observations is not affected by the shifting of all times of observations forward or backward by any integer amount k. That is, if the joint probability density function associated with n observations $X_1, X_2, \ldots, X_n$ made

at any set of times $t_1, t_2, \ldots, t_n$, is the same as that associated with n observations $X_{1+k}, X_{2+k}, \ldots, X_{n+k}$ made at times $t_{1+k}, t_{2+k}, \ldots, t_{n+k}$. For a process to be *strictly stationary*, it is necessary for the entire probability structure to be time invariant.

A stationary stochastic process may be described by its mean μ, which can be estimated by

$$\bar{x} = \frac{1}{n} \sum_{t=1}^{n} x_t , \qquad (2.1.1)$$

the sample mean of the time series, and by the variance, σ_x^2, of the stochastic process, which can be estimated by

$$\hat{\sigma}_x^2 = \frac{1}{n} \sum_{t=1}^{n} (x_t - \bar{x})^2, \qquad (2.1.2)$$

which is called the sample variance of the time series. As mentioned earlier, the values of the time series at different points in time are serially correlated. This correlation is of great importance to this study; hence, the covariance function of the stochastic process is of great importance to us. The covariance, γ_k, between x_t and x_{t+k}, k intervals of time apart, is called the *autocovariance* at lag k. $\gamma_k = \text{cov}\,(X_t, X_{t+k})$ can be estimated by

$$c_{xx}(k) = \frac{1}{n} \sum_{t=1}^{n-k} (x_t - \bar{x})(x_{t+k} - \bar{x}), \quad k = 0, 1, \ldots, n-1 , \qquad (2.1.3)$$

the *sample autocovariance* function of the time series. Of equal importance, or possibly greater, is the *autocorrelation* at lag k, $\rho_k = \gamma_k/\gamma_o$, which acts like a correlation coefficient, and can be estimated by

$$r_{xx}(k) = \frac{c_{xx}(k)}{c_{xx}(0)} , \; k = 0, 1, \ldots, n-1 , \qquad (2.1.4)$$

the *sample autocorrelation* function of the time series. Note that when $k = 0$, $r_{xx}(0)$ is 1. Both the autocovariance function and autocorrelation function are even functions because of the stationary assumption. In practice it is only necessary to compute the sample autocovariance and autocorrelation functions for lags up to n/4.

One of the most important assumptions made with respect to a time series is that the corresponding stochastic process is stationary, [3]*. In general, the properties of a stochastic process are time dependent; that is, the current value x_t will depend only on the time which has elapsed since the process began. We can make a simplifying assumption that the time series corresponding to the stochastic process has reached some form of *steady state* or *equilibrium*, in the sense that the statistical properties of the time series are independent of absolute time.

2.2 STATIONARY STOCHASTIC PROCESSES

Stationary stochastic processes are used to model time series of many practical situations. Consider the discrete process Z_t where the random variables Z_t, t=1, 2, ..., n, are mutually independent and are normal with mean zero and variance σ_Z^2--this constitutes the simplest form of a stationary stochastic process. For this process the autocovariance function is zero for all lags except the zeroeth. Such a sequence of random variables is called a *purely random process* or *white noise*.

An important class of stochastic processes can be generated by the passing of a purely random process through a linear system, (see Figure 2.1).

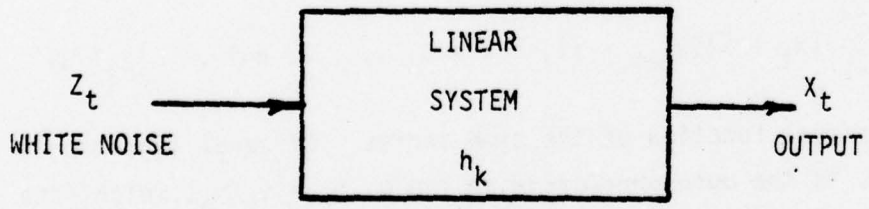

FIGURE 2.1: REPRESENTATION OF A LINEAR SYSTEM

If the system is linear, we may express the relationship between the output process X_t and the input process Z_t as

$$X_t - \mu = \sum_{k=0}^{\infty} h_k Z_{t-k}. \qquad (2.2.1)$$

* Chapter 5

h_k is called the *weighting function* or the *impulse response function* of the linear system. The resulting stochastic process derived from a purely random process using (2.2.1) is called a *linear process*.

The variance of the linear process is given by

$$\sigma_X^2 = \sigma_Z^2 \sum_{j=0}^{\infty} h_j^2. \tag{2.2.2}$$

The convergence of the above series ensures that the linear process has finite variance. We shall now show an equivalent conditon, [4], [3], which also assures the variance to be finite. We will use Z-transforms, [5], to obtain the characteristic equation of the linear process and, then, by restricting the roots of the characteristic equation to a certain region, we will be in a position to establish the conditions necessary to ensure *stationarity* and/or *invertibility* of the process.

Consider the following difference equation:

$$y_r = a_1 y_{r-1} + a_2 y_{r-2} + \ldots + a_m y_{r-m} + b_o x_r + \ldots + b_n x_{r-n} , \tag{2.2.3}$$

where $a_1, \ldots, a_m, b_o, \ldots, b_n$ are the parameters, and x_r is assumed given for all values of r. The general solution to (2.2.3) is

$$y_r = \sum_{k=0}^{\infty} h_k x_{r-k} , \tag{2.2.4}$$

where h_k is as defined in (2.2.1).

The x's and the y's in equation (2.2.3) can be considered as being obtained by sampling the continuous signals x(t) and y(t) at the moments of time $t = r\Delta, (r-1)\Delta, \ldots, (r-n)\Delta$, and $t = r\Delta, (r-1)\Delta, \ldots, (r-m)\Delta$, respectively. Of course, Δ represents the *spacing interval* used. We can now rewrite (2.2.3) as

$$\begin{aligned} y(t) - a_1 y(t-\Delta) - a_2 y(t-2\Delta) - \ldots - a_m y(t-m\Delta) \\ = b_o x(t) + b_1 x(t-\Delta) + \ldots + b_n x(t-n\Delta) . \end{aligned} \tag{2.2.5}$$

The Fourier transform of (2.2.5) is given by

$$[1 - a_1 e^{-j2\Pi f\Delta} - \ldots - a_m e^{-j2\pi fm\Delta}]\, Y(f)$$
$$= [b_o + b_1 e^{-j2\pi f\Delta} + \ldots + b_n e^{-j2\pi fn\Delta}]\, X(f) \,. \tag{2.2.6}$$

Solving for Y(f), we have

$$Y(f) = \frac{[b_o + b_1 e^{-j2\pi f\Delta} + \ldots + b_n e^{-j2\pi fn\Delta}]}{[1 - a_1 e^{-j2\pi f\Delta} - \ldots - a_m e^{-j2\pi fm\Delta}]}\, X(f) \,. \tag{2.2.7}$$

Hence, the frequency response function:

$$H(f) = \sum_{k=0}^{\infty} h_k e^{-j2\pi fk\Delta} \,, \tag{2.2.8}$$

which is the Fourier transform of h_k, is given by

$$H(f) = \frac{[b_o + b_1 e^{-j2\pi f\Delta} + \ldots + b_n e^{-j2\pi fn\Delta}]}{[1 - a_1 e^{-j2\pi f\Delta} - \ldots - a_m e^{-j2\pi fn\Delta}]} \,. \tag{2.2.9}$$

The concept of Z-transforms, [5], is used to manipulate the frequency response function H(f). Substituting

$$Z = e^{j2\pi f\Delta} \tag{2.2.10}$$

in equation (2.2.9), one obtains

$$H(Z) = \frac{[b_o + b_1 Z^{-1} + \ldots + b_n Z^{-n}]}{[1 - a_1 Z^{-1} - \ldots - a_m Z^{-m}]} \,, \tag{2.2.11}$$

which is the Z-transform of the impulse response function h_k; that is,

$$H(Z) = \sum_{k=0}^{\infty} h_k Z^{-k} \,. \tag{2.2.12}$$

From an operational point of view, Z may be thought of as a shift operator; that is,

$$Z^{-s}x_r = x_{r-s} .$$

Hence, the linear difference equation (2.2.3) may be expressed as

$$(1 - a_1Z^{-1} - \ldots - a_mZ^{-m})y_r = (b_o + b_1Z^{-1} + \ldots + b_nZ^{-n})x_r . \qquad (2.2.13)$$

Solving for y_r, we have

$$y_r = \frac{[b_o + b_1Z^{-1} + \ldots + b_nZ^{-n}]}{[1 - a_1Z^{-1} - \ldots - a_mZ^{-m}]} x_r ; \qquad (2.2.14)$$

then using (2.2.11), equation (2.2.14) can be written as

$$y_r = H(Z)x_r . \qquad (2.2.15)$$

H(Z) is called the *transfer function* of the discrete linear system. Expanding H(Z) in powers of Z^{-1}, yields

$$y_r = \sum_{k=0}^{\infty} h_kZ^{-k}x_r = \sum_{k=0}^{\infty} h_kx_{r-k} , \qquad (2.2.16)$$

which is the general solution of (2.2.3).

The *characteristic equations* of a linear process can be obtained as follows:

(1) by factoring Z^{-m} out of the *denominator* of (2.2.14), substituting ψ for Z and equating to zero, we have

$$\psi^m - a_1\psi^{m-1} - \ldots - a_m = 0 . \qquad (2.2.17)$$

A linear process is said to be stable if the roots $\zeta_1, \zeta_2, \ldots, \zeta_m$ of the above characteristic equation lie inside the unit circle, [3].* If this condition holds, the process is said to satisfy the *stationary condition*.

* Chapter 5

(2) by factoring Z^{-n} out of the *numerator* of (2.2.14), we have

$$[b_0 Z^n + b_1 Z^{n-1} + \ldots + b_n] Z^{-n} . \qquad (2.2.18)$$

Solving equation (2.2.15) for x_r, one obtains

$$x_r = H(Z)^{-1} y_r . \qquad (2.2.19)$$

Now substituting $\psi = Z$ into (2.2.18) and equating to zero, we obtain another characteristic equation of the system,

$$b_0 \psi + b_1 \psi^{n-1} + \ldots + b_n = 0 . \qquad (2.2.20)$$

A linear process of this type is said to be stable if the roots $\zeta_1, \zeta_2, \ldots, \zeta_n$ of equation (2.2.20) lie within the unit circle, [3]. If this condition is satisfied, the process is said to be *invertible*.

Also, note that the invertibility condition is independent of the stationarity condition, [4], [3].

2.3 THE STATIONARY STOCHASTIC MODELS

Consider the special case of the linear difference equation (2.2.3), in which the first p of the a's are non-zero ($p \leq m$), $b_0 = 1$, and $b_i = 0 \quad i > 1$. This results in the equation,

$$y_r = a_1 y_{r-1} + a_2 y_{r-2} + \ldots + a_p y_{r-p} + x_r . \qquad (2.3.1)$$

This resulting process is called an *autoregressive process of order p*. We shall write the finite autoregressive process in the following form:

$$X_t - \mu = \alpha_1 (X_{t-1} - \mu) + \alpha_2 (X_{t-2} - \mu) + \ldots + \alpha_p (X_{t-p} - \mu) + Z_t . \qquad (2.3.2)$$

Note that μ is the mean of the process and Z_t is a purely random process. As we have just shown in the preceding section, the autoregressive process can be thought of as being stable by satisfying the stationarity condition that the roots of its characteristic equation (2.2.17) lie inside a unit circle.

Next, consider the special case of the linear difference equation (2.2.3), in which the first q of the b's are non-zero ($q \leq n$) with $b_0 = 1$, and all the a's are zero. Thus, we have the resulting equation:

$$y_r = x_r + b_1 x_{r-1} + \ldots + b_q x_{r-q} . \tag{2.3.3}$$

This process is called a *moving average process of order q*. We shall write the finite moving average process in the following form:

$$X_t - \mu = Z_t - \beta_1 Z_{t-1} - \ldots - \beta_q Z_{t-q} . \tag{2.3.4}$$

Thus, the moving average process is said to be stable if it satisfies the invertibility condition; that is, the roots of its characteristic equation (2.2.20) lie inside a unit circle.

We now introduce a *backward shift operator* which will be very useful in manipulating stationary stochastic models. The backward shift operator B is defined by

$$\begin{aligned} Bx_t &= x_{t-1} \\ B^2 x_t &= x_{t-2} \\ &\vdots \\ B^d x_t &= x_{t-d} . \end{aligned} \tag{2.3.5}$$

Using the backward shift operator, it will be shown how a finite autoregressive process can be expressed as an infinite moving average process. Consider a first order autoregressive process with $\mu = 0$,

$$x_t = \alpha_1 x_{t-1} + z_t , \tag{2.3.6}$$

or using the backward shift operator (2.3.6) becomes

$$(1 - \alpha_1 B) x_t = z_t . \tag{2.3.7}$$

Expressing the x's in terms of the z's, we have

$$x_t = (1 - \alpha_1 B)^{-1} z_t . \tag{2.3.8}$$

Expanding $(1 - \alpha_1 B)^{-1}$ we have

$$x_t = z_t + \alpha_1 z_{t-1} + \alpha_2 z_{t-2} + \cdots \quad . \tag{2.3.9}$$

Equation (2.3.9) is an infinite moving average process. Likewise, one can show that the moving average process can be expressed as an infinite autoregressive process.

The point that has been brought out in the above paragraph is that it may be necessary to include parameters from both the autoregressive and moving average processes in order to achieve *parsimony*--employing the smallest possible number of parameters for adequate representation, [6]* Of course, this is due to the fact that a moving average process could not be parsimoniously represented using an autoregressive process, and conversely, an autoregressive process could not be parsimoniously represented using a moving average process. Hence, we will have the stationary stochastic model,

$$\begin{aligned} X_t - \mu = \alpha_1(X_{t-1} - \mu) + \alpha_2(X_{t-2} - \mu) + \cdots + \alpha_p(X_{t-p} - \mu) \\ + Z_t - \beta_1 Z_{t-1} - \cdots - \beta_q Z_{t-q} \quad . \end{aligned} \tag{2.3.10}$$

Equation (2.3.10) is called the *mixed autoregressive-moving average process of order (p, q)*. Writing (2.3.10) in terms of the backward shift operator B, with μ zero, we have

$$(1 - \alpha_1 B - \cdots - \alpha_p B^p) X_t = (1 - \beta_1 B - \cdots - \beta_q B^q) Z_t \quad ,$$

$$X_t = \frac{(1 - \beta_1 B - \cdots - \beta_q B^q)}{(1 - \alpha_1 B - \cdots - \alpha_p B^p)} Z_t \quad . \tag{2.3.11}$$

Hence, the mixed autoregressive-moving average process can be thought of as the output X_t from a linear system, whose impulse response function is the ratio of two polynomials, when the input is white noise Z_t.

As previously mentioned, the stationarity and invertibility condition are independent of each other; thus, we simply have to satisfy the stationarity

* Chapter 1

condition for the autoregressive process and the invertibility condition for the moving average process included in the mixed process for the process (2.3.10) to be stable.

2.4 PROCEDURAL APPROACH FOR FITTING FORECASTING MODELS TO NON-STATIONARY STOCHASTIC REALIZATIONS

At present there exist techniques to analyze stationary time series records. However, the techniques available for the analysis of non-stationary time series are inadequate and do not lend themselves to meaningful interpretations of physical problems. It is possible, however, to adjust non-stationary time series so as to be able to apply the existing techniques of stationary time series analysis directly. This adjustment takes the form of applying a proper filter to the observed non-stationary time series to filter out the non-stationary components. (See section 3.3.1).

In this section we shall illustrate the procedure to identify whether an observed series exhibits stationary or non-stationary properties. If the time series is non-stationary, we explain how it can be filtered and introduce the concept of a "backward filter." We give a procedural approach to determine the stochastic model which gives the best fit to the observed series, and we apply diagnostic checks to determine the goodness-of-fit. Finally, we discuss how the fitted stochastic model can be employed in forecasting and updating.

2.4.1 Identification and Filtering

In a given physical situation, one will have available a stochastic realization $x_1, x_2, \ldots, x_n$, of n observations. The first concern is to identify whether the series x_t exhibits stationary or non-stationary properties. To accomplish this, we make use of certain statistical methods in conjunction with the properties of stationary time series. A stationary time series will have the following properties:

i) it will be in a steady state in the sense that it is in equilibrium about a constant mean level;

ii) it will contain no trend;

iii) its sample autocorrelation function will dampen out rapidly. Hence, we will first plot the series as an aid in exercising some judgment about the behavior of the information. Next, we shall apply various non-parametric trend tests to the data. Finally, and of greatest importance, we calculate the sample autocorrelation function (2.1.4) of the observed data. From these data-analysis tools, we will have sufficient information to identify the given observed series as stationary or non-stationary.

If we identify the observed series as exhibiting non-stationary properties, we need to find a filter that will remove the non-stationary components. One of the most used and most efficient methods of removing non-stationary components from a time series is by differencing. A first-order difference filter is defined by

$$y_t = x_t - x_{t-1} , \tag{2.4.1}$$

where x_t is the observed non-stationary series and y_t is the resulting filtered series. Similarly, a second-order difference filter is defined by

$$w_t = x_t - 2x_{t-1} + x_{t-2} , \tag{2.4.2}$$

and so on.

Since we will be almost exclusively dealing with non-stationary time series, and, since either a first-order or second-order difference filter is usually sufficient to transform most practically occurring non-stationary series into stationary ones, [6], the presentation shall be confined to determining the degree of differencing necessary to result in a stationary series. Using the backward shift operator B (2.3.5), we express the difference filter in the following form:

$$y_t = (1 - B)^d x_t . \tag{2.4.3}$$

We must determine a suitable value for d, either 0, 1, or 2; zero will correspond to the fact that our observed information is stationary; one will correspond to the fact that a first-order difference filter is necessary to filter the observed series, and so on.

The procedure to identify the proper value of d is to compute the first and second differences of the observed series x_t, $t = 1, 2, \ldots, n$. That is,

x_t is processed through a first-order difference filter,

$$y_t = (1 - B)x_t = x_t - x_{t-1} ,$$

which will have (n-1) values and a second-order difference filter,

$$w_t = (1 - B)^2 x_t = x_t - 2x_{t-1} + x_{t-2} ,$$

which will have (n-2) values. For the observed x_t and the filtered y_t and w_t series, we calculate the sample autocorrelation functions and conduct trend tests.

By examining the sample autocorrelation function and the result of the trend test for the separate series, one should be able to infer a suitable value for d, specifically, the degree of differencing necessary to induce the sample autocorrelation function to dampen out fairly rapidly and to cause the trend test to be insignificant. This will yield a stationary series with which to continue the analysis.

It must be noted that in some instances the first-order and the second-order difference filter may fail to remove the non-stationary components. When this occurs, we must continue to search for a proper filter that will leave us with a stationary series. One alternative is to apply a higher-order difference filter, or we can try other types of filters. Jenkins and Watts, [3], list several other types of filters. In some respects, filtering a non-stationary series is a trial and error procedure in that one attempts to transform the observed series into a stationary one by the use of a mathematical function. Unfortunately, this requires us to search for the proper function to accomplish this purpose.

From the examination of the sample autocorrelation function and the sample partial autocorrelation function, which is defined in terms of the sample autocorrelation function as

$$\hat{\phi}(1,1) = r_{xx}(1) , \qquad (2.4.4)$$

and
$$\hat{\phi}(k,k) = \frac{r_{xx}(k) - \sum_{j=1}^{k-1} \hat{\phi}(k-1, j) r_{xx}(k-j)}{1 - \sum_{j=1}^{k-1} \hat{\phi}(k-1, j) r_{xx}(j)}, \qquad (2.4.5)$$

$k = 2, 3, \ldots, n/4$, where,

$$\hat{\phi}(k,j) = \hat{\phi}(k-1, j) - \hat{\phi}(k,k)\, \hat{\phi}(k-1, k-j), \qquad (2.4.6)$$

we may possibly be able to obtain some insight into the identification of the stochastic model and its order that will best fit the data, [6]. The sample autocorrelation function of an autoregressive process of order p tails off, while its sample partial autocorrelation function has a cutoff after lag p. Conversely, the sample autocorrelation function of a moving average process of order q has a cutoff after lag q, while its sample partial autocorrelation function tails off. If both the sample autocorrelations and partial autocorrelations tail off, a mixed process is suggested.

2.4.2 The Fitting Procedure

The process of fitting any one of the three stationary stochastic models under consideration usually involves two stages.

i) deciding the order of the process;

ii) estimating the appropriate set of parameters.

The criterion for selecting the order of the process that will give the best fit is the residual variances of different orders of the process fitted to the data. To compute the residual variances, it is necessary to estimate the parameters for the different order processes. The residual variances are then plotted against the order; the minimum residual variance will correspond to the correct order for the process. After this has been completed for each process (the autoregressive, the moving average, and the mixed autoregressive-moving average), we compare the minimum residual variances; the minimal one will correspond to the process (and its order) that will best describe the data. This procedure is quite well suited for use on a high-speed computer. Note, that when fitting a model to a given set of observations, we keep in mind the principle of parsimony, [6].*

* Chapters 1 and 9

As pointed out by R. A. Fisher, [7], for tests of goodness-of-fit to be relevant, it is necessary to make efficient use of the data in the fitting process. Hence, to obtain efficient estimates of the parameters, we shall use maximum likelihood estimates, or approximate maximum likelihood estimates for the parameters that constitute the different models. The asymptotic properties of maximum likelihood estimates are usually derived for independent observations, but as was shown by Whittle, [8], they may be extended to cover stationary time series.

Suppose there exists a non-stationary series, x_t, $t = 1, 2, \ldots, n+1$, generated by a mixed autoregressive-moving average process of order (p, q), whose first difference, y_t, $t = 1, 2, \ldots, n$, is stationary. We desire to fit a stationary mixed process of order (p, q) to the y's; that is

$$y_t = \alpha_1 y_{t-1} + \ldots + \alpha_p y_{t-p} + z_t - \beta_1 z_{t-1} - \ldots - \beta_q z_{t-q} . \quad (2.4.7)$$

Without loss of generality, one can assume that when $d > 0$, $\mu_y = 0$. We can express (2.4.7) as

$$z_t = y_t - \alpha_1 y_{t-1} - \ldots - \alpha_p y_{t-p} + \beta_1 z_{t-1} + \ldots + \beta_q z_{t-q} . \quad (2.4.8)$$

A recursive technique can now be used to obtain the conditonal sum of squares function. By conditional sum of squares function, we mean that the sum of squares function is conditional on the starting values assigned to the parameters (α's and β's) and for the y's and z's previous to time t. This simple numerical technique will recursively build up the log-likelihood function.

Now, assuming the Z_t process is normal with mean zero and variance σ_Z^2, the joint probability density of the Z's is

$$f(z_1, z_2, \ldots, z_n) \propto \sigma_z^{-n} \exp[- \sum_{t=1}^{n} z_t^2/2\sigma_z^2] . \quad (2.4.9)$$

Given a particular set of data, y_t, $t = 1, 2, \ldots, n$, the conditional log-likelihood associated with the parameter values ($\alpha_1, \ldots, \alpha_p, \beta_1, \ldots, \beta_q, \sigma_z$), conditional on the choice of starting values for the y's and z's, is given by

$$\ell(\alpha_1, \ldots, \alpha_p, \beta_1, \ldots, \beta_q, \sigma_z) = -n\ell n \ \sigma_z - \frac{S(\alpha_1, \ldots, \alpha_p, \beta_1, \ldots, \beta_q)}{2\sigma_z^2}, \tag{2.4.10}$$

and the conditional sum of squares function

$$S(\alpha_1, \ldots, \alpha_p, \beta_1, \ldots, \beta_q) = \sum_{t=1}^{n} z_t^2(\alpha_1, \ldots, \alpha_p, \beta_1, \ldots, \beta_q \mid \text{starting values}). \tag{2.4.11}$$

Notice that the conditional likelihood (2.4.10) involves the data only through the conditional sum of squares function (2.4.11). It follows that contours of (2.4.10) for any fixed value of σ_z in the space (α_1, ..., α_p, β_1, ..., β_q, σ_z) are contours of (2.4.11), that these maximum likelihood estimates are the same as the least squares estimates, and that, in general, one can, on the normal assumption, study the behavior of the conditional likelihood by studying the conditional sum of squares function.

Thus, we will obtain least square estimates (maximum likelihood estimates) by minimizing the sum of squares function. Note that the parameter values are selected to recursively calculate the sum of squares function such that they will satisfy the stationarity and/or the invertibility conditions of the stationary stochastic model. The residual variances can then be obtained by dividing the sum of squares function by the appropriate degrees of freedom. The fitting procedure will be described in greater detail for the autoregressive, the moving average, and the mixed autoregressive-moving average process in Section 3.

2.4.3 The Backward Filter and Diagnostic Checks

Having selected the stationary stochastic model and its order that best describes the data and having estimated its parameters, diagnostic checks are conducted on the model to determine its adequacy. If, in the identification stage of the analysis, a suitable value for d was found to be different from zero, the model has been fitted to the stationary (filtered) data, *not* to the observed non-stationary data. Hence, to use the fitted model to forecast

future values of the observed non-stationary time series, we introduce the concept of a "backward filter." The backward filter is essentially a simple, *but very important*, technique that allows the analysis of non-stationary time series using the well-established methods of stationary time series.

For a better understanding of the above concept, consider the following example: The difference equation,

$$y_t = (1 - B)^d x_t ,$$

was used to filter the observed non-stationary time series, x_t, $t = 1, 2, \ldots, n + d$. To the stationary series, y_t, $t = 1, 2, \ldots, n$, a 2nd order autoregressive model is fitted; that is

$$y_t = \hat{\alpha}_1 y_{t-1} + \hat{\alpha}_2 y_{t-2} + z_t . \qquad (2.4.12)$$

To transform the model (2.4.12), fitted to the stationary data, y_t, to the non-stationary data, x_t, we simply replace y_t in the model with $(1 - B)^d x_t$; that is

$$(1 - B)^d x_t = \hat{\alpha}_1 (1 - B)^d x_{t-1} + \hat{\alpha}_2 (1 - B)^d x_{t-2} + z_t . \qquad (2.4.13)$$

For $d = 1$ and simplifying, we have

$$x_t = \phi_1 x_{t-1} + \phi_2 x_{t-2} + \phi_3 x_{t-3} + z_t \qquad (2.4.14)$$

where $\phi_1 = 1 + \hat{\alpha}_1$, $\phi_2 = \hat{\alpha}_2 - \hat{\alpha}_1$, and $\phi_3 = -\hat{\alpha}_2$. The ϕ's are linear combinations of the $\hat{\alpha}$'s and will depend upon the degree of differencing needed to filter the observed series. For example, if $d = 2$, we have

$$x_t = \phi_1 x_{t-1} + \phi_2 x_{t-2} + \phi_3 x_{t-3} + \phi_4 x_{t-4} + z_t , \qquad (2.4.15)$$

where $\phi_1 = 2 + \hat{\alpha}_1$, $\phi_2 = \hat{\alpha}_2 - 2\hat{\alpha}_1 - 1$, $\phi_3 = \hat{\alpha}_1 - 2\hat{\alpha}_2$, and $\phi_4 = \hat{\alpha}_2$.

We can now conduct diagnostic checks on the fitted model (2.4.14) to determine the goodness-of-fit. Using the model (2.4.14), the behavior of the observed non-stationary series can be simulated. By plotting the simulated series against the observed series, one can obtain a visual conception of the

goodness-of-fit. More substantially, one can calculate the residuals incurred by subtracting the modeled series from the observed series; that is

$$\hat{z}_t = x_t - \hat{x}_t \ . \tag{2.4.16}$$

If the model is adequate, the residuals should be the sum of the z_t process plus a factor of $1/\sqrt{n}$; that is as n increases, the residual $\hat{z}_t$'s should behave approximately like the white noise z_t's. Thus, the study of the residuals could indicate the existence of model inadequacy, in particular, the analysis of the sample autocorrelation function of the residuals, [4].

If the form of the model was known to be accurate and the true parameter values were known, then, by a result of Anderson, [9], the sample autocorrelations $r_{zz}(k)$ of the z_t's would be uncorrelated and distributed, more or less, normally about zero with variance 1/n. Therefore, we could run a statistical test to determine if the deviations of these autocorrelations from their theoretical zero values are significant.

However, in practice, we do not know the correct form of the model nor the true parameter values. The residuals obtained from equation (2.4.16) will be estimates of the residuals, $\hat{z}_t$'s, not the z_t's. Hence, the acceptance of the hypothesis that the sample autocorrelations of the residuals constitute a purely random process on the assumption of a standard error of $1/\sqrt{n}$ can be very dangerous, [10].* Further, it is shown in [6]¢ that, by using $1/\sqrt{n}$ as the standard error for $\hat{r}_{zz}(k)$, the statistical significance of the deviations from zero of the sample autocorrelations at low lags will be underestimated, while at moderate or high lags, $1/\sqrt{n}$ will give an acceptable estimate.

Instead of considering the sample autocorrelations of the residuals separately, an indication is often needed of whether or not the first K autocorrelations of the residuals, taken as a whole, indicate inadequacy of the fitted model, [4]. (The value of K can be taken to be n/10). Now, assume that we have calculated the residual $\hat{z}_t$'s and their first K autocorrelations, $\hat{r}_{zz}(k)$, k = 1, 2, ..., K, resulting when a fitted *mixed* autoregressive-moving average model of order (p,q) is used to model the observed series. Then, it can be shown, [6], that if the fitted model is adequate,

$$Q = n \sum_{k=1}^{K} \hat{r}^2_{zz}(k) \tag{2.4.17}$$

* Chapter 45; ¢ Chapter 8

is approximately chi-square distributed with (K-p-q) degrees of freedom. Here, n is the number of observations used to fit the stationary model. If the model is inadequate, the Q value will be inflated. Therefore, one can make an approximate, general, or "postmanteau" test of the hypothesis of model inadequacy with the information available by referring a calculated value of Q to a table of percentage points of the chi-square distribution, [6].

Note that for fitted autoregressive models of order p and for fitted moving average models of order q, we would have a chi-square with (K-p) and (K-q) degrees of freedom, respectively.

2.4.4 Forecasting and Updating

After having obtained a model to describe the observed time series and having confirmed its adequacy, we desire to use it to forecast future values of the observed series. We shall now illustrate how the fitted model may be used to obtain minimum mean square error forecasts. We would like to forecast a value $x_{t+\ell}$, $\ell = 1, 2, \ldots, L$ steps ahead, when we are presently at time t. That is, the forecast is said to be made at origin t for a lead time ℓ. Of course, the shorter the lead time ℓ, the more accurate one can expect the forecast to be. Also, the spacing, Δ, of the data is of importance in forecasting. That is to say, if the data is recorded daily, then it would be unrealistic to attempt to forecast weeks in advance.

To derive the minimum mean square error forecasts for any lead time ℓ, first consider the general mixed autoregressive-moving average model fitted to the stationary series y_t; that is,

$$y_t = \alpha_1 y_{t-1} + \alpha_2 y_{t-2} + \ldots + \alpha_p y_{t-p} + z_t - \beta_1 z_{t-1} - \ldots - \beta_q z_{t-q} . \tag{2.4.18}$$

Using the backward filter $(1 - B)^d x_t = y_t$, we have

$$x_t = \phi_1 x_{t-1} + \phi_2 x_{t-2} + \ldots + \phi_{p+d} x_{t-p-d} + z_t - \beta_1 z_{t-1} - \ldots - \beta_q z_{t-q} , \tag{2.4.19}$$

or in terms of the backward shift operator B

$$(1 - \phi_1 B - \phi_2 B^2 - \ldots - \phi_{p+d} B^{p+d}) x_t = (1 - \beta_1 B - \beta_2 B^2 - \ldots - \beta_q B^q) z_t . \tag{2.4.20}$$

We may write an observation $x_{t+\ell}$ generated by the process (2.4.19) either as a difference equation,

$$x_{t+\ell} = \phi_1 x_{t+\ell-1} + \phi_2 x_{t+\ell-2} + \cdots + \phi_{p+d} x_{t+\ell-p-d} + z_{t+\ell} - \beta_1 z_{t+\ell-1} - \cdots - \beta_q z_{t+\ell-q} ; \tag{2.4.21}$$

or as an infinite weighted sum of current and previous shocks z_j,

$$x_{t+\ell} = \sum_{j=0}^{\infty} \psi_j z_{t+\ell-j} , \tag{2.4.22}$$

where $\psi_0 = 1$ and the weights may be obtained by equating coefficients in

$$(1 - \phi_1 B - \cdots - \phi_{p+d} B^{p+d})(1 + \psi_1 B + \psi_2 B^2 + \cdots) = (1 - \beta_1 B - \cdots - \beta_q B^q); \tag{2.4.23}$$

or as an infinite weighted sum of previous observations, plus a random shock,

$$x_{t+\ell} = \sum_{j=1}^{\infty} \pi_j x_{t+\ell-j} + z_{t+\ell} . \tag{2.4.24}$$

Now, using equation (2.4.22) and the assumptions of the model, as discussed previously, it will be shown that the minimum mean square error forecast at origin t, for a lead time ℓ, is the conditional expectation of $x_{t+\ell}$ at time t; that is,

$$\hat{x}_t(\ell) = E_t[x_{t+\ell}] . \tag{2.4.25}$$

Suppose at time t we are to forecast $x_{t+\ell}$ with a linear function of current and previous observations x_t, x_{t-1}, x_{t-2}, ... Then, as shown above, it will also be a linear function of current and previous z_t, z_{t-1}, z_{t-2}, ...

Suppose the best (minimum mean square error) forecast is given by

$$\hat{x}_t(\ell) = \psi^*_\ell z_t + \psi^*_{\ell+1} z_{t-1} + \psi^*_{\ell+2} z_{t-2} + \cdots = \sum_{j=\ell}^{\infty} \psi^*_j z_{t+\ell-j} . \tag{2.4.26}$$

Now, from equation (2.4.22),

$$x_{t+\ell} - \hat{x}_t(\ell) = \sum_{j=0}^{\infty} \psi_j z_{t+\ell-j} - \sum_{j=\ell}^{\infty} \psi_j^* z_{t+\ell-j}$$

$$= \sum_{j=0}^{\ell-1} \psi_j z_{t+\ell-j} + \sum_{j=\ell}^{\infty} (\psi_j - \psi_j^*) z_{t+\ell-j} \cdot \tag{2.4.27}$$

Squaring the above expression and taking the expected value, we have

$$E[(x_{t+\ell} - \hat{x}_t(\ell))^2] = E[(\sum_{j=0}^{\ell-1} \psi_j z_{t+\ell-j} + \sum_{j=\ell}^{\infty} (\psi_j - \psi_j^*) z_{t+\ell-j})^2] \cdot$$

Since $E(z_i z_j) = 0$, for $i \neq j$ and σ_z^2 for $i = j$, we have

$$E[(x_{t+\ell} - \hat{x}_t(\ell))^2] = \sum_{j=0}^{\ell-1} \psi_j^2 \sigma_z^2 + \sum_{j=\ell}^{\infty} (\psi_j - \psi_j^*)^2 \sigma_z^2 \tag{2.4.28}$$

The above expression is minimized by setting $\psi_j^* = \psi_j$, $j = \ell, \ell + 1, \ldots, \infty$; this implies:

$$\hat{x}_t(\ell) = \psi_\ell z_t + \psi_{\ell+1} z_{t-1} + \cdots \cdot \tag{2.4.29}$$

Now, it is required to show that $\hat{x}_t(\ell)$ as given in equation (2.4.29) is, in fact, the conditional expectation at time t of $x_{t+\ell}$. Since

$$E_t[z_j] = \begin{cases} 0 & , \text{ for } j > t \\ z_j & , \text{ for } j \leq t \end{cases} , \tag{2.4.30}$$

from equation (2.4.22), we have

$$E_t(x_{t+\ell}) = E_t[\sum_{j=0}^{\infty} \psi_j z_{t+\ell-j}]$$

$$= \sum_{j=0}^{\infty} \psi_j E_t[z_{t+\ell-j}]$$

$$= \sum_{j=\ell}^{\infty} \psi_j z_{t+\ell-j} \cdot \tag{2.4.31}$$

This result also has been shown in [6]*.

For example, if a mixed autoregressive-moving average model of order (p,q) was fitted to the d^{th} difference series of the observed non-stationary series x_t,

$$x_t = \phi_1 x_{t-1} + \ldots + \phi_{p+d} x_{t-p-d} + z_t - \hat{\beta}_1 z_{t-1} - \ldots - \hat{\beta}_q z_{t-q} . \tag{2.4.32}$$

Now, to forecast ahead by a lead time ℓ, we replace t with $t + \ell$ in (2.4.32):

$$x_{t+\ell} = \phi_1 x_{t+\ell-1} + \ldots + \phi_{p+d} x_{t+\ell-p-d} + z_{t+\ell} - \hat{\beta}_1 x_{t+\ell-1} - \ldots - \hat{\beta}_q z_{t+\ell-q} . \tag{2.4.33}$$

The minimum mean square error forecast will be given by

$$E_t [x_{t+\ell}] = \phi_1 E_t[x_{t+\ell-1}] + \ldots + \phi_{p+d} E_t[x_{t+\ell-p-d}] + E_t[z_{t+\ell}]$$
$$-\hat{\beta}_1 E_t[z_{t+\ell-1}] - \ldots - \hat{\beta}_q E_t[z_{t+\ell-q}] . \tag{2.4.34}$$

As discussed previously, the conditional expectation can be obtained from

$$E_t[x_{t+\ell}] = \hat{x}_t(\ell) \text{ and } E_t[z_{t+\ell}] = 0 \tag{2.4.35}$$

for $\ell = 1, 2, \ldots L$, and

$$E_t[x_{t-\ell}] = x_{t-\ell} \text{ and } E_t[z_{t-\ell}] = z_{t-\ell} , \tag{2.4.36}$$

for $\ell = 0, 1, 2, \ldots, L$. Thus, we can rewrite equation (2.4.35) by using the following rules:

i) The data points $x_{t+\ell}$ ($\ell = 1, 2, \ldots, L$), which have not yet been realized, are replaced by their forecasts $\hat{x}_t(\ell)$ at origin t.

ii) The errors $z_{t+\ell}$ ($\ell = 1, 2, \ldots, L$), which cannot be calculated until $x_{t+\ell}$ is realized, are replaced by their unconditional expectation of zero. (See section 3.3.4).

We can also rewrite equation (2.4.36) by the following rules:

i) The data points $x_{t-\ell}$ ($\ell = 0, 1, 2, \ldots, L$), which have already been realized at origin t, assume their realized value.

ii) The errors $z_{t-\ell}$ ($\ell = 0, 1, 2, \ldots L$), which have happened at origin t, are calculated from $x_{t-\ell} - x_{t-\ell-1}(1)$.

* Chapter 5

The variance of the ℓ steps ahead forecast error for any origin t is the expected value of

$$\varepsilon_t^2(\ell) = [x_{t+\ell} - x_t(\ell)]^2 . \tag{2.4.37}$$

It has been shown, [12], that the variance of the lead time ℓ is given by

$$\text{var}(\ell) = [1 + \sum_{j=1}^{\ell-1} \theta_j^2] \sigma_z^2 \tag{2.4.38}$$

where the weights θ_j are given by

$$\begin{aligned}
&\theta_j = 0, \qquad j < 0 \\
&\theta_0 = 1 \\
&\theta_1 = \phi_1 - \hat{\beta}_1 \\
&\theta_2 = \phi_1\theta_1 + \phi_2 - \hat{\beta}_2 \\
&\quad \cdot \\
&\quad \cdot \\
&\quad \cdot \\
&\theta_j = \phi_1\theta_{j-1} + \ldots + \phi_{p+d}\theta_{j-p-d} - \hat{\beta}_j, \qquad j = 1, 2, \ldots, q
\end{aligned} \tag{2.4.39}$$

For j greater than q and p+d-1*, equation (2.4.39) can be reduced to:

$$\theta_j = \phi_1\theta_{j-1} + \phi_2\theta_{j-2} + \ldots + \phi_{p+d}\theta_{j-p-d} . \tag{2.4.40}$$

Note that when one has an autoregressive model, the $\hat{\beta}$'s are zero; similarly, when one has a moving average model, the ϕ's are zero.

We may express the accuracy of the forecasts by calculating probability limits on each forecast. The probability limits are such that when the realized value of the time series occurs, it will be included within these limits with the stated probability. An estimate s_z^2 of the variance σ_z^2 in (2.4.38) is obtained from the time series data. s_z^2 will be the residual sum of squares obtained in the fitting procedure divided by the number of observations used in calculating it. When the number of observations is, say, at least 50, one can approximate the $(1-\alpha)$ probability limits as,

* That is, $j > p+d-1$ if $p+d-1 \geq q$; $j > q$ if $p+d-1 < q$

$$x_{t+\ell} = \hat{x}_t(\ell) \pm t_{\alpha/2} \left[1 + \sum_{j=1}^{\ell-1} \theta_j^2\right]^{1/2} s_z \ , \qquad (2.4.41)$$

where $t_{\alpha/2}$ is the deviate from the student's t-distribution.

We are usually interested in forecasting values of an observed series for $\ell = 1, 2, \ldots, L$ lead times in the future from some origin t. Once these forecasts are obtained and a new piece of information is realized, we may adjust or update the original forecasted values. The new forecast will be related to the old by

$$\hat{x}_{t+1}(\ell) = \hat{x}_t(\ell + 1) + \theta_\ell z_{t+1} \ . \qquad (2.4.42)$$

From the above equation, we see that the t-origin forecast of $x_{t+\ell+1}$ may be updated to become the t + 1 origin forecast of the same $x_{t+\ell+1}$, by adding a constant multiple of the one-step-ahead forecast error z_{t+1}, where z_{t+1} is given by

$$z_{t+1} = x_{t+1} - \hat{x}_t(1) \ , \qquad (2.4.43)$$

and the multiplier θ_ℓ is given by (2.4.39) and (2.4.40).

2.5 THE SPECTRUM

After fitting the appropriate model to the data, additional information can be obtained from the filtered (stationary) series concerning the distribution of the variance with respect to frequency. The Fourier transform of the autocovariance function is another means by which a stationary stochastic process can be characterized. One is forced to conclude, however, that Fourier analysis breaks down when it is applied to non-stationary time series. The reasons are rather obvious; the theory behind Fourier analysis is based on the assumptions that the amplitudes are fixed, as well as the frequencies and phases. This is not the case when we have to deal with time series. Random changes in frequencies, amplitudes, and phases are found here due to the nature of time series.

The *sample spectrum* is the Fourier transform of the *sample autocovariance* function. Its graph shows how the variance of the realization of a stochastic process is distributed with respect to frequency. Furthermore,

having the sample spectrum, one can obtain the sample autocovariance function by taking the inverse Fourier transform of the sample spectrum. That is, the sample spectrum of $c_{xx}(f)$ is given by

$$C_{xx}(f) = \int_{-T}^{T} c_{xx}(u) e^{-j2\pi fu} du, \quad -\infty < f < \infty , \tag{2.5.1}$$

and the sample autocovariance function of $C_{xx}(f)$ is given by

$$c_{xx}(u) = \int_{-\infty}^{\infty} C_{xx}(f) e^{j2\pi fu} df, \quad -T \leq u \leq T \tag{2.5.2}$$

for a continuous time series $x(t)$, while for the discrete case,

$$C_{xx}(f) = \Delta \sum_{k=-(N-1)}^{N-1} c_{xx}(k) e^{-j2\pi fk\Delta} , \quad -\frac{1}{2\Delta} \leq f \leq \frac{1}{2\Delta} \tag{2.5.3}$$

and

$$c_{xx}(u) = \int_{-\frac{1}{2\Delta}}^{\frac{1}{2\Delta}} C_{xx}(f) e^{j2\pi fu} df, \quad -N\Delta \leq u \leq N\Delta . \tag{2.5.4}$$

The *theoretical spectrum* is defined by taking the limit, as the period T tends to infinity, of the expected value of the sample spectrum. That is,

$$\begin{aligned} \Gamma_{xx}(f) &= \lim_{T\to\infty} E[C_{xx}(f)] \\ &= \int_{-\infty}^{\infty} \gamma_{xx}(u) e^{-j2\pi fu} du . \end{aligned} \tag{2.5.5}$$

Similarly, the *theoretical autocovariance* function of the continuous time series $x(t)$ is obtained by taking the inverse Fourier transform of the theoretical spectrum. That is,

$$\gamma_{xx}(u) = \int_{-\infty}^{\infty} \Gamma_{xx}(f) e^{j2\pi fu} df . \tag{2.5.6}$$

The graph of the spectrum $\Gamma_{xx}(f)$, as a function of frequency, shows how the variance of the $x(t)$ process is distributed with respect to frequency. Similarly, the graph of the sample spectrum $C_{xx}(f)$ shows how the variance of

a realization of a stochastic process is distributed with respect to frequency over a period of length T.

Quite frequently in practice we have to compare time series with different scales of measurements. Thus, it is necessary to normalize the spectrum. Normalization in this case is done simply by dividing the theoretical spectrum given by equation (2.5.5) by the variance of the process σ_x^2. That is,

$$\xi_{xx}(f) = \frac{\Gamma_{xx}(f)}{\sigma_x^2} , \qquad (2.5.7)$$

where

$$\sigma_x^2 = \gamma_{xx}(0) = \int_{-\infty}^{\infty} \Gamma_{xx}(f)df .$$

The expression given by equation (2.5.7), $\xi_{xx}(f)$, is called the *spectral density function*. The function $\xi_{xx}(f)$ represents the Fourier transform of the autocorrelation function due to the relationship between the autocovariance and the autocorrelation function. The spectral density function is non-negative and integrates to unity, thus resembling the definition of a probability density function.

2.5.1 Properties of the Spectrum

Sometimes it is highly desirable to obtain the spectrum of the output from a linear system when the input is a stationary process. In the present study, we will be primarily interested in the case where the input is white noise. The general rule is given in Jenkins and Watts [3]*, which states that "the spectrum of the output from a linear system is obtained from the spectrum of the input by multiplying by the square of the frequency response function." Thus, in our case, the input to the system will be white noise denoted by z(t) whose spectrum is given by $\Gamma_{zz}(f) = \sigma_z^2$, and the output process x(t) is a linear process and its spectrum is given by

$$\Gamma_{xx}(f) = \sigma_z^2 |H(f)|^2, \quad -\infty < f < \infty \qquad (2.5.8)$$

* Chapter 6

or

$$\Gamma_{xx}(f) = |H(f)|^2 \Gamma_{zz}(f), \; -\frac{1}{2\Delta} \leq f \leq \frac{1}{2\Delta} \qquad (2.5.9)$$

where H(f) is the *frequency response function.*

In our presentation of the spectral analysis of the ionospheric, man/machine interface,and climatological information, we shall utilize the spectrum of the three basic models we discussed in sections 2.1 through 2.4, namely, the autoregressive, the moving averages, and a mixture of auto-regressive-moving averages. Thus, in what follows, we shall give the basic definitions of the above models for both the continuous and the discrete case.

i) *Continuous First Order Autoregressive Process*

The spectrum of a continuous realization of a stochastic process x(t) is given by

$$\Gamma_{xx}(f) = \frac{\sigma_z^2}{1+ (2\pi fT)^2}, \; -\infty < f < \infty . \qquad (2.5.10)$$

Note that from the form of the theoretical spectrum, $\Gamma_{xx}(f)$, one can conclude that most of the power (variance) is concentrated at low frequencies.

ii) *Discrete First Order Autoregressive Process*

The spectrum of a discrete realization of a stochastic process x(t) is defined by

$$\Gamma_{xx}(f) = \frac{\Delta\sigma_z^2}{1+\alpha_1^2-2\alpha_1 \cos 2\pi f\Delta} , \; -\frac{1}{2\Delta} < f < \frac{1}{2\Delta} . \qquad (2.5.11)$$

It should be mentioned that if α_1 is negative, the spectrum has most of its power concentrated at higher frequencies, while when α_1 is positive, the power will be concentrated at lower frequencies.

iii) *Continuous Second Order Autoregressive Process*

The spectrum of a continuous realization of a stochastic process x(t) is given by

$$\Gamma_{xx}(f) = \frac{\sigma_z^2}{(a_0-a_2 4\pi^2 f^2)^2 + (2\pi f a_1)} , \; -\infty < f < \infty . \qquad (2.5.12)$$

Here the distribution of the power of the process will depend on how a_0, a_1 and a_2 are inter-related. This relationship is inherent in the form of the characteristic equation of the process.

iv) *Discrete Second Order Autoregressive Process*

The spectrum of the continuous realization of a stochastic process x(t) is given by

$$\Gamma_{xx}(f) = \frac{\Delta\sigma_z^2}{1+\alpha_1^2+\alpha_2^2-2\alpha_1(1-\alpha_2)\cos 2\pi f\Delta-2\alpha_2\cos 4\pi f\Delta}, \quad -\frac{1}{2\Delta} \leq f \leq \frac{1}{2\Delta}. \tag{2.5.13}$$

Again, the location of where most of the power is concentrated is characterized by the values of α_1 and α_2.

v) *General Autoregressive-Moving Average of a Continuous Process*

The spectrum of a continuous realization of a stochastic process x(t) is given by

$$\Gamma_{xx}(f) = \sigma_z^2 \left| \frac{b_0+b_1 j2\pi f+\ldots+b_\ell (j2\pi f)^\ell}{a_0+a_1 j2\pi f+\ldots+a_m (j2\pi f)^m} \right|^2, \quad -\infty \leq f \leq \infty. \tag{2.5.14}$$

vi) *General Autoregressive-Moving Average of a Discrete Process*

The spectrum of a continuous realization of a stochastic process (x(t) is defined by

$$\Gamma_{xx}(f) = \Delta\sigma_z^2 \left| \frac{1+\beta_1 e^{-j2\pi f\Delta}+\ldots+\beta_\ell e^{-j2\pi f\Delta\ell}}{1-\alpha_1 e^{-j2\pi f\Delta}-\ldots-a_m e^{-j2\pi f\Delta m}} \right|^2, \quad \frac{1}{2\Delta} \leq f \leq \frac{1}{2\Delta}. \tag{2.5.15}$$

In the last two definitions, various peaks or spikes will appear in the spectrum if the roots of the corresponding characteristic equations are complex. The behavior of the above will be displayed in Section 4.

2.6 ESTIMATE OF THE SPECTRUM

In the previous section, we have given a brief discussion of the basic definitions and properties of the theoretical spectrum. With respect to the aims of the present study, we shall give in this section a smoothed estimate

of the theoretical spectrum and some of its properties that are essential in the final analysis of the experimental data.

Bartlett, [11], introduced a very useful procedure for estimating the spectrum of a stochastic realization. This estimate of the spectrum for a purely random process is given by

$$C_{zz}(f) = \frac{\Delta}{N}\left[\{\sum_{t=-n}^{n-1} z_t \cos 2\pi f t\Delta\}^2 + \{\sum_{t=-n}^{n-1} z_t \sin 2\pi f\Delta\}^2\right]$$

$$= \frac{\Delta}{N}\left[A^2(f) + B^2(f)\right] , \; -\frac{1}{2\Delta} \leq f \leq \frac{1}{2\Delta} \quad , \tag{2.6.1}$$

where

$$A^2(f) = \{\sum_{t=-n}^{n-1} z_t \cos 2\pi f t\Delta\}^2 \tag{2.6.2}$$

and

$$B^2(f) = \{\sum_{t=-n}^{n-1} z_t \sin 2\pi f\Delta\}^2 \; . \tag{2.6.3}$$

Bartlett's procedure consists of splitting up the series of length N into k sub-series of length $\frac{N}{k}$, evaluates a sample spectrum $C_{zz}^{(i)}(f)$ for each of the k sub-series, i = 1, 2, ..., k, and finally takes the mean of the sub-series as his estimator at frequency f. That is,

$$\bar{C}_{zz}(f) = \frac{1}{k}\sum_{i=1}^{k} C_{zz}^{(i)}(f) \; . \tag{2.6.4}$$

The estimate given by equation (2.6.4) is called a *smoothed spectral estimate* at frequency f and the method to obtain (2.6.4), *Bartlett's smoothing procedure*. More generally, Bartlett's smoothing procedure suggests that a smoothed spectral estimator of a stochastic realization x(t) is given by

$$\bar{C}_{xx}(f) = \int_{-\infty}^{\infty} w(u) c_{xx}(u) e^{-j2\pi f u} du = \int_{-\infty}^{\infty} \bar{c}_{xx}(u) e^{-j2\pi f u} du \; . \tag{2.6.5}$$

The smoothed sample spectrum will have a smaller variance than the unsmoothed sample spectral estimator, $C_{xx}(f)$. The smoothed estimate of the spectrum is a function of the type of lag window, w(u), one utilizes.

However, in all cases the following properties hold with respect to w(u):

i) $w(0) = 1$;

ii) $w(u) = w(-u)$;

iii) $w(u) = 0, \ |u| > T$;

iv) $w(u) = 0, \ |u| > M, \ M < T$.

In section 2.8 the above concept of the window will be explored extensively. As will be stated, the bandwidth of a spectral window will be defined as follows:

$$b = \frac{1}{\int_{-\infty}^{\infty} w^2(f)df} \quad . \tag{2.6.6}$$

Another form of the bandwidth is the standardized bandwidth, b_1, which is given by placing

$$M = \frac{N}{k} = 1 \quad .$$

and

$$b = \frac{b_1}{M} = \frac{1}{\int_{-\infty}^{\infty} w^2(f)df} \quad .$$

We can conclude that the variance of a spectral estimator is inversely proportional to the bandwidth of the spectral window. Also the degrees of freedom, ν, of the smoothed estimator are directly proportional to the bandwidth of the spectral window due to the relationship

$$\nu = \frac{2T}{\int_{-\infty}^{\infty} w^2(u)du} = 2(\frac{T}{M})b_1 \quad . \tag{2.6.7}$$

On the other hand, the bias is directly proportional to the bandwidth of the window.

The notion of *the smoothed spectral density estimate* denoted by $\overline{R}_{xx}(f)$ shall now be introduced. This estimate is defined as follows:

$$\bar{R}_{xx}(f) = 2 \{1 + 2 \sum_{k=1}^{L-1} r_{xx}(k)w(k)\cos 2\pi fk\}, \quad 0 \leq f \leq \frac{1}{2} \quad , \qquad (2.6.8)$$

where,

$$r_{xx}(k) = \frac{c_{xx}(k)}{c_{xx}(0)} \quad . \qquad (2.6.9)$$

The mean smoothed spectral density $\frac{\bar{\Gamma}_{xx}(f)}{\sigma^2_x}$ is given by

$$\frac{\bar{\Gamma}_{xx}(f)}{\sigma^2_x} = 2 \left[1 + \sum_{k=1}^{L-1} \rho_{xx}(k)w(k)\cos 2\pi fk\right] . \qquad (2.6.10)$$

Equation (2.6.10) is the expected value of the smoothed spectral denisty estimator. By plotting $\frac{\Gamma_{xx}(f)}{\sigma^2_x}$ versus $\frac{\bar{\Gamma}_{xx}(f)}{\sigma^2_x}$, as shall be done with the ionospheric phenomenon under investigation, one will be able to detect how the bias varies with frequency.

Also, the variation of bias with bandwidth can be observed by simply plotting different curves for the different values of L, the truncation point. One other relationship can be plotted as well. This plot consists of $\bar{R}_{xx}(f)$ versus $\frac{\Gamma_{xx}(f)}{\sigma^2_x}$ and displays how the variance varies with respect to frequency.

Similarly, the variation of variance with bandwidth can be observed simply by plotting the estimate with different values of L.

Jenkins and Watts, in their efforts to point out the criteria for determining optimal lag windows, argue that window carpentry is not as important as window closing. In Section 4 of the present study, we will examine these factors in detail with actual data to determine an optimal lag window.

Two criteria, which would seem logical at first sight but whose value is debatable in determining an optimal lag window, are listed as follows. (They are classified as the "optimality approach to smoothing."):

i) The mean squared error criterion,

$$E[\{\overline{C}_{xx}(f) - \Gamma_{xx}(f)\}^2] ,$$

and

ii) The integrated mean squared error,

$$\int_{-\infty}^{\infty} E[\{\overline{C}_{xx}(f) - \Gamma_{xx}(f)\}^2]df .$$

Nevertheless, the above optimality criteria are rejected, a fact which brings into play the formulation of *high stability* and *high fidelity* as useful criteria. They are widely accepted in practice. The previous criteria, namely, the mean squared error and the integrated squared error, are not useful because they are arbitrary; they have no flexibility (strictly mathematical); they do not allow an *a priori* design and analysis of the data; and they only indicate what is best on the average. Therefore, the two main requirements for estimating the theoretical spectrum $\Gamma_{xx}(f)$ as accurately as possible are:

i) High fidelity, which implies that

$$\overline{\Gamma}_{xx}(f) - \Gamma_{xx}(f) = B(f)$$

be small, and

ii) High stability, which implies that

$$Var[\overline{C}_{xx}(f)] \simeq \frac{\Gamma_{xx}^2(f)}{T}\left(\frac{M}{b_1}\right)$$

be small.

High fidelity and high stability are two conflicting requirements. In minimizing the covariance, we increase the bias; and, conversely, by minimizing the bias, we increase the variance. An ideal situation would be one where M is large enough for high fidelity and M is small enough for high stability. The logic here dictates a compromise of some form.

In summary, we can say that smoothing the estimate of the theoretical spectrum consists of determining the shape or the mathematical form of the window (section 2.8 discusses window carpentry) on one hand and the value of

the bandwidth (window closing) on the other. By window closing we mean computing window estimates using a wide bandwidth and then progressively using narrower bandwidths until we achieve a state of high fidelity and high stability. The numerous and various problems involved will be studied in subsequent chapters.

2.7 THE CROSS SPECTRUM

In this section, the concepts we have already dealt with shall be extended so as to be able to treat pairs of time series $x_1(t)$ and $x_2(t)$.

The autocovariance function of the stochastic realization is given by

$$\gamma_{x_1x_1}(u) = E[(X_1(t)-\mu_1)\ (X_1(t+u)-\mu_1)] = \gamma_{11}\ , \tag{2.7.1}$$

where the expression for γ_{22} can be obtained by changing the subscripts, and the cross-covariance function is given by:

$$\gamma_{x_1x_2}(u) = E[(X_1(t)-\mu_1)(X_2(t+u)-\mu_2)] = \gamma_{12} \tag{2.7.2}$$

where

$$\mu_i = E[X_i(t)],\ i = 1,\ 2.$$

The cross correlation function is given by

$$\rho_{12}(u) = \frac{\gamma_{12}(u)}{\sqrt{\gamma_{11}(0)\gamma_{22}(0)}} = \frac{\gamma_{12}(u)}{\sigma_1\sigma_2}\ . \tag{2.7.3}$$

The cross covariance function is estimated by

$$c_{x_1x_2}(u) = \begin{cases} \frac{1}{T}\int_{-T/2}^{T/2-u} (X_1(t)-\overline{X}_1)\ (X_2(t+u)-\overline{X}_2)dt,\ 0 \le u \le T \\ \frac{1}{T}\int_{-T/2+u}^{T/2} (X_1(t)-\overline{X}_1)\ (X_2(t+u)-\overline{X}_2)dt,\ -T \le u \le 0\ , \end{cases} \tag{2.7.4}$$

where

$$\bar{X}_i = \frac{1}{T}\int_{-T/2}^{T/2} X_i(t)dt, \quad i = 1, 2 . \tag{2.7.5}$$

An estimate of the cross correlation function is obtained by

$$r_{x_1x_2}(k) = \frac{c_{x_1x_2}(k)}{\sqrt{c_{x_1x_1}(0)c_{x_2x_2}(0)}} \tag{2.7.6}$$

Using the above equations as a foundation, one can define the theoretical *autospectrum*, $\Gamma_{11}(f)$, and *sample autospectrum*, $C_{11}(f)$, by

$$\Gamma_{11}(f) = \int_{-\infty}^{\infty}\gamma_{11}(u)e^{-j2\pi fu}du , \tag{2.7.7}$$

and

$$C_{11}(f) = \int_{-T}^{T}c_{11}(u)e^{-j2\pi fu}du, \tag{2.7.8}$$

respectively. Hence, we arrive at the notion of the cross spectrum. As in the univariate case, the *sample cross spectrum* is the Fourier transform of the *sample cross covariance* function. That is,

$$C_{12}(f) = \int_{-T}^{T}c_{12}(u)e^{-j2\pi fu}du . \tag{2.7.9}$$

Note that the inverse Fourier transform of $C_{12}(f)$ gives rise to $c_{12}(f)$. Another form of $C_{12}(f)$ that is commonly used is

$$C_{12}(f) = A_{12}(f)e^{jF_{12}(f)} = L_{12}(f) - jQ_{12}(f) , \tag{2.7.10}$$

which is the product of a real function $A_{12}(f)$, called the *sample cross amplitude spectrum*, and a complex function called the *sample phase spectrum*, $e^{jF_{12}(f)}$.

The *theoretical cross spectrum* is the Fourier transform of the *theoretical cross-covariance function;* that is,

$$\Gamma_{12}(f) = \int_{-\infty}^{\infty}\gamma_{12}(u)e^{-j2\pi fu}du = \alpha_{12}(f)e^{j\phi_{12}(f)}$$

$$= \Lambda_{12}(f) - j\Psi_{12}(f) , \qquad (2.7.11)$$

which is the product of the *cross amplitude spectrum* and the *phase spectrum.*

The expected value of the cross spectrum estimate is given by

$$E[C_{x_1x_2}(f)] = \int_{-T}^{T}(1 - \frac{|u|}{T})\gamma_{x_1x_2}(u)e^{-j2\pi fu}du . \qquad (2.7.12)$$

As T goes to infinity, the above mean value approaches the cross spectrum. Therefore,

$$\lim_{T\to\infty} E[C_{x_1x_2}(f)] = \Gamma_{x_1x_2}(f) = \int_{-\infty}^{\infty}\gamma_{x_1x_2}(u)e^{-j2\pi fu}du \quad -\infty < f < \infty . \qquad (2.7.13)$$

Furthermore, the *co-spectrum,* $\Lambda_{12}(f)$, is defined as

$$\Lambda_{12}(f) = \int_{-\infty}^{\infty}\lambda_{12}(u)e^{-j2\pi fu}du$$

$$= \frac{1}{2}\int_{-\infty}^{\infty}\{\gamma_{12}(u) + \gamma_{12}(-u)\ \cos\}2\pi fudu , \qquad (2.7.14)$$

where

$$\lambda_{12}(u) = \frac{1}{2}\{\gamma_{12}(u) + \gamma_{12}(-u)\} . \qquad (2.7.15)$$

Similarly, the *sample co-spectrum,* $L_{12}(f)$, is defined by

$$L_{12}(f) = \int_{-T}^{T}\ell_{12}(u)e^{-j2\pi fu}du$$

$$= \frac{1}{2}\int_{-T}^{T}\{c_{12}(u) - c_{12}(-u)\}\cos\ 2\pi fudu , \qquad (2.7.16)$$

where

$$\ell_{12}(u) = \frac{1}{2}\{c_{12}(u) - c_{12}(-u)\} . \qquad (2.7.17)$$

On the other hand, the *quadrature spectrum*, $\Psi_{12}(f)$, is defined by

$$\Psi_{12}(f) = \int_{-\infty}^{\infty}\psi_{12}(u)e^{-j2\pi fu}du$$

$$= \frac{1}{2}\int_{-\infty}^{\infty}\{\gamma_{12}(u) - \gamma_{12}(-u)\ \sin\}2\pi fudu , \qquad (2.7.18)$$

where

$$\psi_{12}(u) = \frac{1}{2}\{\gamma_{12}(u) - \gamma_{12}(-u)\} , \qquad (2.7.19)$$

and the *sample quadrature spectrum*, $Q_{12}(f)$, is defined by

$$Q_{12}(f) = \int_{-T}^{T}q_{12}(u)e^{-j2\pi fu}du$$

$$= \frac{1}{2}\int_{-T}^{T}\{c_{12}(u) - c_{12}(-u)\}\sin\ \pi fudu , \qquad (2.7.20)$$

where

$$q_{12}(u) = \frac{1}{2}\{c_{12}(u) - c_{12}(-u)\} .$$

Thus, with the above definitions, we can define the *cross amplitude spectrum* as follows:

$$\alpha_{12}(f) = |\Gamma_{12}(f)| = \sqrt{\Lambda_{12}^2(f) + \Psi_{12}^2(f)} . \qquad (2.7.21)$$

Also, the *sample cross amplitude spectrum* is defined by

$$A_{12}(f) = |C_{12}(f)| = \sqrt{\Lambda_{12}^2(f) + Q_{12}^2(f)} . \qquad (2.7.22)$$

On the other hand, the *phase spectrum* can be written by

$$\Phi_{12}(f) = \arctan \frac{-\psi_{12}(f)}{\Lambda_{12}(f)} \quad , \tag{2.7.23}$$

and the *sample phase spectrum* is given by

$$F_{12}(f) = \arctan \frac{-Q_{12}(f)}{L_{12}(f)} \quad . \tag{2.7.24}$$

Having a graph of the cross amplitude spectrum, one can detect whether frequency components in one series are associated with large or small amplitudes at the same frequency in the other series. The graph of the phase spectrum helps to determine whether frequency components in one series are in phase or out of phase (lag or lead) with the components at the same frequency in the other series.

The cross amplitude spectrum and the phase spectrum would suffice to provide a complete description of a bivariate stochastic process. However, a more efficient spectrum, namely, the *coherency spectrum,* will be introduced in sub-section 2.7.1 to take the place of the cross amplitude spectrum.

For the discrete case, we simply replace the integral with a sum and make the necessary notational changes.

2.7.1 The Squared Coherency Spectrum

The squared coherency, $k_{12}^2(f)$, is

$$k_{12}^2(f) = \frac{\alpha_{12}^2(f)}{\Gamma_{11}(f)\Gamma_{22}(f)} = \frac{1}{1+(\Gamma_{22}(f)/G^2(f)\Gamma_{11}(f))} \quad . \tag{2.7.25}$$

The *squared coherency spectrum* is the plot of $k_{12}^2(f)$ versus frequency. The cross amplitude spectrum $\alpha_{12}(f)$ is a measure of the covariance between the two time series $x_1(t)$ and $x_2(t)$ at frequency f. $\Gamma_{11}(f)$ is the variance of the input at frequency f, and G(f) is the gain of the spectrum defined by

$$G(f) = \frac{\sqrt{\Lambda_{12}^2(f) + \psi_{12}^2(f)}}{\Gamma_{11}(f)} = \frac{\alpha_{12}(f)}{\Gamma_{11}(f)} \quad . \qquad (2.7.26)$$

In general, the coherency spectrum plays the role of a correlation coefficient with respect to the frequencies. When $\Gamma_{zz}(f) = 0$, the squared coherency is equal to one. When the output is nothing else but noise, the squared coherency is equal to zero.

The usefulness of the squared coherency spectrum lies in the fact that dimensions do not enter the picture when the correlation is measured with respect to frequency. Unlike the squared coherency spectrum, the cross amplitude spectrum depends on the dimensions of $x_1(t)$ and $x_2(t)$. This is the reason why the squared coherency spectrum is preferred over the cross amplitude spectrum, and, together with the phase spectrum, it gives us a complete picture of the cross correlation properties of two time series.

2.8 THE ROLE OF THE LAG WINDOWS

One of the goals of the present study is to perform spectral analysis on univariate and bivariate stochastic realizations obtained from ionospheric soundings. The purpose of such an analysis is important to the systems design engineer and to the communication/ADP scientist. One of the basic and essential factors which enters in the mathematical formulation of the power spectrum is the lag window. There are specifically four lag windows that are commonly used in spectral analysis. These lag windows are as follows:

i) rectangular window
ii) Bartlett's lag window
iii) Tukey's lag window
iv) Parzen's lag window.

The object of this section is to briefly introduce these lag windows. A specific discussion about their behavior in estimating the spectrum will be given in Section 4, where we consider the analysis of vertical incidence and oblique incidence ionospheric information.

An exact determination of the autocovariance function or the power spectrum function is quite impractical since it would require both a collection of pieces of infinite length and an infinite number of computations.

An approximate determination is therefore proposed in order for workable estimates to be obtained. The results obtained by Tukey, [12], show that, although the autocovariance function and the power spectrum are Fourier transforms of each other, the latter, in most practical situations, is preferred as yielding better results. By reducing the data, the estimates will be subject to the usual sampling variations and statistical biases. It should be pointed out again that estimates of the power spectrum exhibit bias and sampling variability characteristics much easier to study than estimates of the autocovariance function.

The unsmoothed sample spectrum is given by

$$C_{xx}(f) = \int_{-T}^{T} c_{xx}(u) e^{-j2\pi fu} du, \quad -\infty \leq f \leq \infty . \qquad (2.8.1)$$

The first moment of $C_{xx}(f)$, the unsmoothed sample spectrum estimator, is given by

$$E[C_{xx}(f)] = \int_{-T}^{T} E[c_{xx}(u)] e^{-j2\pi fu} du , \qquad (2.8.2)$$

which can be written as

$$E[C_{xx}(f)] = \int_{-T}^{T} \gamma_{xx}(u)(1 - \frac{|u|}{T}) e^{-j2\pi fu} du , \qquad (2.8.3)$$

using the fact that

$$E[c_{xx}(u)] = \begin{cases} \gamma_{xx}(u)(1 - \frac{|u|}{T}), & |u| \leq T \\ 0 , & |u| > T . \end{cases} \qquad (2.8.4)$$

Therefore, using the convolution theorem, the expected value of the unsmoothed sample spectrum can be written as

$$E[C_{xx}(f)] = \int_{-\infty}^{\infty} T\{\frac{\sin \pi T_g}{\pi T_g}\}^2 \Gamma_{xx}(f-g) dg . \qquad (2.8.5)$$

In expression (2.8.5) the quantity

$$T\{\frac{\sin \pi T_g}{\pi T_g}\}^2$$

in the integrand is referred to as the *spectral window* of the sample spectrum. The Fourier transform of the spectral window is the *lag window* which will be denoted by w(u).

In actual practice we utilize a smoothed form of expression (2.8.5) to obtain an estimate of the theoretical spectrum given by

$$\bar{C}_{xx}(f) = 2[c_{xx}(0) + 2\sum_{k=1}^{L-1} c_{xx}(u)w(u)\cos 2\pi f_k], \quad 0 < f < \frac{1}{2} , \tag{2.8.6}$$

where $c_{xx}(k)$ is the sample autocovariance at lag k, w(k) being the lag window, and L the truncation point of the series.

It is clear from a practical point of view that the resulting estimate of the power spectrum, equation (2.8.6) depends on the choice of the lag window that we are utilizing in our estimate. In what follows, these lag windows shall be defined and, for a more thorough investigation of their origin and properties, the recent books of Jenkins and Watts, [3], and Box and Jenkins, [6], are recommended.

2.9 USEFUL LAG WINDOWS

In this section the basic useful windows mentioned above shall be defined, namely, the *rectangular, Bartlett's, Tukey's, and Parzen's lag windows*. A specific comparison of these lag windows in actual problems will be given in Section 4.

We shall denote W(f)asthe portion of the integrand given by $T\{\frac{\sin \pi Tf}{\pi Tf}\}^2$ of equation (2.8.5). That is,

$$W(f) = T\{\frac{\sin \pi Tf}{\pi Tf}\}^2 . \tag{2.9.1}$$

Equation (2.9.1) is called the *spectral window*. Its Fourier transform is called the *lag window*.

2.9.1 The Rectangular Lag Window

Definition 2.9.1 The function given by

$$w_R(u) = \begin{cases} 1, & |u| \leq M \\ 0, & \text{otherwise} \end{cases} \tag{2.9.2}$$

is called the *rectangular lag window.* The Fourier transform of $w_R(u)$ is

$$W_R(f) = 2M\left[\frac{\sin 2\pi fM}{2\pi fM}\right], \quad -\infty < f < \infty , \tag{2.9.3}$$

and is called the *rectangular spectral window.* The above lag window was the first window that was used by many scientists, especially engineers. However, due to its mathematical simplicity in being able to characterize complicated phenomena, it is not very useful. Further details to this addendum will be given in a later discussion.

2.9.2 Bartlett's Lag Window

Definition 2.9.2 The function defined by the expression

$$w_B(u) = \begin{cases} 1 - \frac{|u|}{M} , & u \leq M \\ 0, & \text{otherwise} \end{cases} \tag{2.9.4}$$

is called *Bartlett's lag window.* The Fourier transform of $w_B(u)$ is given by

$$W_B(f) = M\left[\frac{\sin \pi fM}{\pi fM}\right]^2 \tag{2.9.5}$$

and is called *Bartlett's spectral window.* The above lag window, which was introduced in the 1950's, has been used extensively in spectral analysis. It possesses some interesting features that will be discussed later. However, its side lobes are much larger than any of the other windows known.

2.9.3 Tukey's Lag Window

Definition 2.9.3 The function w_T, defined by the following expression,

$$w_T(u) = \begin{cases} \frac{1}{2}(1 + \cos \frac{\pi u}{M}), & |u| \leq M \\ 0 & , \text{otherwise}, \end{cases} \tag{2.9.6}$$

is called *Tukey's lag window*. The Fourier transform of equation (2.9.6) is called *Tukey's spectral window* and it is given by

$$W_T(f) = M\{\frac{\sin 2\pi fM}{2\pi fM}\} + \frac{1}{2} \frac{\sin 2\pi M(f + \frac{1}{2}M)}{2\pi M(f + \frac{1}{2}M)}$$
$$+ M(\frac{\sin 2\pi fM}{2\pi fM}) (\frac{1}{1-[2fM]^2}), \quad -\infty \leq f \leq \infty . \tag{2.9.7}$$

Tukey's window possesses the property of having most of its power concentrated at low frequencies. Furthermore, Tukey's window results in smaller bias in the spectral estimate than Bartlett's window.

2.9.4 Parzen's Lag Window

Definition 2.9.4 The function defined by

$$w_p(u) = \begin{cases} 1-6[\frac{|u|}{M}]^2 + 6[\frac{|u|}{M}]^3, & |u| \leq \frac{M}{2} \\ 2[1 - \frac{|u|}{M}]^3 & , \frac{M}{2} \leq |u| \leq M \\ 0 & , |u| > M \end{cases} \tag{2.9.8}$$

is called *Parzen's lag window*. The Fourier transform of equation (2.9.8) is called *Parzen's spectral window* and is given by

$$W_p(f) = \frac{3}{4} M [\frac{\sin(f\pi M/2)}{\pi fM/2}]^4, \quad -\infty \leq f \leq \infty . \tag{2.9.9}$$

The above window, which was introduced in the early 1960's, gives much wider lobes and its power is not concentrated primarily at lower frequencies as in the previous window.

2.10 Some Remarks Concerning the Lag Windows

Scientists who have been involved in choosing the shape of a lag window, w(u), have taken into consideration the fact that the spectral window, W(f) (that is, the Fourier transform of the lag window), should be concentrated near the zero frequency. Blackman and Tukey, [13], looking at the problem from the communications engineering point of view, almost identified it with that of choosing the intensity distribution along an antenna, so that the variation will fall in a narrow beam. The *principal maximum* and the *subsidiary extrema* of W(f) are called, respectively, main and side lobes. A window should be an even function so that it can equally treat positive and negative values of the spectral density function on both sides of a given point of the time series. It should integrate to unity; that is,

$$\int_{-\infty}^{\infty} W(f)df = 1 \ , \qquad (2.10.1)$$

and should achieve a maximum value at the frequency f = 0. That is,

$$|W(f)| \leq W(0), \text{ for all } f.$$

It should be concentrated as much as possible about f = 0 so that the behavior of the spectral density function is concentrated as much as possible in that neighborhood.

It is my opinion that there is no agreed valid criterion for comparing the degree of concentration of any window. One criteria could be the ratio of the size of the second largest peak to the size of the largest peak. However, again this would be powerful only in the case where the second largest peak would occur at the same point. This fact explains why one has to consider all the different windows, in addition to the most popular, in one's search for the most appropriate case.

For the main lobe of W(f) to be concentrated, the graph of w(u) should be flat due to the way the two concepts are related. Also, for the side lobes to be small, w(u) should be smooth and should not change rapidly as in

the case of the rectangular window. Therefore, one should compromise. The above authors' investigations have been done along the lines of compromise, and as a result, there exist numerous windows among which to choose.

Taking Bartlett's spectral window, $W_B(f)$, as an example, we find that when it is graphed against frequency, it is found to be symmetric about the origin and has zeros at $f = \pm\frac{1}{M}, \pm\frac{2}{M}, \pm\frac{3}{M}, \ldots$.

The distance between the first zeros on either side of the origin is called *base width*. The base width for Bartlett's window is equal to $\frac{2}{M}$. It is inversely proportional to M and also to the variance. On the other hand, by increasing the base width, the bias, B(f), increases as well. Thus, one is forced to compromise between bias and variance in choosing a particular window.

The rectangular window is more concentrated about the center frequency than any of the other windows under consideration. Nevertheless, although it has the smallest bandwidth, which implies small bias, it also has the largest side lobes. This makes it very impractical. The first side lobe is about 1/5 of the height of the main lobe which shows unrealistic characterization of the estimate of the power spectrum.

Tukey claims that the window he proposed with Blackman, the use of which is called "Hanning" after the Austrian meteorologist Julius Von Han, is simple and convenient. Two facts about it are: that the main lobe is four times as wide as the side lobes; and that the side lobes are 1% or 2% of the height of the main lobe.

The above remarks will be extensively examined with the analysis of the ionospheric information in Section 4.

3. MODELING AND ANALYSIS OF IONOSPHERIC INFORMATION

3.1 INTRODUCTION

HF communications are provided by systems not specifically limited by line-of-sight, extended distance, or intervening terrain obstacles. However, ionospheric disturbances, both natural and man-made, complicate the use of the HF media, [2]. The HF communicator had as his only propagation aid, the monthly predictions for undisturbed conditions prepared three months in advance by the Department of Commerce, and distributed by the U. S. Army Strategic Communications Command. While valid for long range planning, they do not account for diurnal variations or disturbed ionospheric conditions that may degrade communications. It is, therefore, necessary to develop a system to provide tactical communicators with propagation predictions in near real-time, and prepared specifically for medium and long range distances.

The aim of this section, therefore, is two-fold:

a. to introduce a widely accepted statistical concept for the prediction of oblique incidence soundings including application for the prediction of vertical incidence soundings, and

b. to develop more suitable statistical models to forecast either the oblique or vertical incidence soundings over specific paths or at specific terminals, one, two, three, ..., k time slots ahead, beginning with a certain origin.

It is shown that for a 500 Km path, both oblique and vertical incidence recordings are non-stationary stochastic realizations. That is, they form a discrete time series that is not in statistical equilibrium. A procedure is proposed to handle this type of information and to investigate the possibility of characterizing the data with either an autoregressive process, a moving average model, or a mixture of autoregressive-moving average processes.

A systematic presentation of recording ionospheric soundings for the purpose of forecasting is given in section 3.2. An autoregressive model has been developed for the discrete realization representing the 13^{th} day vertical incidence (VI) and oblique incidence (OI) critical frequencies observed for the 500 Km path, Fort Monmouth, N. J. - Fort Drum, N. Y., in section 3.3. The complete procedure of fitting the models is given, along with the associated confidence intervals. Also included in this section is the development of

another autoregressive model that characterizes the behavior of the 18-day overall VI and OI soundings for the experiment. A prediction process based on the widely accepted Ames-Egan approach, [1], is given in section 3.4. In this section, the limitations of the process and suggested improvements are covered. Finally, in section 3.5, a summary and conclusion are presented.

3.2 DESIGN OF THE EXPERIMENT

To accomplish the task of developing both a functional relationship between OI and VI maximum observed frequencies (MOF) and a forecasting model, the Communications/ADP Laboratory, of the U. S. Army Electronics Command, had been involved in an extensive collection of VI and short-path OI ionospheric data at three different distances with Fort Monmouth, N. J., as the base station. Experimentation was performed in the 2-16 MHz range, using two ionosondes, one as a fixed terminal and the other as a mobile terminal, as shown in figure 3.1. The mobile terminal was situated at Fort Dix, N. J., establishing a 60 Km path; at Aberdeen Proving Ground, Md., to establish a 200 Km path; and at Camp Drum, N. Y., to establish a nominal 500 Km path (figure 3.2). This section will address only the 500 Km experiment.

Each terminal made scheduled soundings every ten minutes for an 18-day experiment. While the fixed terminal was transmitting and receiving its own signal, the mobile terminal would simultaneously receive the same transmissions. The same procedure was followed for the mobile terminal with respect to the fixed terminal (figures 3.1 and 3.2). Both ionosondes were synchronized to the WWV (HF) time standard (National Bureau of Standards) so that the "remote" sounder scans would be precise with the Fort Monmouth terminal. The number of days each experiment was performed has no significance with respect to the results obtained, but was a matter of funding. The basic instruments used were two Granger Associates Model 3905-5 Ionospheric Sounders, matched with wide responde delta antennas.

The frequency range of the ionosondes was limited from 2-16 MHz, in three octaves, with 400 discrete frequency channels per octave. Transmissions consisted of successively "stepping" through the channels of each octave with a pulse width of 100 micro-seconds to maximize the system sensitivity. The data is a recording of the time delay from ionosonde to ionospheric reflecting layer and return. Time delay is a measure of the virtual height of reflection

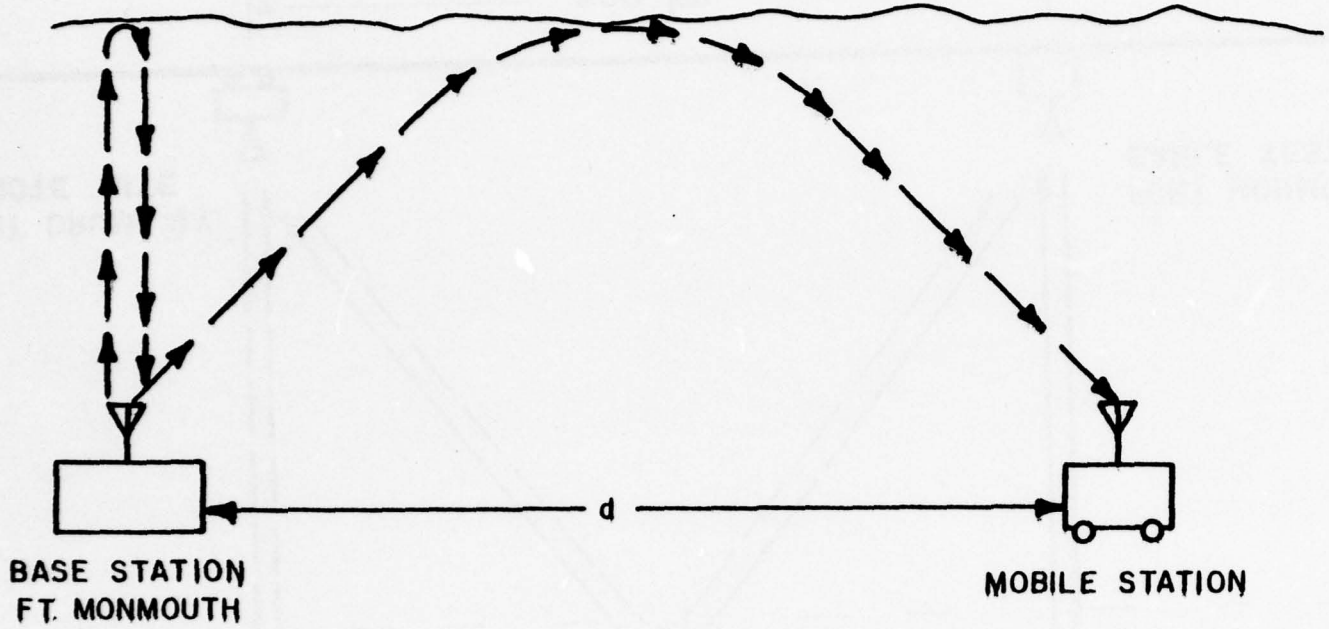

FIGURE 3.1 FIELD TESTS FOR A NEAR-REAL TIME IONOSPHERIC FORCASTING SCHEME

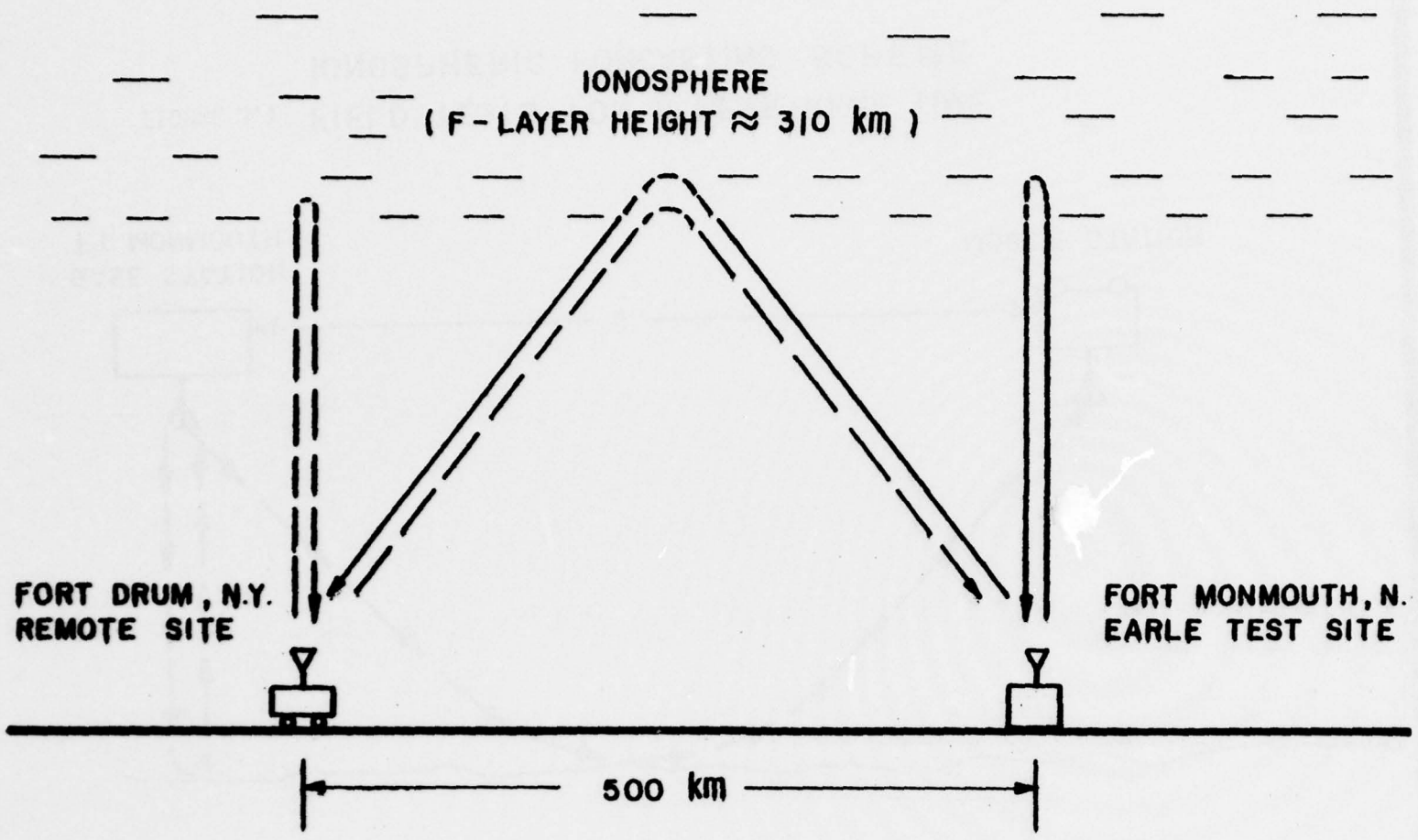

FIGURE 3.2 500 Km PATH SCHEMATIC

from the layer. The trace of the returned pulse on a scale of frequency versus time delay (virtual height) is the ionogram record, figure 3.3. Ionogram records of the data were taken on 35mm film at Fort Monmouth and on light sensitive oscillograph paper at the remote terminals. After collection and development, the ionograms were scaled for the extraordinary critical frequencies, f_xF_2, as shown in figure 3.4. The f_xF_2 data was then compiled for computer analysis and for comparison between the observed VI and observed OI critical frequencies.

The experiment results were dependent upon ionospheric conditions and man-made noise. Conditions were characterized by the Space Disturbance Forecast Center, Institute of Telecommunication Sciences, Boulder, Colorado, as generally undisturbed, but some interference occurred. Some data (ionograms) were unreadable due to man-made noise, and solar and geomagnetic activity. For those few records that were unreadable (though signal was detected), simulated data was prepared. The occurrence of obscured data was negligible over the experiment.

3.3 FORECASTING MODELS FOR IONOSPHERIC SOUNDINGS

In this section, we shall propose a step-by-step procedure in:

a. identifying and filtering the ionospheric information,
b. fitting the most appropriate model to the data,
c. applying the backwards filter technique and diagnostic checking, and
d. forecasting and updating of the appropriate model.

Specific reasons and mathematical formulations for this sequence of steps are stated in Section 2. Therefore, the basic idea and philosophy of this section is the implementation of the procedural approach proposed in this study for analyzing non-stationary information. The approach has yielded better results for fitting and forecasting than those obtainable with other methods, [1], [14], [15], [16], [17], [18], that exist in the literature.

In the previous section, the manner in which our time series were generated was outlined for the vertical incidence (VI) and oblique incidence (OI) ionospheric soundings. Specifically, we have available 18 days of data where each day is divided into 144 time slots. The data was taken over consecutive days under the same conditions; however, due to diurnal ionospheric changes, there is an inherent and uncontrollable diurnal variation in the

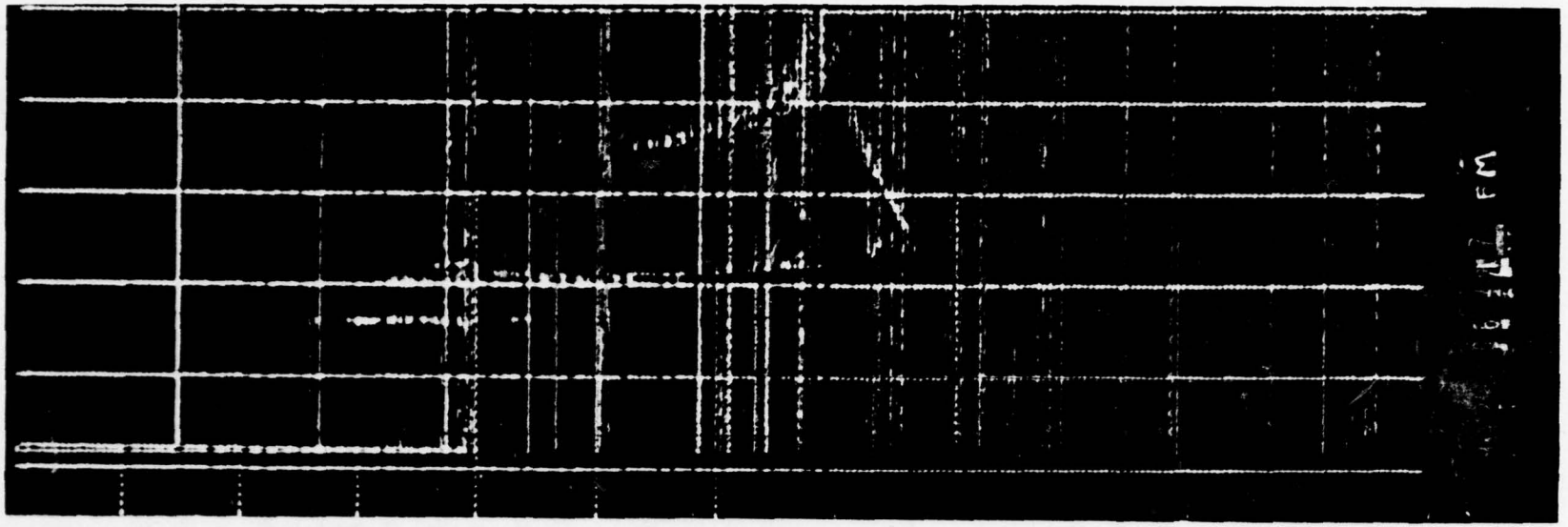

FIGURE 3.3 A TYPICAL 500 km OBLIQUE INCIDENCE IONOGRAM (FORT MONMOUTH TO CAMP DRUM)

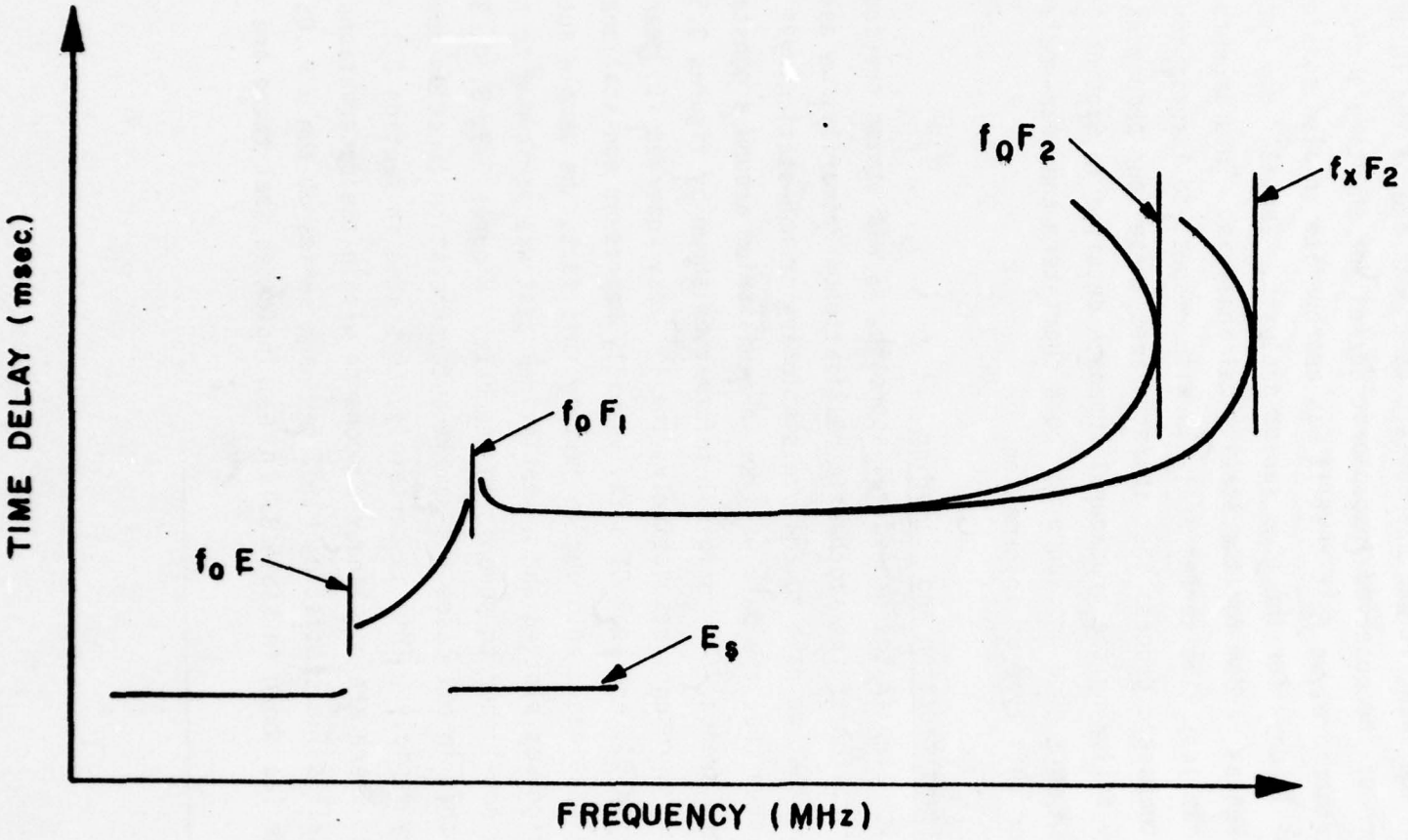

FIGURE 3.4 SCHEMATIC 500 km OBLIQUE INCIDENCE IONOGRAM

soundings. Thus, the observed data is a stochastic realization that consists of 144 data points with the corresponding time of day. In view of the diurnal differences in the data, it was appropriate to choose one of the 18 days at random for each of the observed ionospheric series for the time series analysis. Furthermore, we felt that it was appropriate to also consider the *average* of the 18 days for the time series analysis. The 13^{th} day (April 5, 1971) was chosen at random for the statistical analysis. This amounts to doing a very explicit time series analysis with respect to identifying the appropriate stochastic process that characterizes these four phenomena. We shall begin by following the procedural approach detailed in Section 2, which we believe is a very good procedure for both short-term and near-real-time forecasting for this type of information.

3.3.1 Model Identification and Filtering

The initial step in the procedural approach, as was stated previously, is the identification of the stochastic realization. Primarily, we ask, "is the information that we have to analyze stationary or non-stationary?" By stationary we mean that the data will be in equilibrium around a constant mean without any trends. The original information shown by figures 3.5, 3.6, 3.7, 3.8, which represent, respectively, the 13^{th} day observed VI, mean VI, 13^{th} day observed OI, and mean OI data, visually represent non-stationary stochastic realizations. In order to justify this fact, the sample autocorrelation function was plotted and a statistical test was performed to see if there were any non-linear components in the data. Figures 3.9, 3.10, 3.11, and 3.12 show that in all cases the sample autocorrelation function does not dampen out very rapidly. This is certainly, as stated in section 2.4, an indication that there are non-linear components within the observations. Secondly, Kendall's Tau statistic, [19]*, for each series at the $\alpha = .05$ level of significance (as shown in table 3.1, p. 63) indicates that there are non-linear trends.

* Chapter 5

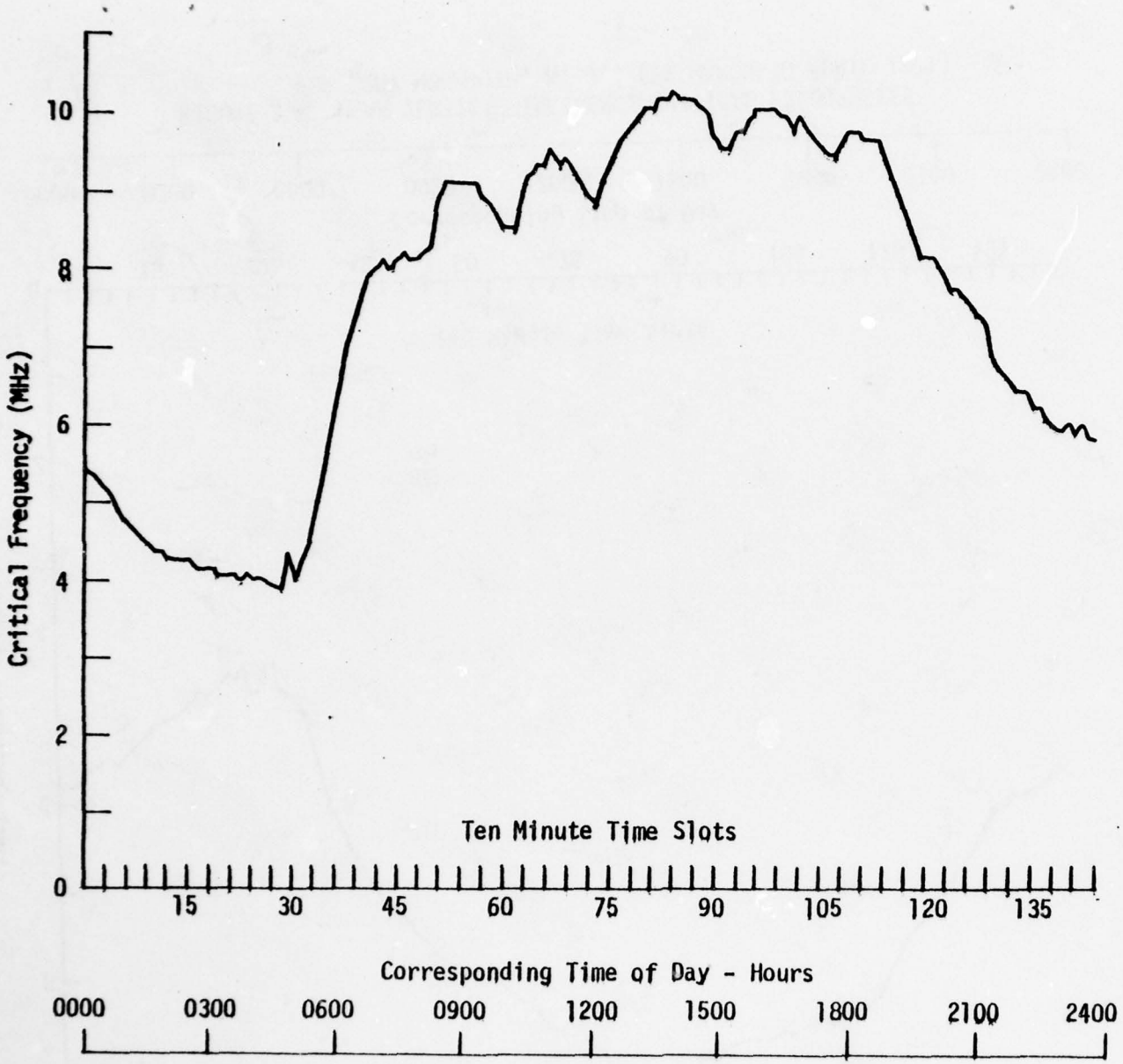

FIGURE 3.5 OBSERVED VERTICAL INCIDENCE CRITICAL FREQUENCIES FOR FORT MONMOUTH, N. J., 5 APRIL 1971

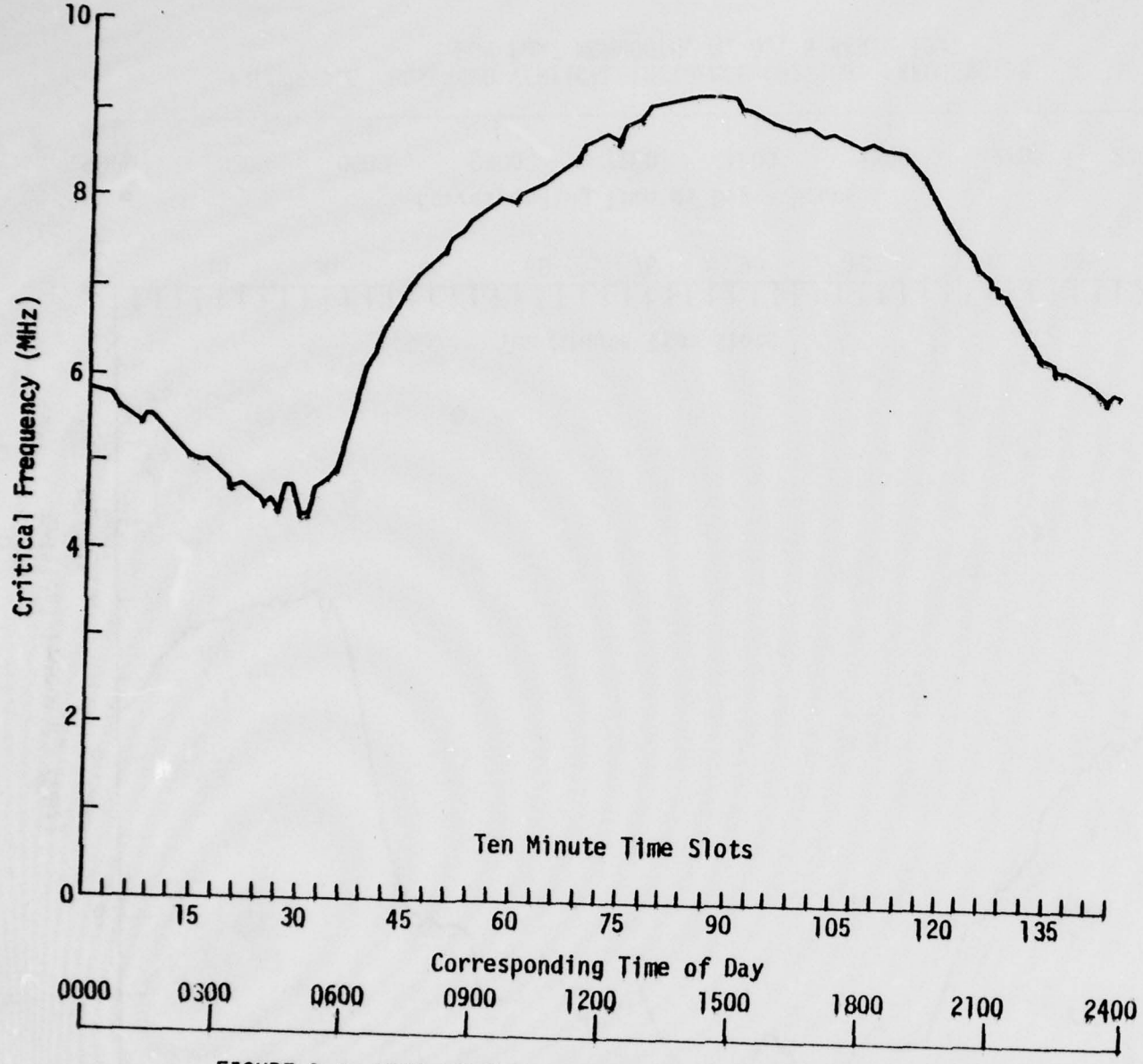

FIGURE 3.6 MEAN VERTICAL INCIDENCE CRITICAL FREQUENCIES FOR FORT MONMOUTH, N. J., (22 MARCH-10 APRIL 1971)

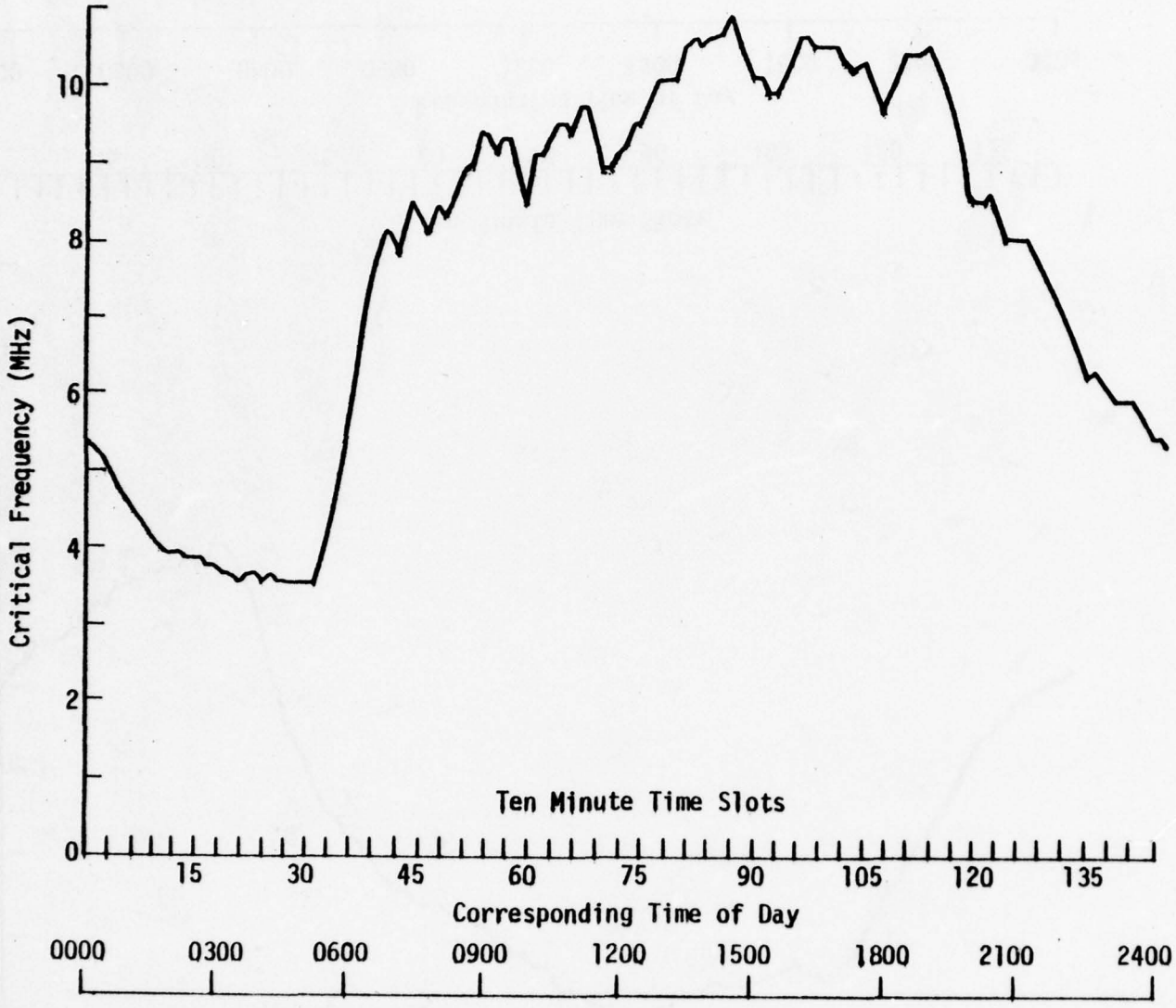

FIGURE 3.7 OBSERVED 500 Km OBLIQUE INCIDENCE CRITICAL FREQUENCIES BETWEEN FT. MONMOUTH, N. J., AND FT. DRUM, N. Y., 5 APRIL 1971

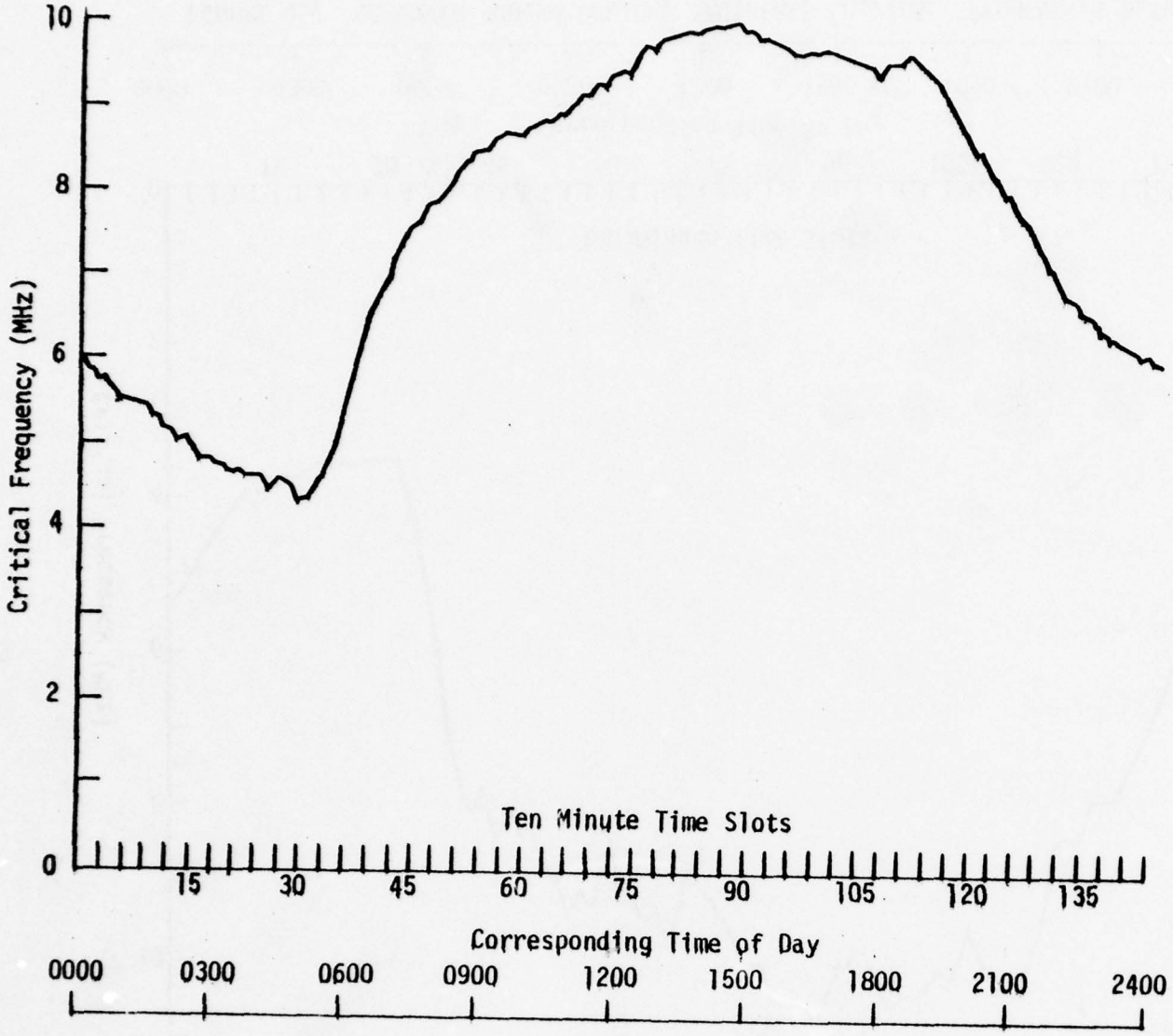

FIGURE 3.9 Mean 500 Km Oblique Incidence Critical Frequencies Between Ft. Monmouth, N. J., and Ft. Drum, N. Y., 22 March-10 April 1971

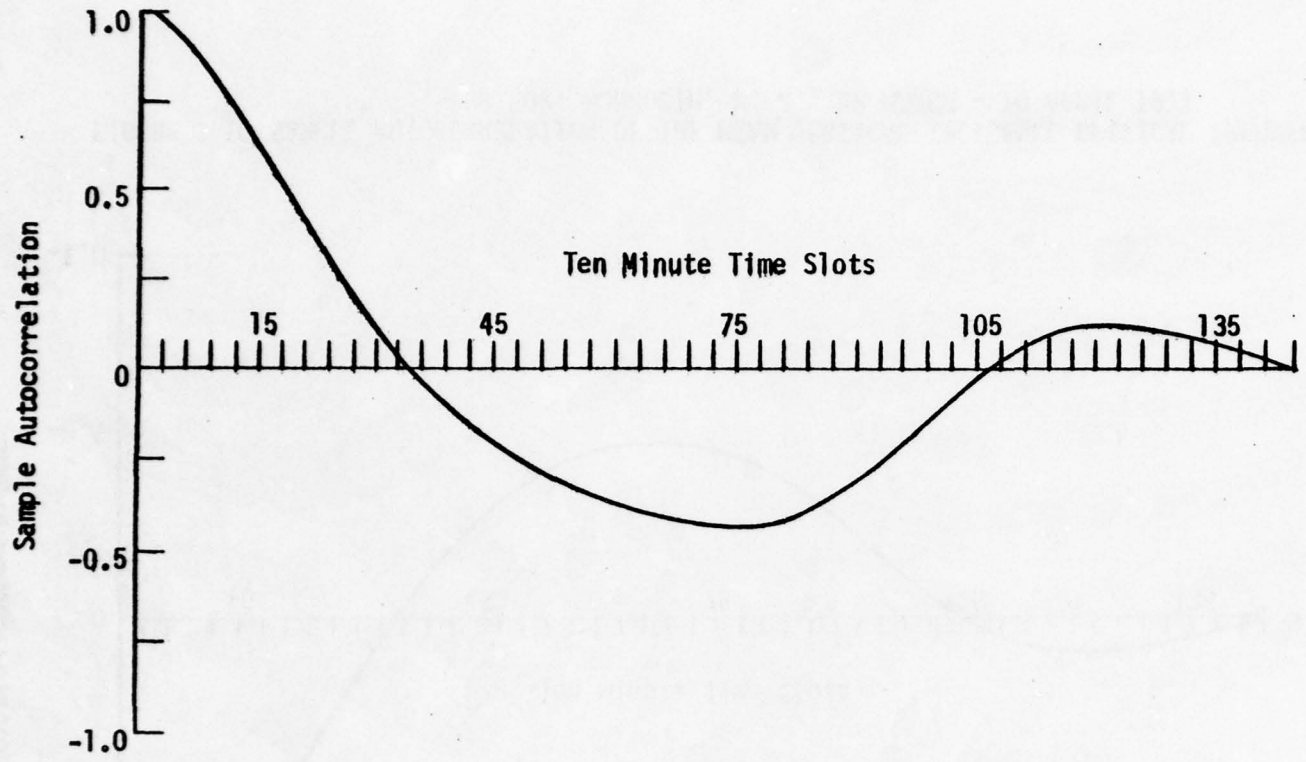

FIGURE 3.9 SAMPLE AUTOCORRELATION OF THE OBSERVED VERTICAL INCIDENCE CRITICAL FREQUENCIES AT FORT MONMOUTH, N. J., 5 APRIL 1971

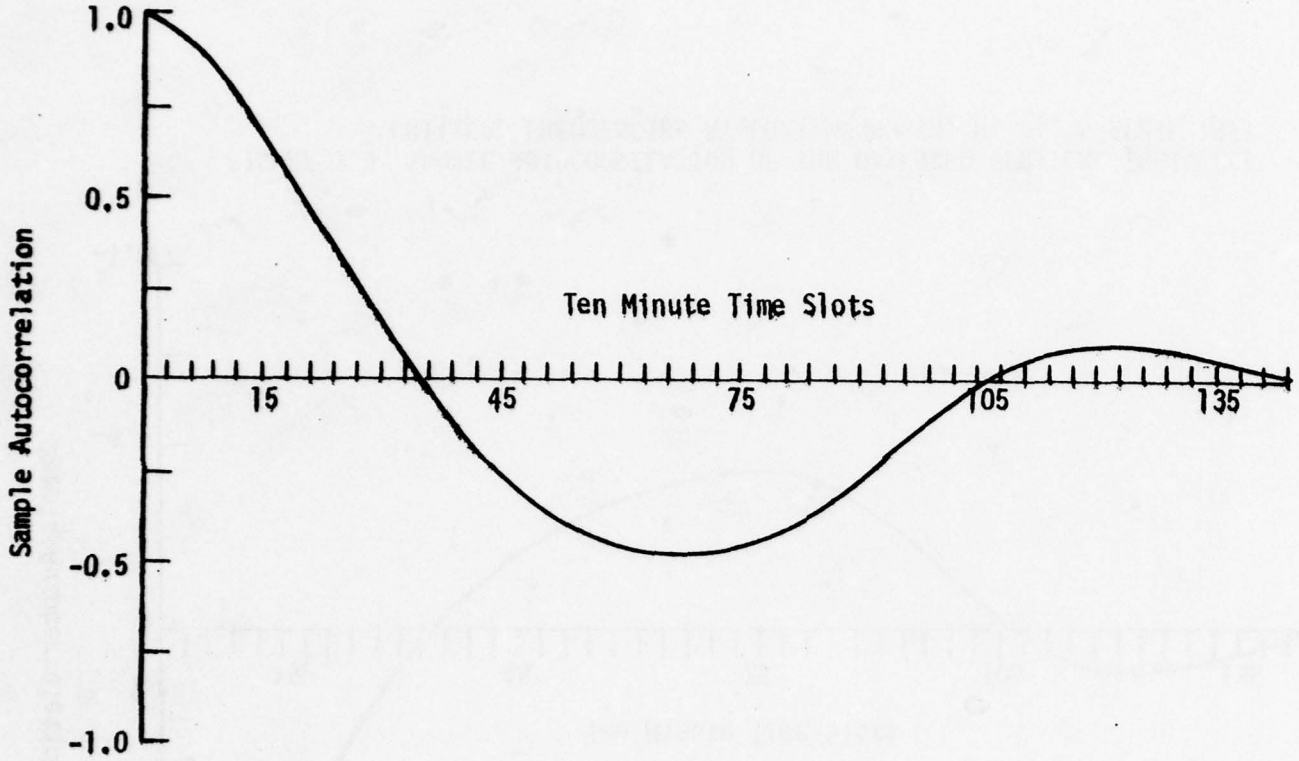

FIGURE 3.10 SAMPLE AUTOCORRELATION OF THE MEAN VERTICAL INCIDENCE CRITICAL FREQUENCIES FOR FORT MONMOUTH, N. J., 22 MARCH - 10 APRIL 1971

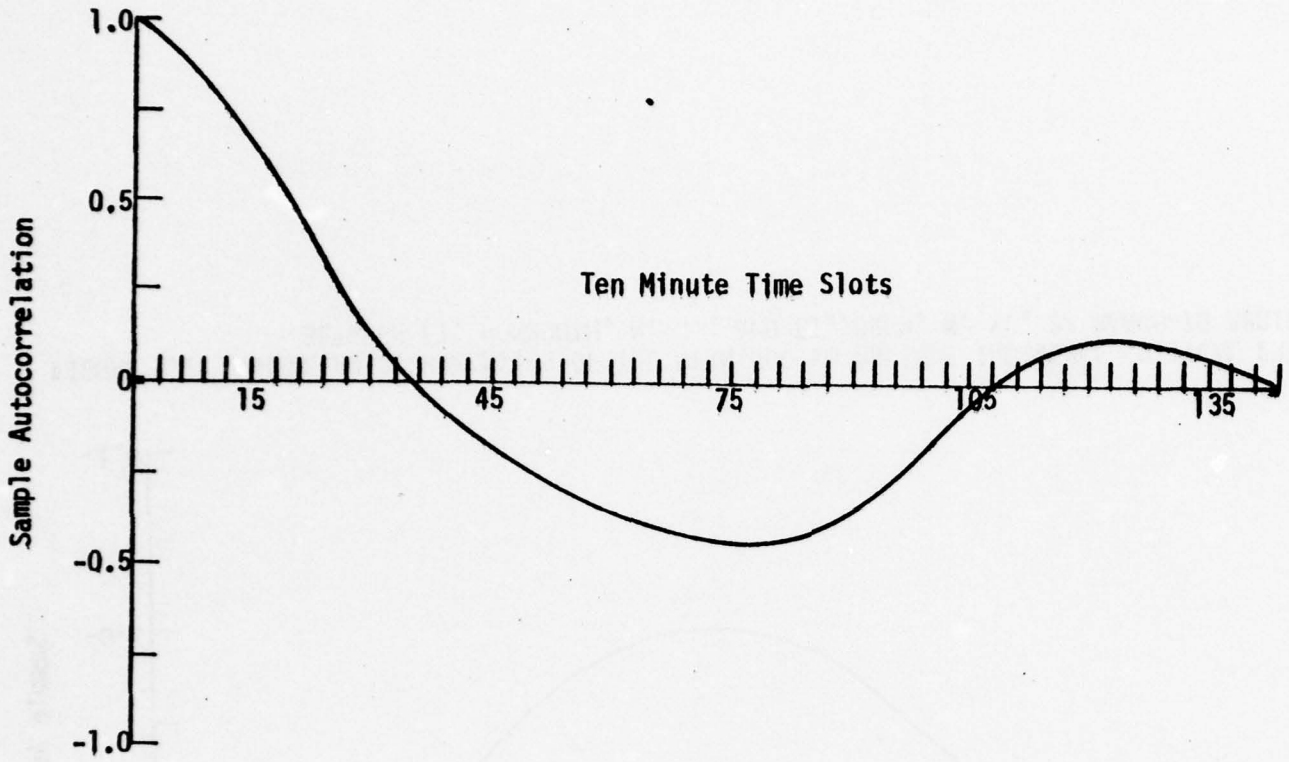

FIGURE 3.11 SAMPLE AUTOCORRELATION OF THE OBSERVED 500 Km OBLIQUE INCIDENCE CRITICAL FREQUENCIES BETWEEN FT. MONMOUTH, N. J. AND FT. DRUM, N. Y., 5 APRIL 1971

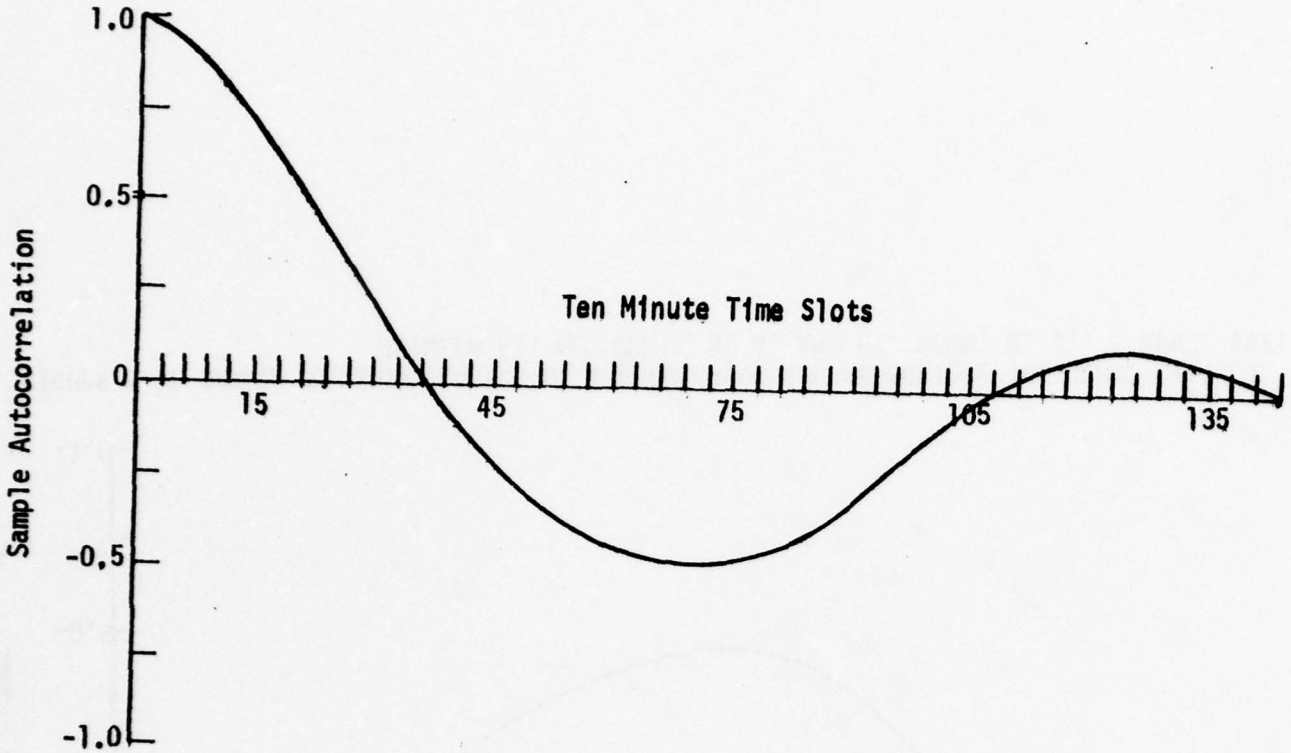

FIGURE 3.12 SAMPLE AUTOCORRELATION OF THE MEAN 500 Km OBLIQUE INCIDENCE CRITICAL FREQUENCIES BETWEEN FT. MONMOUTH, N. J., AND FT. DRUM, N. Y., 22 MARCH-10 APRIL 1971

Table 3.1 Kendall's Tau Statistics for Trend

Ionospheric Series	Calculated Statistic	$Z_{.05}$	Decision
13^{th} day VI observed	5.192	±1.645	reject H_o
18-day VI averaged	4.874	±1.645	reject H_o
13^{th} day OI observed	5.641	±1.645	reject H_o
18-day OI averaged	4.964	±1.645	reject H_o

Thus, we are certain that the ionospheric information is not in statistical equilibrium. The next step in the proposed procedure is to develop a filter that will eliminate the non-stationary components from the series. The initial step towards this end is to implement a first difference filter, namely:

$$y_t = x_t - x_{t-1}, \quad t = 1, \ldots, 144,$$

to each of the four realizations. Upon applying this filter, the sample autocorrelation functions were computed for the four cases and are shown in figures 3.13, 3.14, 3.15, and 3.16. It is evident by inspecting these autocorrelation functions that the 13^{th} day observed OI and VI information dampen out fairly rapidly about the zero axis except at the zero point. Kendall's Tau test was conducted on the filtered data. Results indicate that in both of these cases the non-stationary components had been removed as shown in table 3.2.

Table 3.2 Kendall's Tau Statistics for the First Difference Filtered Data

Ionospheric Series	Calculated Statistic	$Z_{.05}$	Decision
13^{th} day VI observed	-0.379	±1.645	accept H_o
18-day VI averaged	-4.577	±1.645	reject H_o
13^{th} day OI observed	-0.574	±1.645	accept H_o
18-day OI averaged	-4.616	±1.645	reject H_o

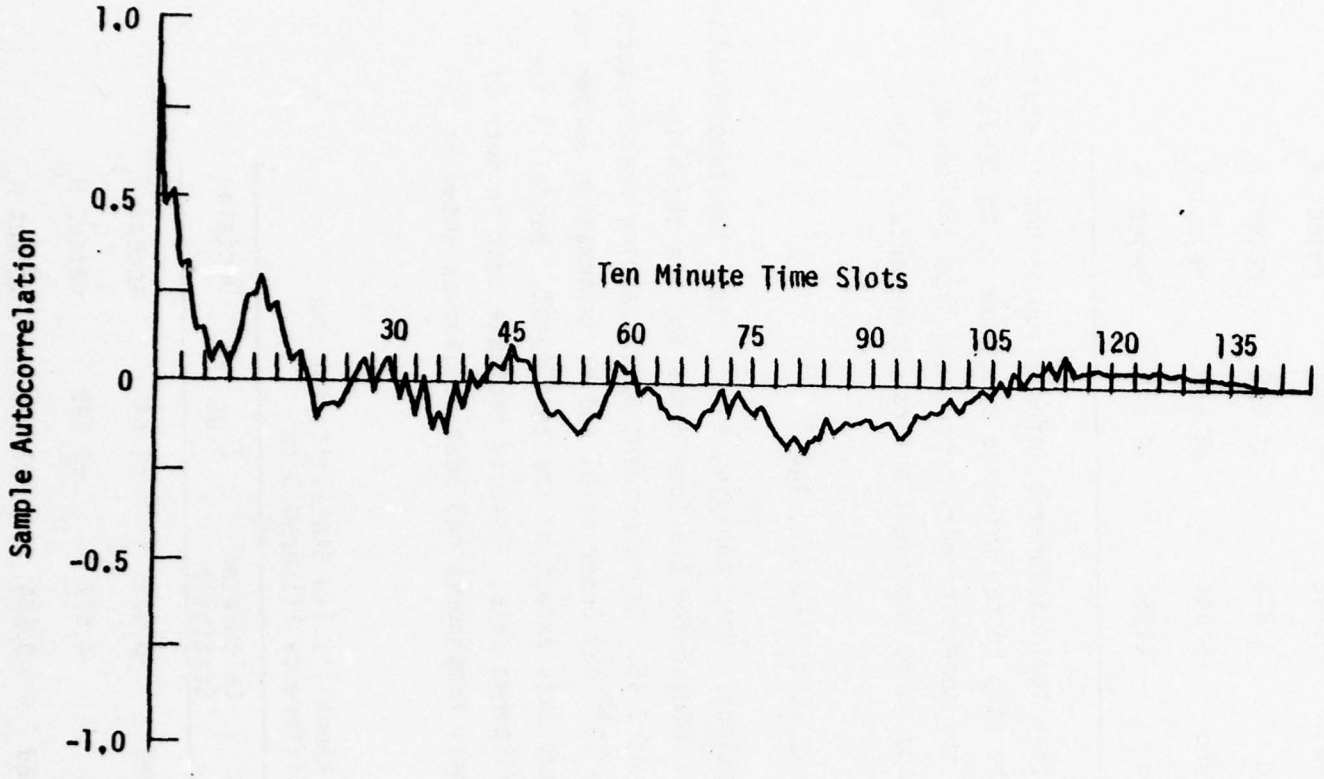

FIGURE 3.13 SAMPLE AUTOCORRELATION OF THE FIRST DIFFERENCE DATA FOR THE VERTICAL INCIDENCE CRITICAL FREQUENCIES AT FORT MONMOUTH, N. J., 5 APRIL 1971

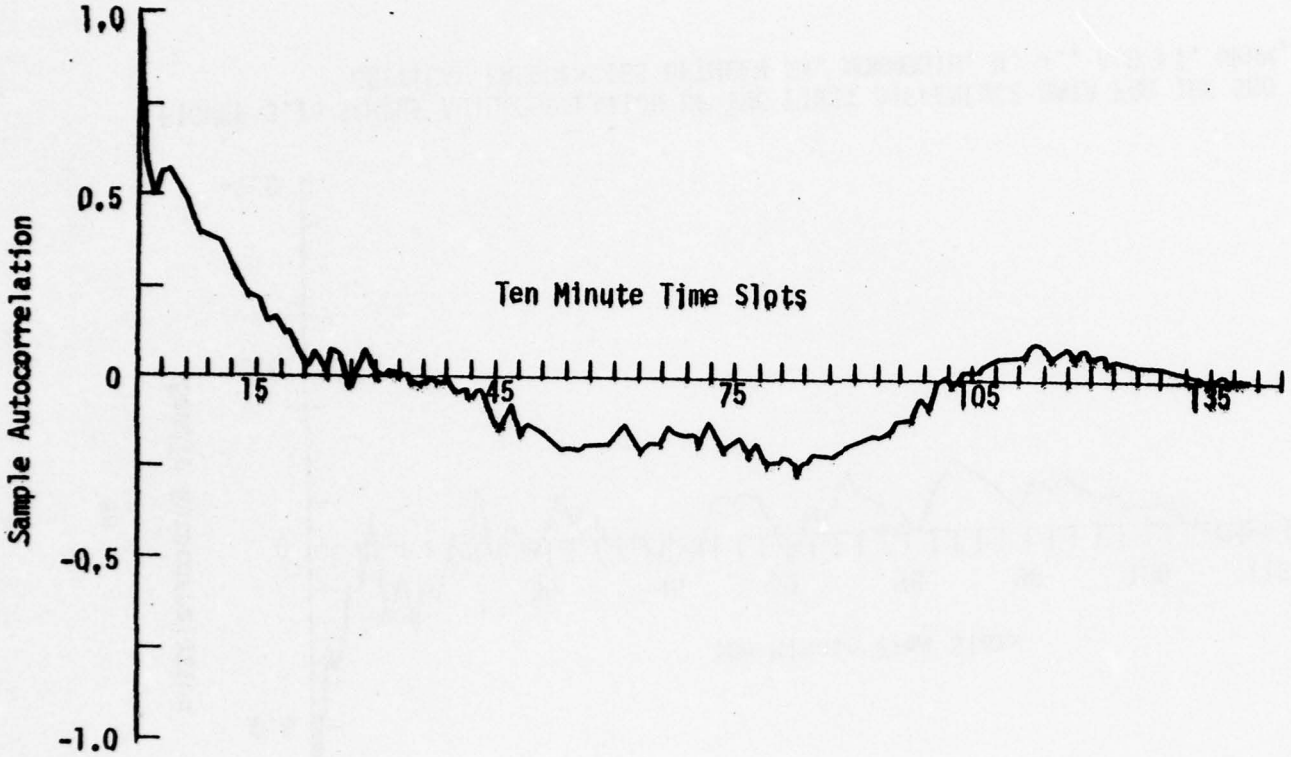

FIGURE 3.14 SAMPLE AUTOCORRELATION OF THE FIRST DIFFERENCE DATA OF THE MEAN VERTICAL INCIDENCE CRITICAL FREQUENCIES AT FORT MONMOUTH, N. J., 22 MARCH - 10 APRIL 1971

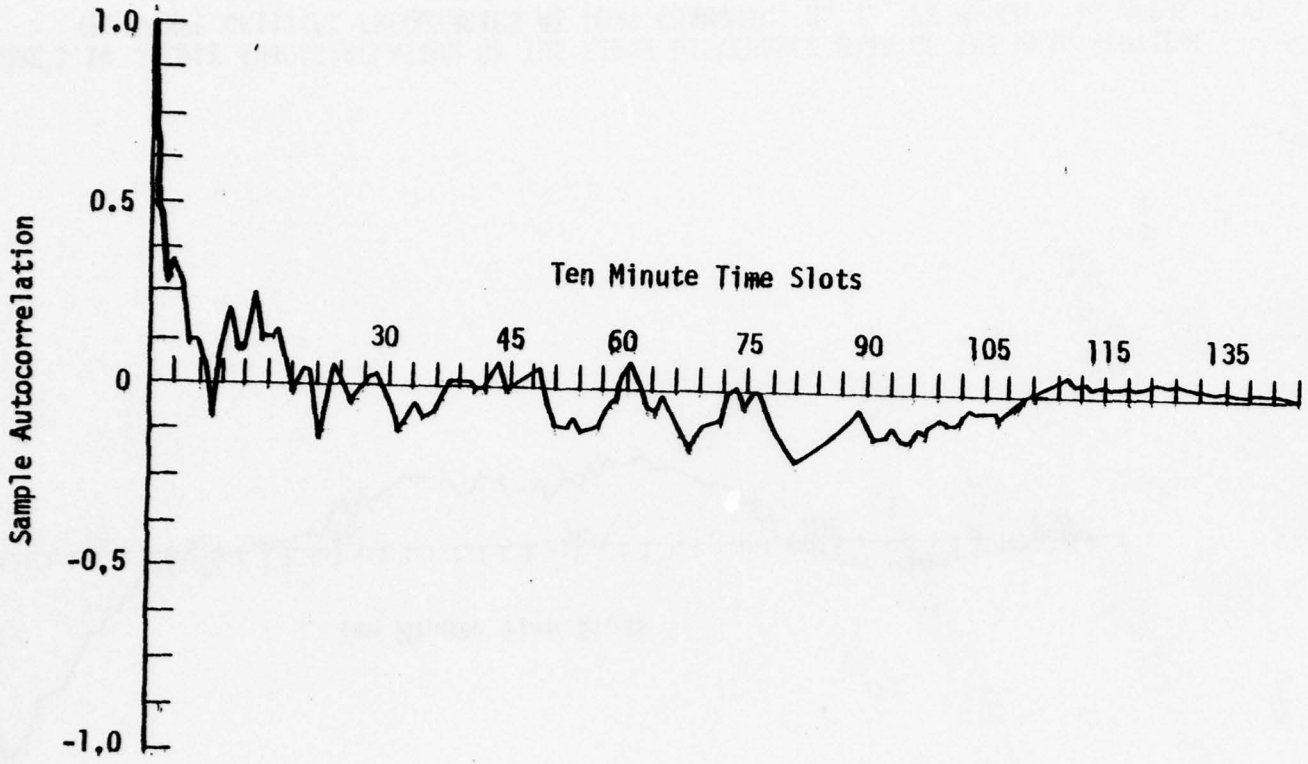

FIGURE 3.15 SAMPLE AUTOCORRELATION OF THE FIRST DIFFERENCE DATA FOR THE 500 Km OBLIQUE INCIDENCE CRITICAL FREQUENCIES BETWEEN FT. MONMOUTH, N. J., AND FT. DRUM, N. Y., 5 APRIL 1971

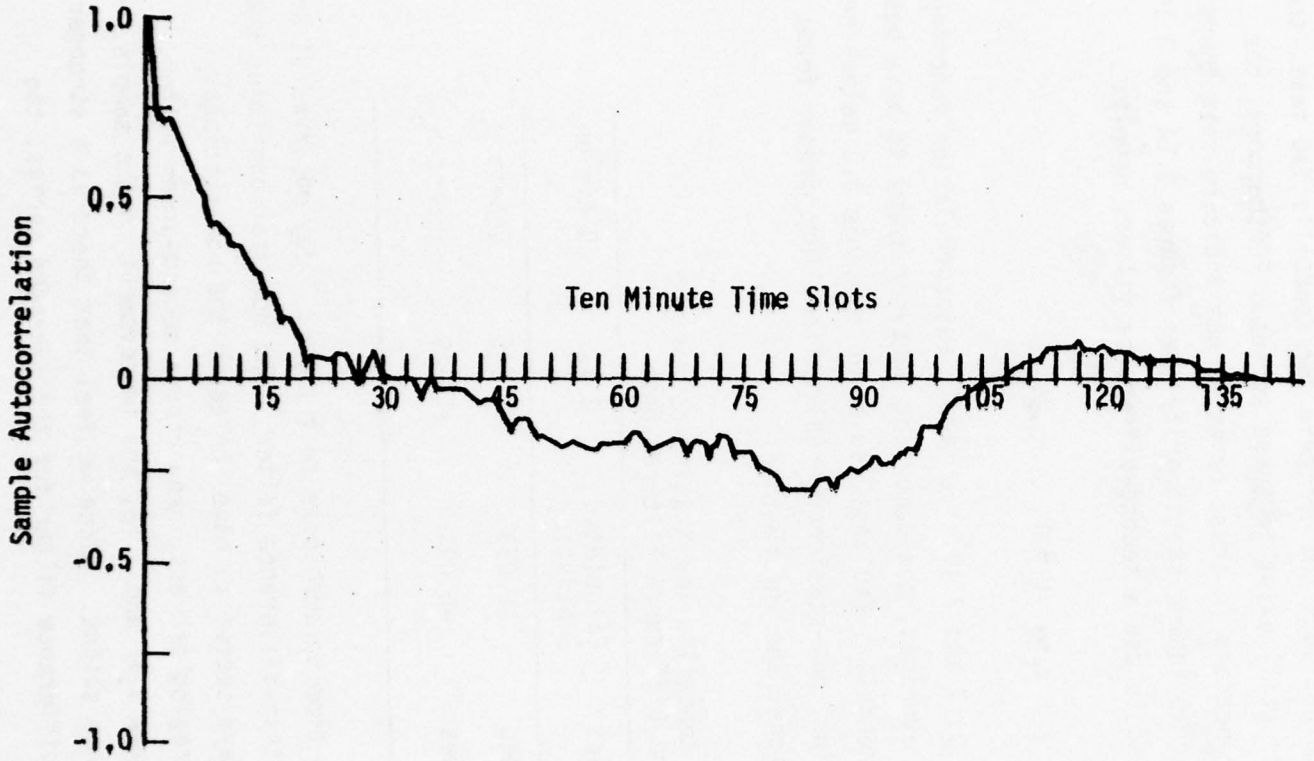

FIGURE 3.16: SAMPLE AUTOCORRELATION OF THE FIRST DIFFERENCE DATA OF THE MEAN 500 Km OBLIQUE INCIDENCE CRITICAL FREQUENCIES BETWEEN FT. MONMOUTH, N. J., AND FT, DRUM, N. Y., 22 MARCH - 10 APRIL 1971

Thus, Kendall's Tau test and the visual interpretation of the sample autocorrelation function indicate that we have reduced the two 13^{th} day observed stochastic realizations (OI and VI) into stationary series. Thus, they are in the proper form to proceed in identifying the appropriate model that characterizes their behavior. However, since the average of the 18 days of OI and VI soundings do not pass the criteria for Kendall's Tau test, then one concludes that trends still exist in these series. Furthermore, the sample autocorrelation functions in these cases do not indicate that there is rapid enough dampening to insure stationarity (see figures 3.14 and 3.16). Therefore, we must proceed to use a second-difference filter, namely:

$$w_t = x_t - 2x_{t-1} + x_{t-2}, \; t = 1, \ldots, 144 \; .$$

As shown in figures 3.17 and 3.18, the sample autocorrelation functions of the second-difference averages, the dampening behavior seems to have been improved. Furthermore, Kendall's Tau test (as shown in table 3.3 below) seems to have reduced the original non-stationary realizations into proper form; thus, we can proceed to model the information.

Table 3.3 Kendall's Tau Statistics for the Second Difference Filtered Data

Ionospheric Series	Calculated Statistic	$Z_{.05}$	Decision
18-day VI averaged	0.053	±1.645	accept H_o
18-day OI averaged	-0.093	±1.645	accept H_o

It is appropriate at this time to emphasize that the 13^{th} day observed OI and VI data needed only the first-difference filter. The non-stationarities that occur in each of the 18 days seemed to have increased the non-stationary components during the averaging process, requiring a second-order filter. However, as shown in figures 3.17 and 3.18, the improvement in the sample autocorrelation function was slight. Since we feel that there is a stronger decision with the second-difference filter for the averaged series, the

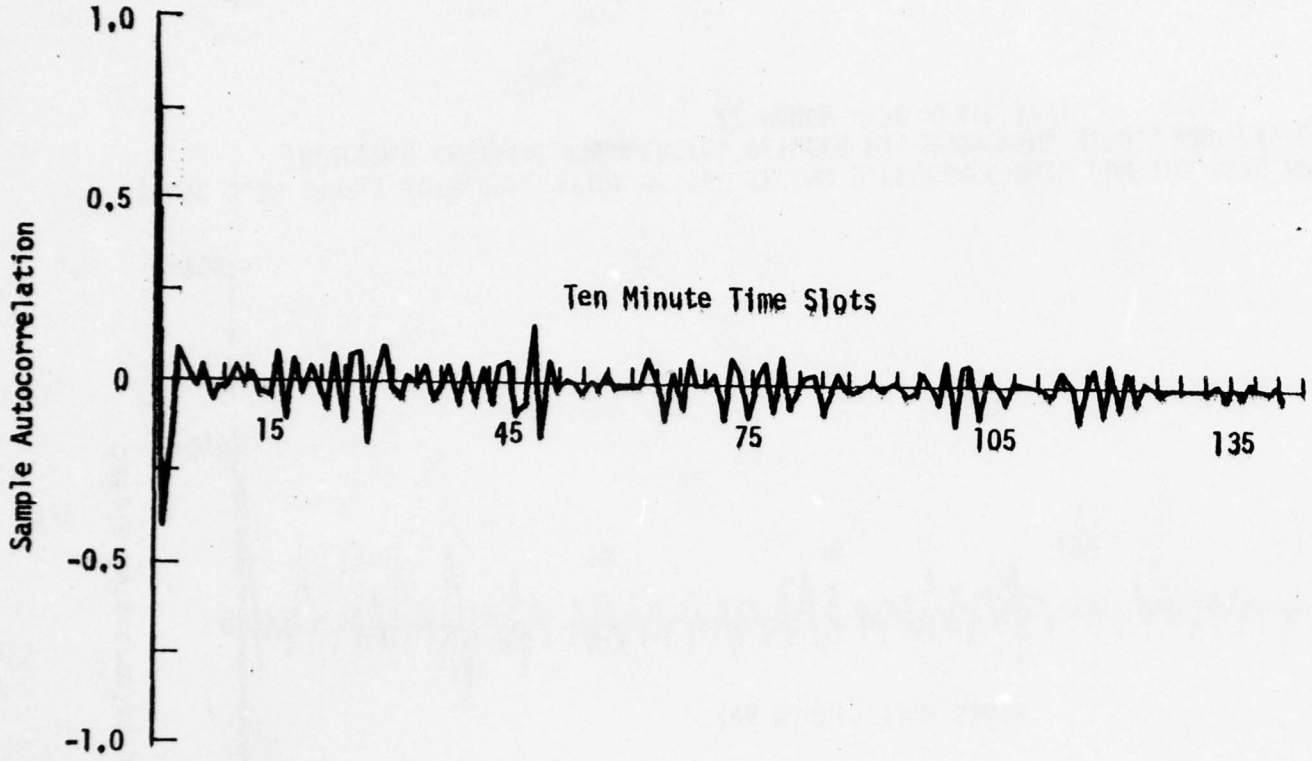

FIGURE 3.17 SAMPLE AUTOCORRELATION OF THE SECOND DIFFERENCE DATA FOR THE MEAN VERTICAL INCIDENCE CRITICAL FREQUENCIES AT FORT MONMOUTH, N. J., 22 MARCH - 10 APRIL 1971

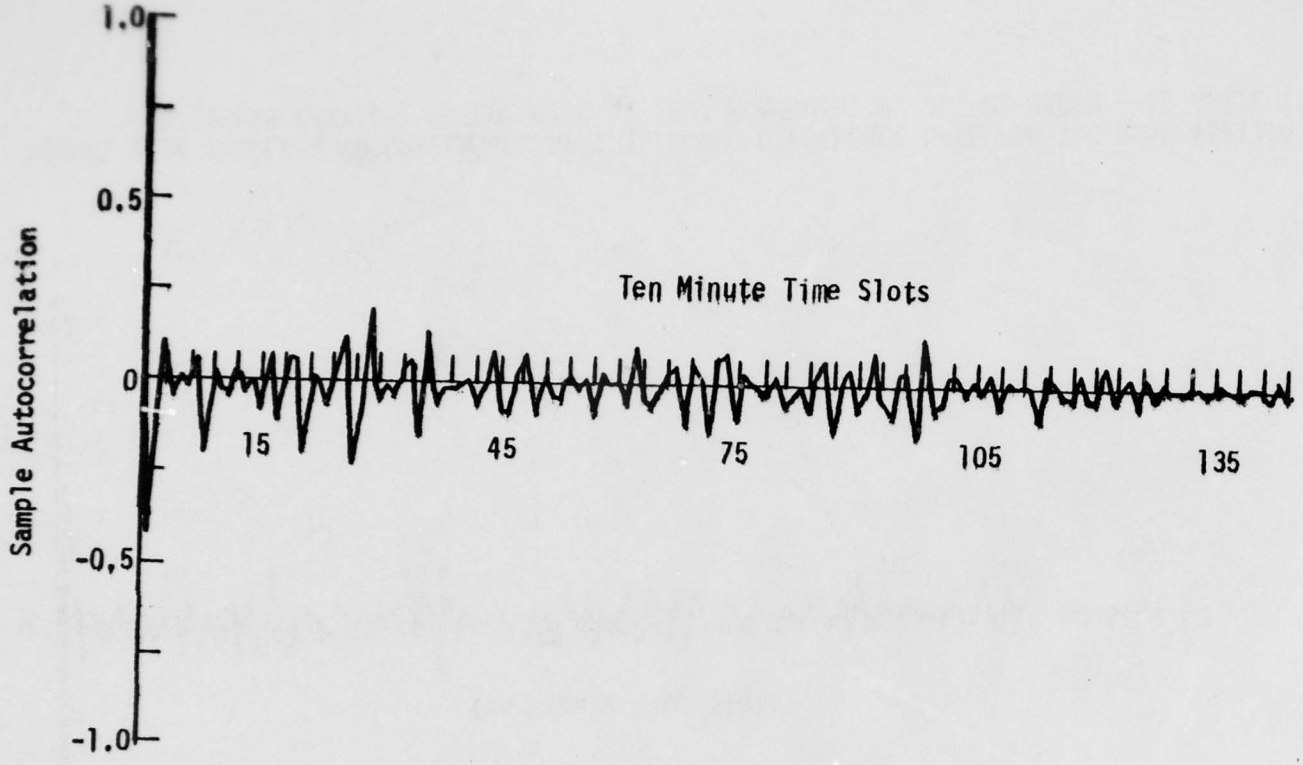

FIGURE 3.18 SAMPLE AUTOCORRELATION OF THE SECOND DIFFERENCE DATA FOR THE MEAN 500 Km OBLIQUE INCIDENCE CRITICAL FREQUENCIES BETWEEN FT. MONMOUTH, N. J., AND FT. DRUM, N. Y., 22 MARCH - 10 APRIL 1971

procedural approach will be continued with the first-order filter in analyzing the 13th day observed data, and with the second-order filter in analyzing the averaged information.

3.3.2 Fitting The Model

Now, having reduced the stochastic realizations into stationary form, the next step in the procedural approach is the fitting process. Specifically, we are interested in identifying the appropriate model, and secondly, having identified the model as either autoregressive (AR), moving-averages (MA), or a mixture of the two (ARMA), the order of the particular process must be determined. In deciding on the order of a particular process, one has to be concerned with estimating the parameters that are associated with the specific model. Specifically, with regard to the four ionospheric series, we have a *simultaneous* investigation of both the *model* that fits that data and the estimation of the *parameters* associated with the model. As indicated in the recommended procedure for identifying the model, graphic displays have been structured as shown by figures 3.19, 3.20, 3.21, and 3.22, for each of the four realizations that give the residual variance of *each* of the realizations as a function of the order of the three models involved. The decision as to which model best characterizes these series resulted from the criterion of minimum residual variance as stated in section 2.4.2.

As shown in the four graphs, the order (m,q) refers to the order m of the autoregressive process and the order q of the moving averages process. Thus, for example, (3,0) is a purely AR process of order 3; (0,2) is a purely MA process of order 2; and (3,2) is a mixture of a third order AR and a second order MA process. As depicted in the figures, with respect to the residual variance, it is clear that the "best" models that should be selected are:

i) (2,0) process for the 13th day observed VI soundings,
ii) (3,0) process for the 18-day mean VI soundings,
iii) (3,0) process for the 13th day observed OI soundings,
iv) (3,0) process for the 18-day mean OI soundings.

It will be shown later, that the difference equations that have been identified above are the most appropriate ones to characterize our data. Of course, in reaching the decisions with respect to the selection of these models, the principle of "parsimony" was also taken into consideration. Specifically, this means that if there was a lower order model (refer to

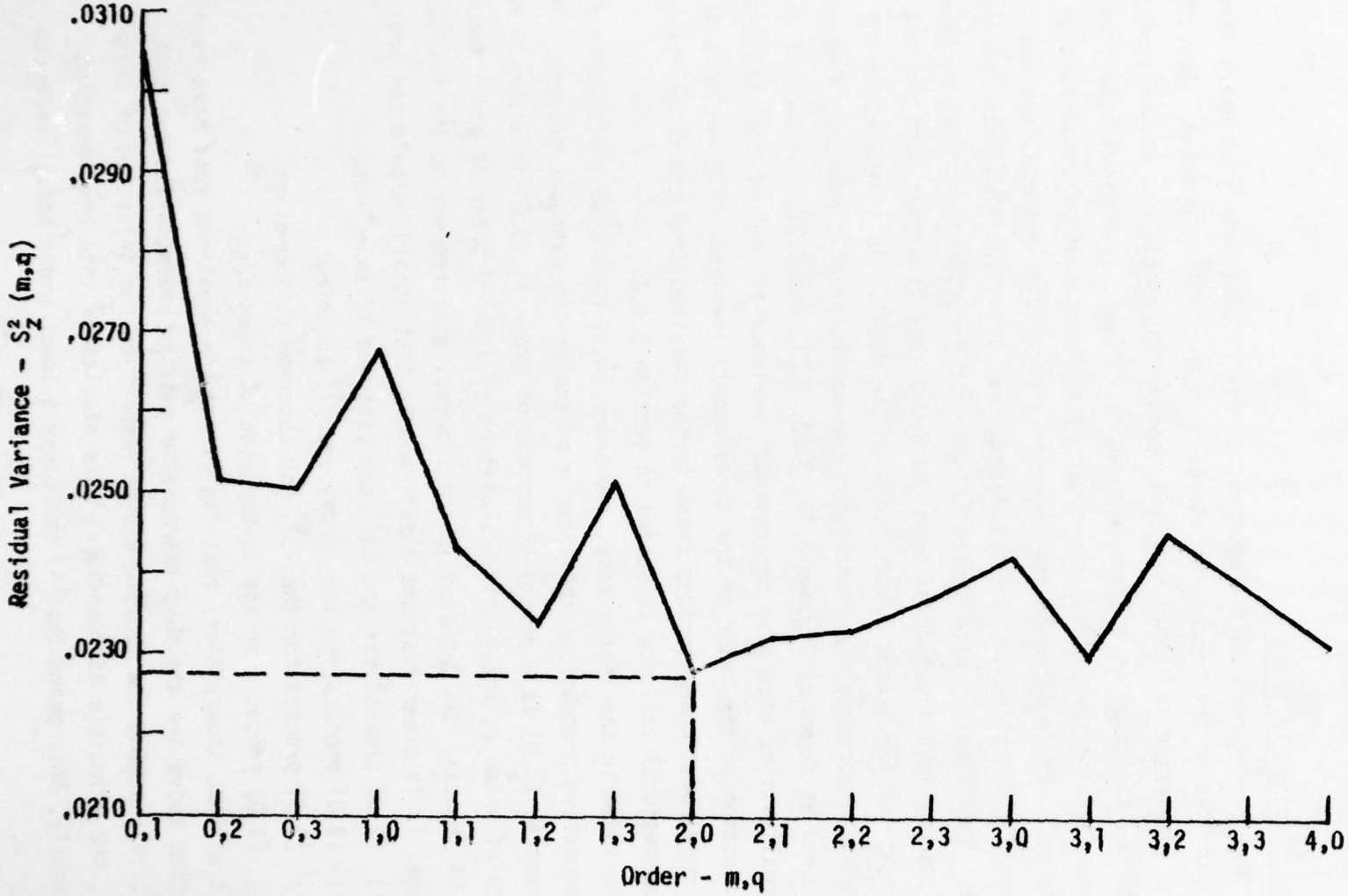

FIGURE 3.19 MODEL ORDER vs. RESIDUAL VARIANCE FOR THE VERTICAL INCIDENCE IONOSPHERIC DATA, FT. MONMOUTH, N. J., FOR 5 APRIL 1971

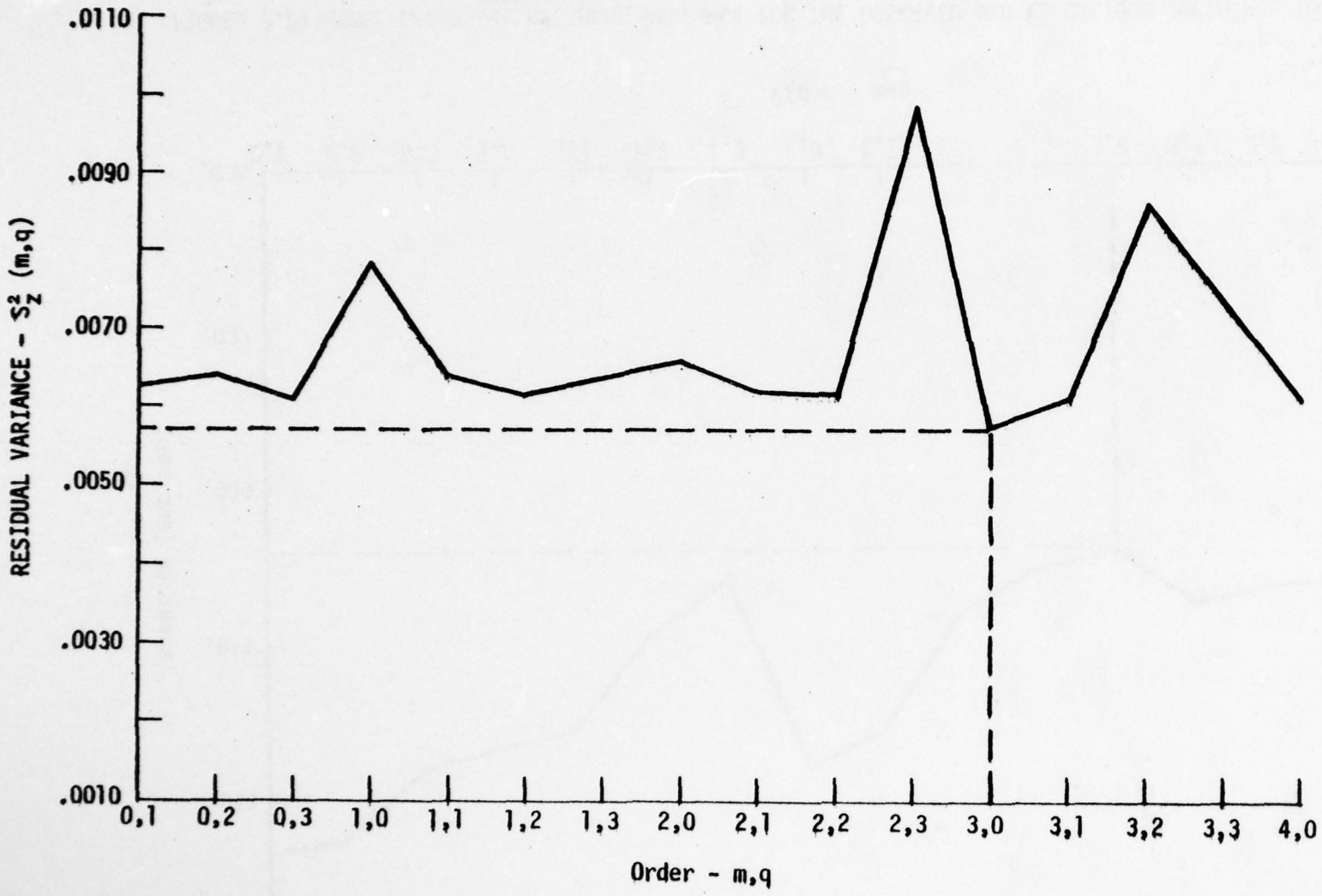

FIGURE 3.20 MODEL ORDER vs. RESIDUAL VARIANCE FOR THE VERTICAL INCIDENCE IONOSPHERIC DATA, FT. MONMOUTH, N. J. - MEAN FOR 22 MARCH-10 APRIL 1971

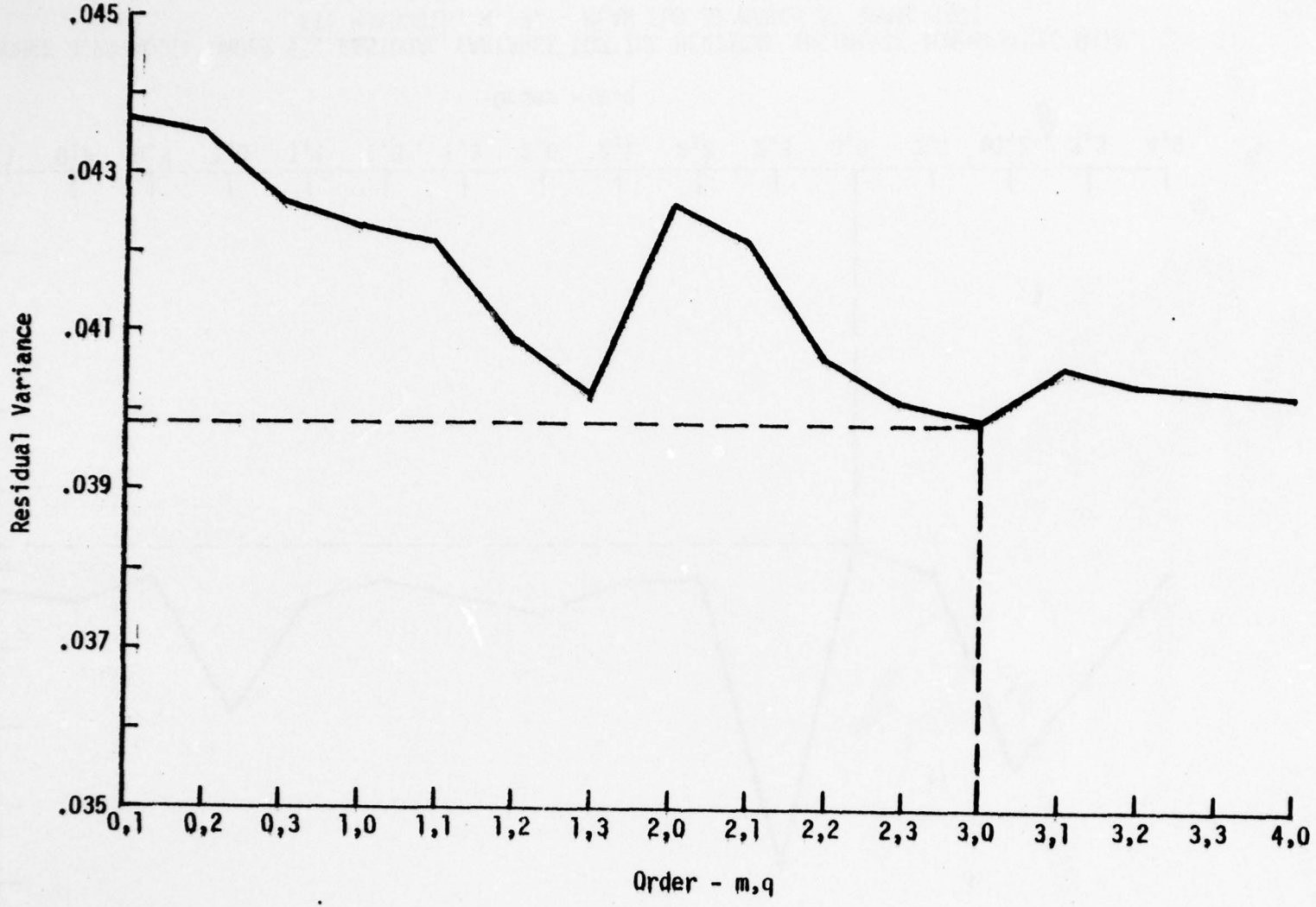

FIGURE 3.21 MODEL ORDER vs. RESIDUAL VARIANCE FOR THE OBSERVED 500 Km OBLIQUE INCIDENCE IONOSPHERIC DATA BETWEEN FT. MONMOUTH, N. J., AND FT. DRUM, N. Y., FOR 5 APRIL 1971

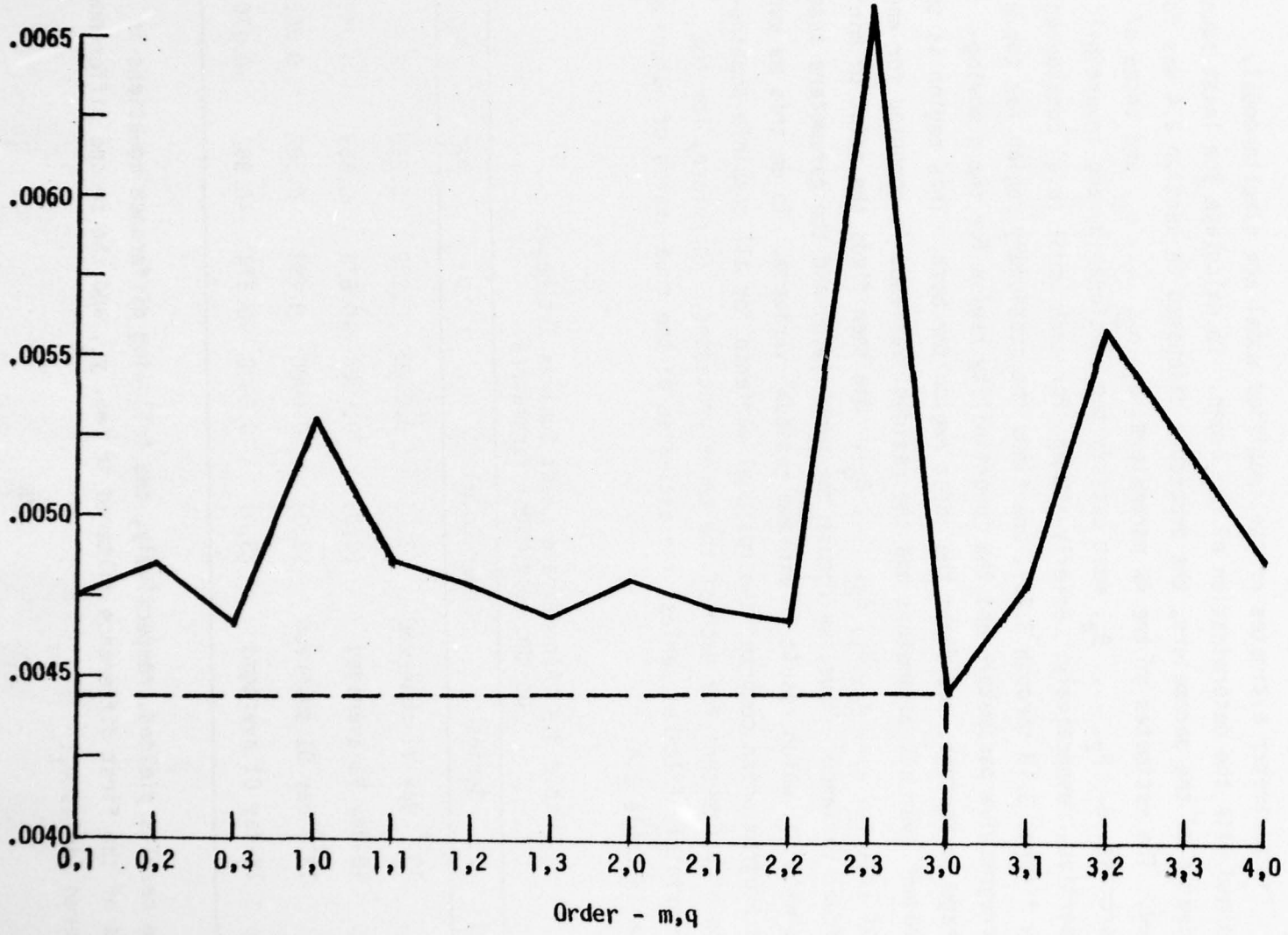

FIGURE 3.22 MODEL ORDER vs. RESIDUAL VARIANCE FOR THE 500 Km OBLIQUE INCIDENCE IONOSPHERIC DATA BETWEEN FT. MONMOUTH, N. J., AND FT. DRUM, N. Y., - MEAN FOR 22 MARCH-10 APRIL 1971

figures 3.19 through 3.22) that had an equal or slightly higher residual variance than a higher order model, the lowest order model would be selected because the number of parameters and convenience that such a model offers computationally is desirable, and will usually have little effect on the near-real-time forecasts of the data.

The parameter estimates of the specified model are simultaneously obtained with the determination of the order. To calculate the least squares estimates of the parameters, the procedure discussed in section 2.4 was followed. The estimates of the AR parameters, $\alpha_1, \alpha_2, \ldots, \alpha_m$, and those of the MA process, $\beta_1, \beta_2, \ldots, \beta_q$, must satisfy the stationarity and invertibility properties, respectively. Briefly stated, for each model (m,q) considered (see figures 3.19 through 3.22), one finds the stationary region for the m autoregressive parameters and the invertibility region for the q moving-average parameters, and forms the joint region for both. This region is then "gridded" over all parameters and the residual variance is computed for each point $(\alpha_1, \alpha_2, \ldots, \alpha_m, \beta_1, \beta_2, \ldots, \beta_q)$. One then finds the point of minimum residual variance. Thus, we choose the model (m,q) and the parameters associated with it, which result in minimum residual variance. To do this we used a grid program which computed the residual variance for all possible combinations of parameters for each of the three processes. Therefore, for the appropriately filtered series, the estimates of the true states of nature are shown in table 3.4.

Table 3.4 Approximate Least Squares Estimates of the Best Model Parameters

Model	Series	Order (m,q)	$\hat{\mu}$	$\hat{\alpha}_1$	$\hat{\alpha}_2$	$\hat{\alpha}_3$
i.	13^{th} day VI observed	(2,0)	0.0020	0.289	0.395	---
ii.	18-day VI averaged	(3,0)	0.0004	-0.676	-0.559	-0.258
iii.	13^{th} day OI observed	(3,0)	0.0000	0.484	-0.102	0.266
iv.	18-day OI averaged	(3,0)	0.0008	-0.574	-0.352	-0.070

These results yielded, respectively, the following difference equations in terms of the first difference filtered series, y_t, and the second difference filtered series w_t:

i. $(y_t - .002) = .289\ (y_{t-1} - .002) + .395\ (y_{t-2} - .002) + Z_t$ (3.3.1)

ii. $(w_t - .0004) = -.676\ (w_{t-1} - .0004) - .559\ (w_{t-2} - .0004) - .258\ (w_{t-3} - .0004) + Z_t$ (3.3.2)

iii. $(y_t - 0.000) = .484\ (y_{t-1} - 0.000) - .102\ (y_{t-2} - 0.0000) + .266\ (y_{t-3} - 0.000) + Z_t$ (3.3.3)

iv. $(w_t - .0008) = -.574\ (w_{t-1} - .0008) - .352\ (w_{t-2} - .0008) - .070\ (w_{t-3} - .0008) + Z_t$ (3.3.4)

3.3.3 Inserting the Backwards Filter and Diagnostic Check of the Models

The next step in the procedural approach to forecasting is the implementation of the backwards filter and diagnostic check of the models. Having selected the appropriate stationary stochastic model and its order, a diagnostic check must be performed to determine the adequacy of the models. As indicated in Section 2, if the original information was filtered to put it into the proper form to perform time-series analysis, we must, at this point incorporate *back* into the model the non-stationarities that the filter has eliminated. That is, we must introduce the concept of the *backward filter* into our model. This backward filtering concept is very important because it puts back into the model some of the basic characteristics that the initial data contained so that the final interpretation of the observed realizations would be more meaningful. Thus, we insert the appropriate filter, either:

$$y_t = x_t - x_{t-1},$$

or

$$w_t = x_t - 2x_{t-1} + x_{t-2}$$

into equations (3.3.1), (3.3.2), (3.3.3), and (3.3.4).

Given below are the forecasting models, having been modified to include the filtering concept. That is,

i. $\hat{x}_t = 1.289x_{t-1} + 0.106x_{t-2} - 0.395x_{t-3} + 0.007 + Z_t$ (3.3.5)

ii. $\hat{x}_t = 1.324x_{t-1} - 0.207x_{t-2} + 0.184x_{t-3} - 0.043x_{t-4} - 0.258x_{t-5} + .001 + Z_t$ (3.3.6)

iii. $\hat{x}_t = 1.484x_{t-1} - 0.586x_{t-2} + 0.368x_{t-3} - 0.266x_{t-4} + Z_t$ (3.3.7)

iv. $\hat{x}_t = 1.426x_{t-1} + 0.204x_{t-2} - 0.060x_{t-3} - 0.212x_{t-4} - 0.070x_{t-5} + .0016 + Z_t$ (3.3.8)

Having formulated the above difference equations for the stochastic realizations, the next step is to investigate the goodness-of-fit of the structured models. This is done as outlined in section 2.4 by calculating the residuals incurred, that is, by subtracting the modeled series from the observed series. In other words, if x_t is the observed series and $\hat{x}_t$ is the modeled series, then their difference r_t, is the residual (equation 2.4.16); that is: $r_t = x_t - \hat{x}_t$. The residuals should behave as a purely random process, with a zero mean and a variance in the order of 1/n. As a first step in simulating the x_t, the unknown value of Z_t is set to its unconditional expectation of zero in equations (3.3.5) through (3.3.8), and it is assumed that the values of x_{t-1}, x_{t-2}, x_{t-3}, ..., x_{t-m}, are known. As shown by figures 3.23*, 3.24, 3.25, and 3.26, we have an excellent fit of the estimated models with respect to the observed series. One, of course, can perform a statistical test to justify the fit. That is, the resulting residuals should behave approximately like a purely random process; in other words, they should be normally distributed with a mean of zero and a variance of 1/n. Clearly, for this sample size, the variance becomes very small. Thus, the standard deviation of the sample autocorrelation is $1/\sqrt{n} = 1/\sqrt{144} = .0833$. The 95% confidence intervals of the sample autocorrelation $r_{zz}(k)$ are ± 1.96 (.0833) $= \pm 0.163$. At the 5% level of significance, one could expect (.05)144 or 8 out of the sample autocorrelations to lie outside the confidence interval. Only two autocorrelations for the 13th day observed VI and OI, and two autocorrelations for the 18-day averaged information lie outside of the confidence interval (see tables 3.5, 3.6, 3.7 and 3.8). Hence, one

*Note: In the simulation graphs, the lines connecting the points are aids to see the relationship of the points.

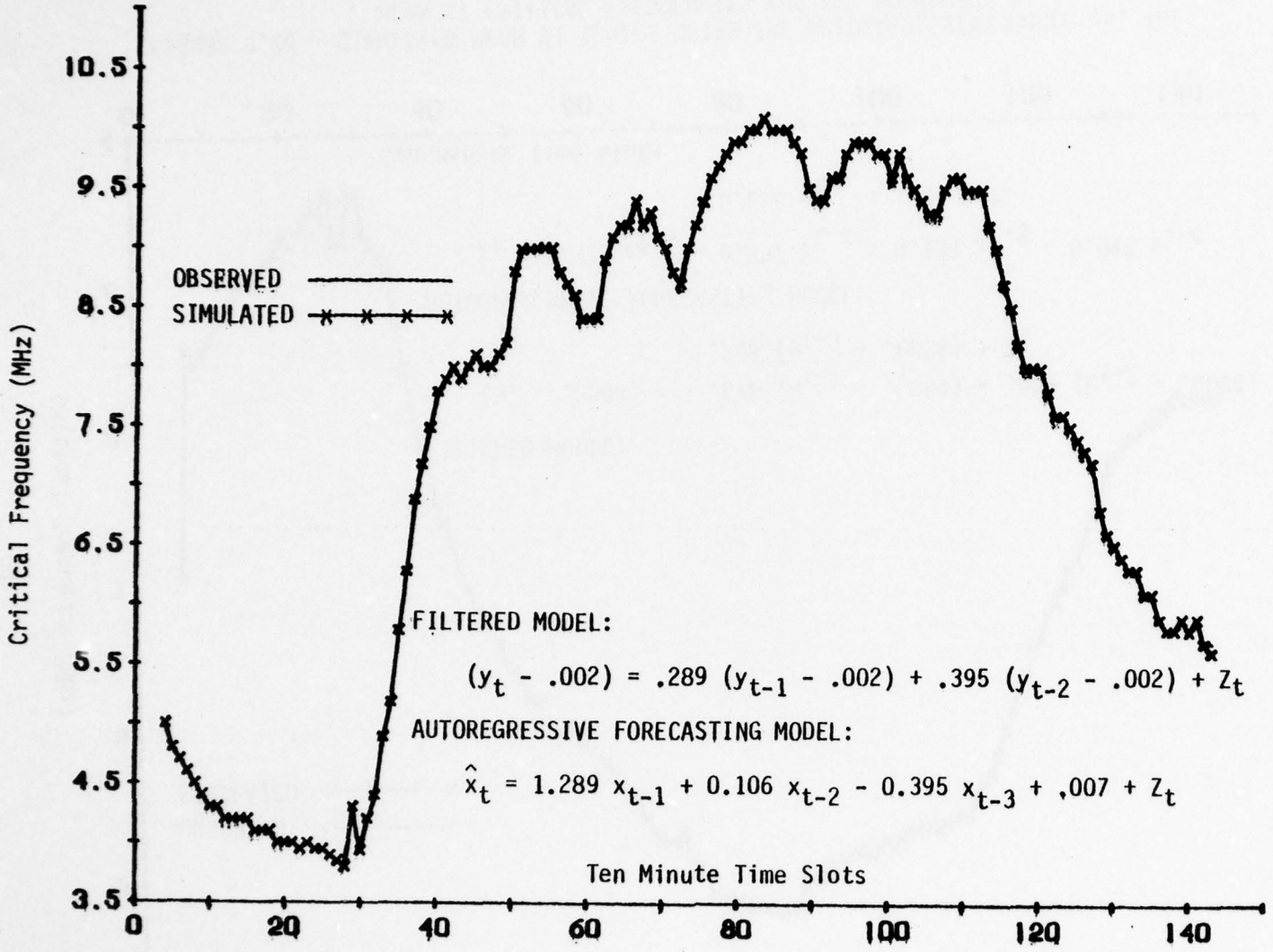

FIGURE 3.23 SIMULATED VI SERIES USING THE AUTOREGRESSIVE MODEL vs. THE OBSERVED VI CRITICAL FREQUENCIES FOR FT. MONMOUTH, N.J., 5 APRIL 1971

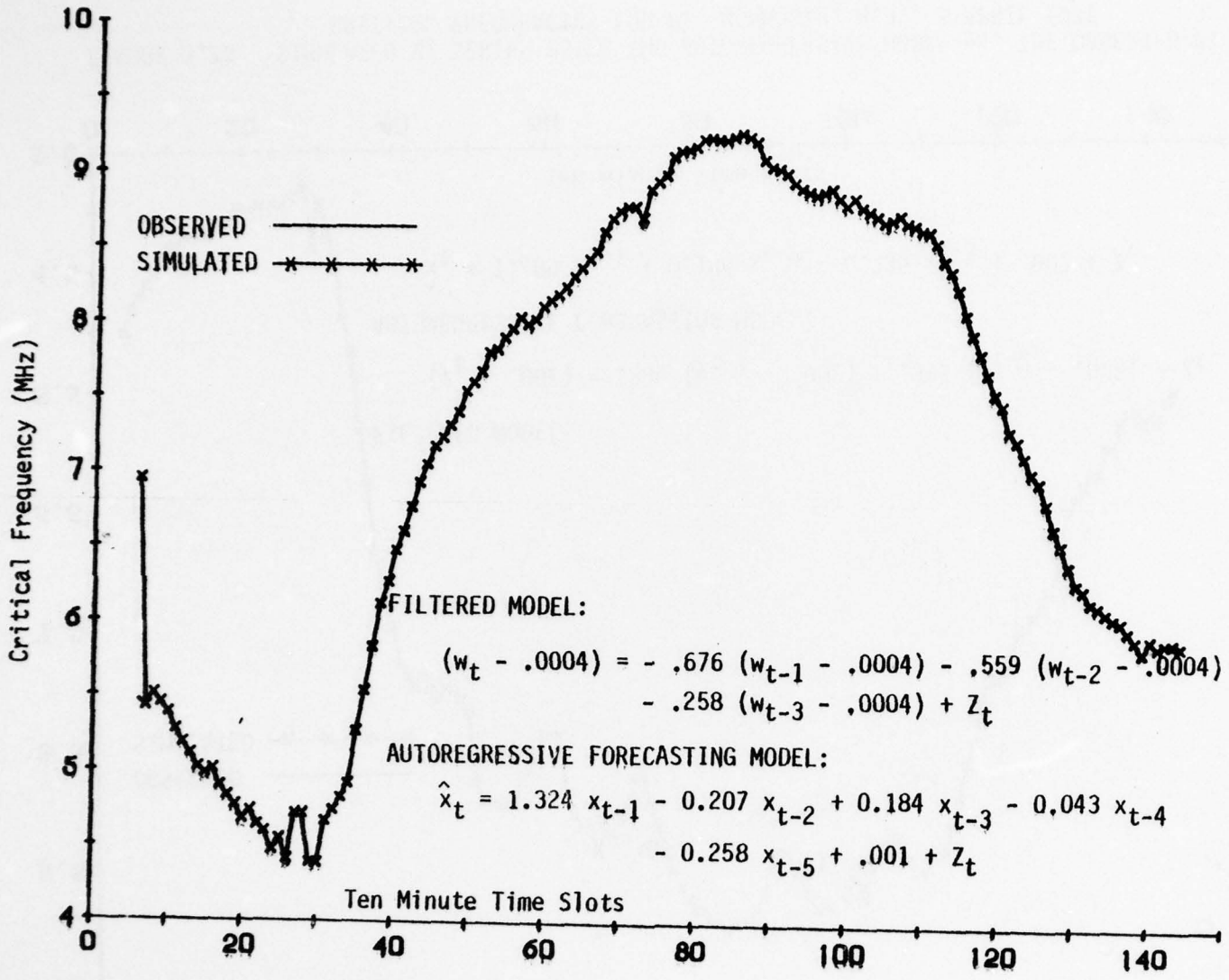

FIGURE 3.24 SIMULATED MEAN VI SERIES USING THE AUTOREGRESSIVE MODEL vs. THE MEAN VI CRITICAL FREQUENCIES FOR FT. MONMOUTH, N. J., 22 MARCH - 10 APRIL 1971

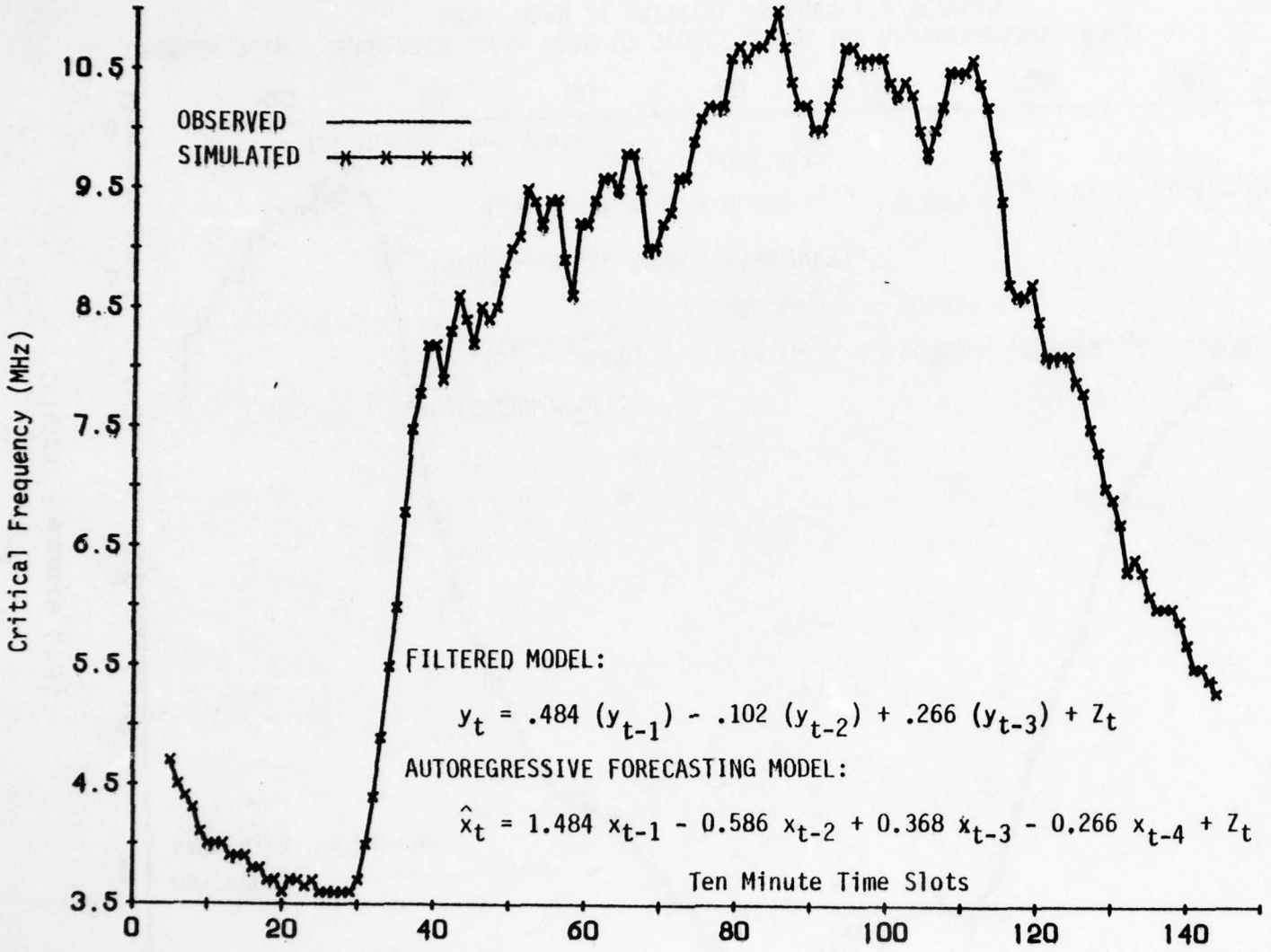

FIGURE 3.25 SIMULATED 500Km OI SERIES USING THE AUTOREGRESSIVE MODEL vs. THE OBSERVED 500Km OI CRITICAL FREQUENCIES BETWEEN FT. MONMOUTH, N.J., AND FT. DRUM, N.Y., 5 APRIL 1971

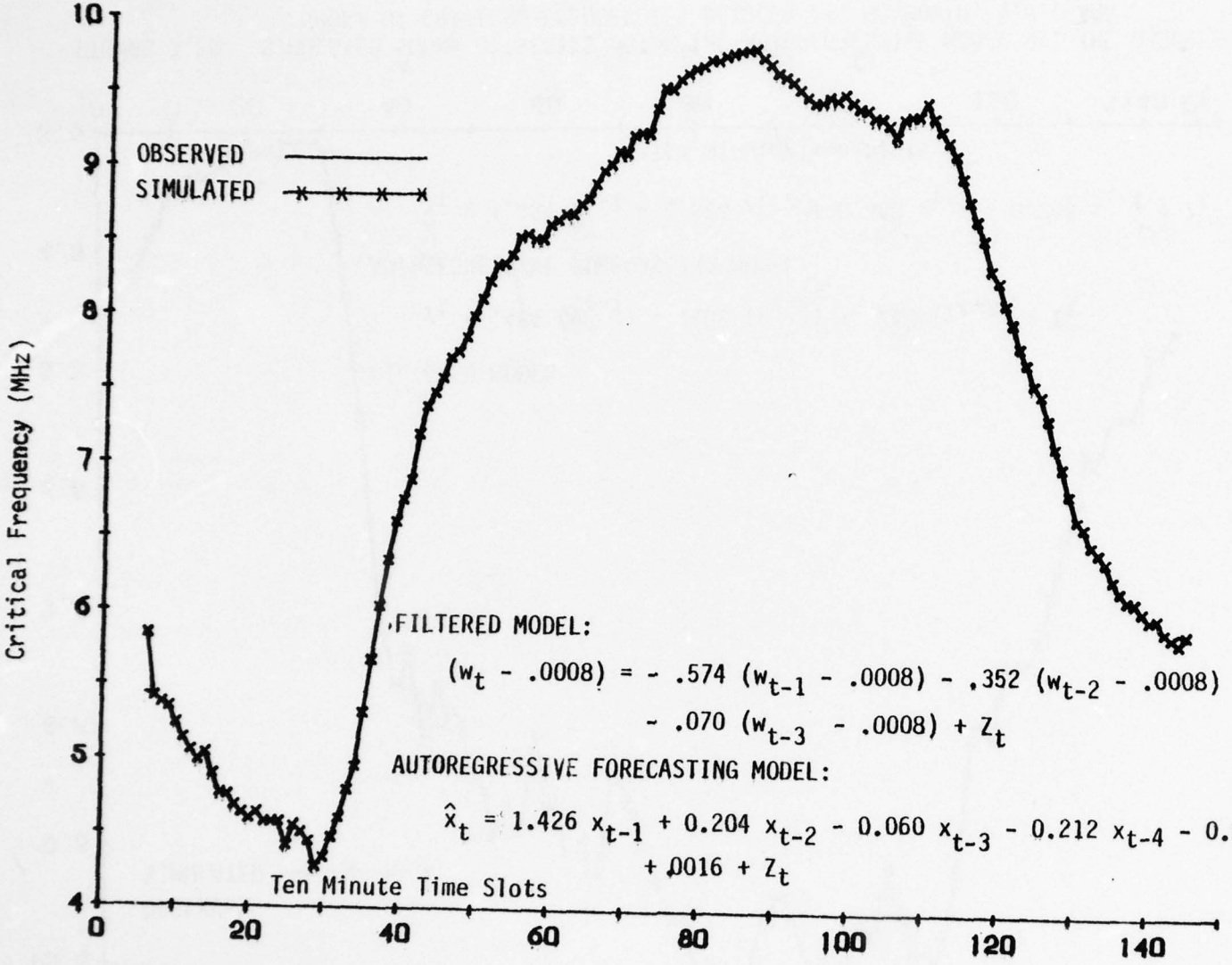

FIGURE 3.26 SIMULATED 500Km MEAN OI SERIES USING THE AUTOREGRESSIVE MODEL vs. THE 500Km MEAN OI CRITICAL FREQUENCIES BETWEEN FT. MONMOUTH, N.J., AND FT. DRUM, N.Y., 22 MARCH-10 APRIL 1971

Table 3.5 Sample Autocorrelations $r_{zz}(k)$ for the Simulated 13th Day Observed VI Data With a 95% Confidence Interval of ±0.163

Lag k (Time Slots)	Sample Autocorrelation $r_{zz}(k)$ $\times 10^{+2}$									
1-10	-14.1	-31.8	-.003	-.001	-.051	-.040	-.023	-.023	-.037	-.039
11-20	-.005	-.033	-.021	.008	.011	-.036	-.010	.010	-.038	-.019
21-30	-.008	-.026	.007	-.008	-.002	-.008	-.093	-.069	.157	-.096
31-40	-.097	-.031	.042	-.002	.056	.103	.166	.094	.069	.103
41-50	.072	.045	-.051	.003	.058	-.033	-.055	-.077	-.089	.155
51-60	.157	.025	-.010	.017	.039	-.037	-.027	-.020	-.084	-.111
61-70	-.120	.095	.122	.029	.003	.072	-.021	.036	-.004	-.024
71-80	-.111	-.153	.002	.042	.039	.055	.026	.021	.025	-.007
81-90	.009	.005	.038	-.023	-.013	.021	.019	.009	-.099	-.119
91-100	-.059	.025	-.018	.035	.057	.023	.009	-.009	-.019	-.074
101-110	.066	.000	-.039	-.035	-.079	-.067	.041	.077	.031	-.032
111-120	.019	.073	-.121	-.037	-.056	-.040	-.097	-.119	-.014	.056
121-130	-.032	-.087	-.011	-.006	-.023	.018	.041	-.096	-.106	-.041
131-140	-.038	-.027	.009	-.040	.005	-.051	-.087	-.029	.025	-.036
141-143	-.455	-.342	1.147							

AD-A058 630 ARMY COMMUNICATIONS RESEARCH AND DEVELOPMENT COMMAND --ETC F/G 4/1
TIME-SERIES MODELING AND ANALYSIS OF HIGH FREQUENCY (HF) VERTIC--ETC(U)
JUL 78 R J D'ACCARDI

UNCLASSIFIED CORADCOM-78-7 NL

2 OF 2
AD
A058630

END
DATE
FILMED
11-78
DDC

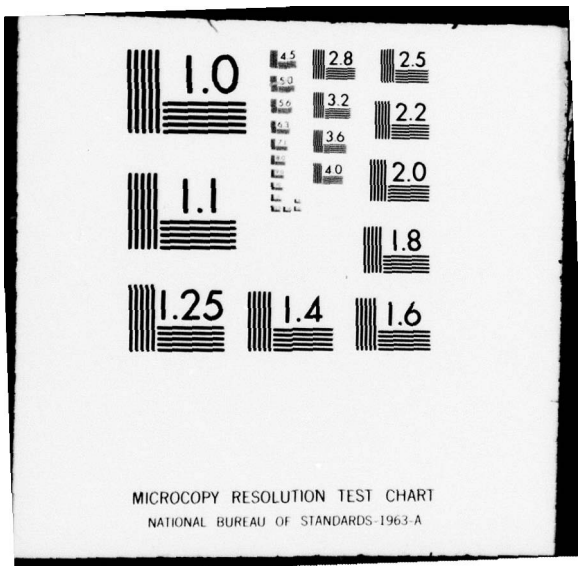
1.0
1.1
1.25
1.4
1.6
1.8
2.0
2.2
2.5
2.8
3.2
3.6
4.0
4.5
5.0
5.6
MICROCOPY RESOLUTION TEST CHART
NATIONAL BUREAU OF STANDARDS-1963-A

Table 3.6 Sample Autocorrelations, $r_{zz}(k)$ for the Simulated 18-Day Averaged VI Data With a 95% Confidence Interval of ±0.163

Lag k (Time Slots)	Sample Autocorrelation $r_{zz}(k)$ $\times 10^{+2}$									
1-10	-13.5	.84	-17.1	-20.2	-.050	.032	.067	-.005	.035	-.064
11-20	-.014	-.011	-.003	.017	.032	-0.21	.017	-.044	-.002	.048
21-30	-.037	.028	-.097	.072	-.068	.180	-.095	-.031	-.078	-.023
31-40	.060	.046	-.106	.067	.014	.099	.008	-.028	.018	-.059
41-50	.033	-.006	.008	.005	-.033	.000	-.019	.031	-.011	.013
51-60	.000	-.015	.035	-.032	.027	-.043	.004	-.013	.013	.012
61-70	-.016	.001	-.003	.002	-.009	.033	.015	.016	-.023	-.029
71-80	-.059	.058	-.031	.075	-.003	-.018	.017	-.029	-.011	.019
81-90	-.011	.007	-.011	.012	.020	.005	-.001	-.045	.001	-.013
91-100	.021	-.004	-.014	-.006	.008	.018	.012	-.008	-.009	.011
101-110	-.019	.025	-.037	.002	.018	.013	.003	.013	-.017	.029
111-120	-.001	-.004	.000	-.018	-.003	-.016	-.013	.000	-.005	.015
121-130	-.031	.035	-.022	.031	.014	-.016	-.009	-.021	-.027	.006
131-140	.006	-.006	.034	-.010	.018	.000	-.014	.098	.028	.028
141-143	.086	-.417	.206							

Table 3.7 Sample Autocorrelations, $r_{zz}(k)$, for the Simulated 13th Day Observed OI Data With a 95% Confidence Interval of ±0.163

Lag k (Time Slots)	Sample Autocorrelation $r_{zz}(k)$ $\times 10^{+2}$									
1-10	-42.5	17.5	-20.2	-.031	-.021	-.052	-.018	-.031	-.044	-.033
11-20	-.041	-.004	-.009	.002	.002	-.017	.022	-.045	.015	-0.55
21-30	.013	-.011	.004	.024	-.033	.007	-.033	-.021	-.044	-.061
31-40	-.046	-.013	.019	.079	.062	.151	.195	.189	.208	.093
41-50	-.021	.041	.007	.086	-.023	.010	-.089	.033	-.018	.048
51-60	.033	.121	.029	.044	.031	-.002	-.009	-.160	-.009	-.095
61-70	.145	.022	.058	-.004	.085	.026	.073	-.104	-.116	-.090
71-80	-.042	.088	-.032	.088	.019	.059	.032	-.038	.050	.031
81-90	.044	.027	-.025	.026	.093	.010	.026	-.106	-.049	-.097
91-100	-.051	-.040	-.003	.099	.059	.044	.009	-.017	.025	-.018
101-110	-.018	-.017	.003	-.004	-.013	-.105	-.055	-.044	.101	.062
111-120	.078	.022	.090	-.047	-.012	-.211	-.092	-.149	.046	-.009
121-130	-.035	-.054	-.058	.049	-.008	.046	-.062	-.002	-.083	-.036
131-140	-.037	-.102	-.005	-.076	-.002	-.036	-.033	.005	.012	-.399
141-143	.088	-.758	1.42							

Table 3.8 Sample Autocorrelations, $r_{zz}(k)$ for the Simulated 18-Day Averaged OI Data With a 95% Confidence Interval of ±0.163

Lag k (Time Slots)	Sample Autocorrelation $r_{zz}(k)$ $\times 10^{+2}$									
1-10	-18.9	-6.59	-19.1	-5.33	-.012	.018	.006	.009	-.013	-.010
11-20	-.007	.000	.029	-.016	-.009	-.005	-.004	.008	-.010	.019
21-30	-.005	.006	.000	-.028	.041	-.017	.011	-.063	-.001	.004
31-40	.011	.001	-.025	.024	.015	.036	.009	.000	-.021	-.022
41-50	.023	.008	.003	-.019	-.001	-.015	.000	.000	.012	.008
51-60	.003	-.014	.000	.011	.000	-.012	-.018	.014	.000	.007
61-70	-.019	.004	-.008	.013	.005	-.004	.008	-.020	.016	-.018
71-80	-.008	.013	.019	-.003	.000	-.012	.007	-.006	.003	-.006
81-90	.004	-.001	.005	.002	.006	-.009	-.002	-.011	.004	.000
91-100	-.002	-.007	-.007	.003	.012	.000	.013	-.012	-.001	-.002
101-110	-.004	.001	-.009	-.018	.022	.004	.015	.018	-.014	.001
111-120	-.010	.007	-.004	-.009	-.005	.003	-.013	.013	-.009	.011
121-130	-.015	.008	-.004	.020	-.005	-.006	-.009	-.011	-.009	.011
131-140	-.004	.017	-.002	-.007	-.005	-.006	.012	-.073	-.272	-.135
141-143	-.385	1.17	-.319							

can conclude that the residuals constitute a purely random process and that the fitted models give satisfactory representation of the observed series.

There is a further statistical test described in section 2.4.3 that reflects on the accuracy of our models. From equation (2.4.17), the calculated value of $Q \sim \chi^2_{k-m-q}$ for the first K autocorrelations, where $K = n/10$, m = the order of the AR process, q = the order of the MA process. When this value is tested against the appropriate χ^2 value, and if

$$Q < \chi^2_{k-m-q}\,(1 - \alpha/2)\ ,$$

then the fitted model is adequate, [12]. For the stationary stochastic ionospheric realizations,

i. for the 13th day observed VI data, $Q = 16.67 < \chi^2_{12}\,(.975) = 24.7$

ii. for the 18-day averaged VI data, $Q = 12.72 < \chi^2_{12}\,(.975) = 24.7$

iii. for the 13th day observed OI data, $Q = 21.29 < \chi^2_{13}\,(.975) = 23.3$

iv. for the 18-day averaged OI data, $Q = 10.41 < \chi^2_{12}\,(.975) = 24.7$.

Clearly, then, the four estimated models are adequate.

By the mean approaching zero, it is meant that in using these types of models there is a tendency to either under- or over-forecast a particular estimate at a given time slot. However, in the long run, if the over- and under-estimates are averaged, this average would be zero. The basic idea of the "purely random process" means that as $n \to \infty$, the variance approaches zero. This is not the case, however, because if the variance is zero, we would have a degenerate phenomenon where the mass would be concentrated at a point, and interpretation would be impossible.

3.3.4 Forecasting and Updating

The final step in the procedural approach to time series modeling is to state the model in such a form that forecasts ℓ steps ahead are possible, where $\ell = 1, 2, \ldots, n$. Given below are the four estimated ionospheric models in the appropriate form for ℓ step-ahead forecasts:

i. for the 13th day observed VI information, $\hat{x}_t(\ell) = 1.289\, x_{t+\ell-1}$

$$+ 0.106\, _{t+\ell-2} - 0.395\, _{t+\ell-3} + .007 + Z_{t+\ell} \qquad (3.3.9)$$

ii. for the 18 - day averaged VI information, $\hat{x}_{t(\ell)} = 1.324x_{t+\ell-1}$
$- 0.207x_{t+\ell-2} + 0.184x_{t+\ell-3} - 0.043x_{t+\ell-4} - 0.258x_{t+\ell-5}$
$+ .001 + Z_{t+\ell}$ (3.3.10)

iii. for the 13^{th} day observed OI information, $\hat{x}_{t(\ell)} = 1.484x_{t+\ell-1}$
$- 0.586x_{t+\ell-2} + 0.368x_{t+\ell-3} - 0.266x_{t+\ell-4} + Z_{t+\ell}$ (3.3.11)

iv. for the 18 - day averaged OI information, $\hat{x}_{t(\ell)} = 1.426x_{t+\ell-1}$
$- 0.204x_{t+\ell-2} + 0.060x_{t+\ell-3} - 0.212x_{t+\ell-4} - 0.070x_{t+\ell-5}$
$+ Z_{t+\ell} + .0016$. (3.3.12)

Of course, the accuracy of these models will be much better for small ℓ. As ℓ becomes large, i.e., $\ell >> m + d + q$, where d is the order of the filter and m and q are as previously defined, the accuracy decreases substantially. However, one can forecast any number of steps ahead and *update* the forecasts as additional information becomes available.

To illustrate how one may update the forecasts for a time t (origin), suppose that a new piece of data, x_{t+1}, becomes available. With the new origin at time t+1, we update the time t forecasts by equation (2.4.42) as:

$$\hat{x}_{t+1}(\ell) = \hat{x}_t(\ell+1) + \theta_\ell Z_{t+1}, \quad \ell=1, 2, \ldots, 11,$$

where $Z_{t+1} = x_{t+1} - \hat{x}_t(1)$ and θ_ℓ is as described in section 2.4.

Given in tables 3.9, 3.10, 3.11, and 3.12 below are ℓ steps ahead forecasts (up to ℓ=11) at an arbitrary t = 72 origin, with updating, along with their 95% confidence intervals.

Table 3.9 Forecasted Values of the 13th Day Observed VI Series at Origin t = 72 and Updating Under the Assumption x_{73} Becomes Available

TIME	ACTUAL VALUE	LEAD TIME	FORECAST	95% PROBABILITY LIMITS	UPDATED FORECAST
1150	9.00	--	-----	----	-----
1200	8.80	1	8.875	± .404	-----
1210	8.70	2	8.885	± .596	8.788
1220	9.00	3	9.022	± .778	8.889
1230	9.20	4	9.047	± .962	9.198
1240	9.40	5	9.064	±1.139	9.235
1250	9.60	6	9.086	±1.310	9.270
1300	9.70	7	9.106	±1.474	9.302
1310	9.80	8	9.127	±1.631	9.331
1320	9.90	9	9.148	±1.782	9.359
1330	9.90	10	9.169	±1.926	9.386
1340	10.00	11	9.190	±1.926	9.411

Table 3.10 Forecasted Values of the 18-Day Averaged VI Series at Origin t = 72 and Updating Under the Assumption x_{73} Becomes Available

TIME	ACTUAL VALUE	LEAD TIME	FORECAST	95% PROBABILITY LIMITS	UPDATED FORECAST
1150	8.79	--	-----	----	-----
1200	8.71	1	8.721	± .214	-----
1210	8.90	2	8.729	± .292	8.879
1220	8.96	3	8.752	± .371	8.969
1230	9.00	4	8.749	± .473	8.949
1240	9.13	5	8.737	± .562	8.987
1250	9.16	6	8.745	± .616	9.005
1300	9.17	7	8.752	± .641	8.972
1310	9.19	8	8.752	± .644	8.902
1320	9.19	9	8.753	± .656	8.803
1330	9.24	10	8.758	± .735	8.868
1340	9.25	11	8.763	± .735	9.043

Table 3.11 Forecasted Values of the 13th Day Observed OI Series at Origin t = 72 and Updating Under the Assumption x_{73} Becomes Available

TIME	ACTUAL VALUE	LEAD TIME	FORECAST	95% PROBABILITY LIMITS	UPDATED FORECAST
1150	9.20	--	-----	----	-----
1200	9.30	1	9.305	± .586	-----
1210	9.60	2	9.439	± .791	9.509
1220	9.60	3	9.467	± 1.006	9.547
1230	9.90	4	9.495	± 1.229	9.585
1240	10.10	5	9.541	± 1.438	9.651
1250	10.20	6	9.568	± 1.638	9.678
1300	10.20	7	9.584	± 1.831	9.704
1310	10.20	8	9.601	± 2.016	9.721
1320	10.60	9	9.615	± 2.193	9.745
1330	10.70	10	9.624	± 2.362	9.754
1340	10.60	11	9.631	± 2.362	9.761

Table 3.12 Forecasted Values of the 18-Day Averaged OI Series at Origin t = 72 and Updating Under the Assumption x_{73} Becomes Available

TIME	ACTUAL VALUE	LEAD TIME	FORECAST	95% PROBABILITY LIMITS	UPDATED FORECAST
1150	9.26	--	-----	----	-----
1200	9.25	1	9.249	± .198	-----
1210	9.42	2	9.260	± .287	9.360
1220	9.56	3	9.274	± .395	9.474
1230	9.55	4	9.283	± .514	9.483
1240	9.62	5	9.294	± .652	9.594
1250	9.66	6	9.307	± .801	9.347
1300	9.69	7	9.320	± .959	9.360
1310	9.71	8	9.334	±1.129	9.384
1320	9.75	9	9.349	±1.649	9.399
1330	9.75	10	9.365	±1.495	9.425
1340	9.78	11	9.382	±1.495	9.442

It is clear from tables 3.9 and 3.11 that, for a small number of steps, i.e., $\ell = 1, 2, 3$, our forecasts of the observed series are quite good. For larger L, the forecasted values generally tend to underestimate the future values. Updating the forecasts in these cases improves the estimates. The ℓ step ahead forecasts for the 18-day averaged series are also very good for $\ell = 1, 2, 3$, steps ahead. The necessity for updating in these cases is obvious since, here again, updating yielded an excellent gain of accuracy.

3.4 A Prediction Process Based on The Sample Autocorrelation Function

Ames and Egan, [1], have developed a prediction process based upon the sample autocorrelation function to make short-term predictions for the maximum observed frequency (MOF), the lowest observed frequency (LOF), and other high frequency (HF) propagation parameters dealing with the ionosphere. The acquisition of the data for their model was similar to the 500 Km experiment described in section 3.2.

Their data was collected from oblique incidence soundings which were transmitted every 10 minutes from the U. S. Naval Station at Lualualei, Hawaii, and received at Palo Alto, California, a distance of about 4400 Km. The analysis was based on ionograms recorded from January 7 through March 12, 1965. For each 24-hour period, there were 144 increments and, in duration, there were 45 days of data available.

For each 10-minute increment of the 24-hour period, the mean and the standard deviation were calculated for the MOF and LOF. It was pointed out that the standard deviation represents the variation of the MOF and LOF from day to day within each particular time slot and not fluctuations with time on a single day. It was discovered that the standard deviation of the MOF was higher during the day than at night by a factor of 2.17, while the MOF ratio between these periods was 2.4 to 1. The plot of the MOF vs. standard deviation further demonstrated the dependence of the standard deviation upon the MOF.

Next, the sample autocorrelation function of the MOF was calculated with values from five previous 10-minute periods and then plotted as hourly averages. It was found that the autocorrelation of the MOF was high during

the morning and evening ionospheric transition periods. The autocorrelation is a measure of the current stability relative to the mean-value function, whereas the standard deviation is a measure of the day-to-day variance.

3.4.1 Short-Term Prediction

Ames and Egan fitted forecasting models to the maximum observed frequency series and to the lowest observed frequency series to be able to predict eight successive 10-minute periods following each observation. Their prediction (or forecasting) model is, [1],

$$\hat{x}(t+T) = \bar{x}(t+T) + [x(t) - \bar{x}(t)]\, \rho(t,T) \ , \qquad (3.4.1)$$

where t is the present time; T is the lead time; x(t) is the observed value for time t; $\bar{x}(t)$ is the mean value for the time slot t; $\bar{x}(t+T)$ is the long-term mean value for a prediction T minutes in the future; $\rho(t,T)$ is the sample autocorrelation between values at t and t + T; and $\hat{x}(t+T)$ is the future value of the MOF or the LOF predicted for any of eight 10-minute periods following each observation. That is, equation (3.4.1) states that a prediction for T minutes in the future consists of the long-term mean value for that time plus a weighted term correcting it for the present difference between observed and average values.

The input data Ames and Egan used in equation (3.4.1) consisted of current MOF and LOF running averages and standard deviations determined only from previous data (except for the first few days of "start up"), and values of autocorrelation derived from all the data. The MOF and LOF running averages were computed and stored separately for each of the 10-minute increments of the 24-hour day; the standard deviations were computed for each 10-minute increment and then combined into hourly averages. These values were then updated when a new measurement was realized by the running average function:

$$\bar{x}_n = \left(1 - \frac{1}{K}\right) \bar{x}_{n-1} + \frac{x_n}{K} = \left(1 - \frac{1}{K}\right)^{n-1} x_1 + \frac{1}{K} \sum_{i=2}^{n} \left(1 - \frac{1}{K}\right)^{n-i} x_i \ . \qquad (3.4.2)$$

It was stated that for the means, x_n represented an observed value and for the standard deviation, it represented the absolute value of the difference

between an observed value and the corresponding mean. The value of K was set equal to 10 for the means, and 100 for the standard deviations.

Data was used from the full experimental period in calculating the sample autocorrelation function in order to obtain relatively smooth estimates of the autocorrelation. The following equation was used to estimate the autocorrelation:

$$\rho(t,T) = \frac{\sum_{i=1}^{N} [x_i(t) - \bar{x}(t)][x_i(t - T) - \bar{x}(t - T)]}{\sqrt{\sum_{i=1}^{N} [x_i(t) - \bar{x}(t)]^2 \sum_{i=1}^{N} [x_i(t - T) - \bar{x}(t - T)]^2}} \tag{3.4.3}$$

where N is the number of days measurements were available. In real-time, values of the autocorrelation could be computed once each month and then when new values are realized, they could be updated using equation (3.4.2).

The 24 hourly values of the autocorrelation, ρ, for a delay of 10 minutes plus a set of corresponding time constants, τ, derived from the least squares fit to the ρ data between delays of 10 to 60 minutes, were used as input to the prediction process. For delays greater than 10 minutes, values of ρ were calculated from:

$$\rho = \rho_{10} \exp-(T - 10)/\tau \tag{3.4.4}$$

The values of ρ calculated from equation (3.4.4) were found to be a few percent larger than the observed values of autocorrelation. Ames and Egan concluded that the smoothing of the measured ρ values over 1-hour periods plus the abstracting of all delays greater than 10 minutes into corresponding time constants appears to have reduced the unrealistic benefit from this partial view of the future to a negligible amount.

Ames and Egan express the expected error in predicting with the process (3.4.1) in terms of the autocorrelation. The expected error is given by:

$$\frac{\sigma_\rho(t + T)}{\sigma(t + T)} = \sqrt{1 - \rho^2 (t, T)} \quad . \tag{3.4.5}$$

The above equation predicts the degree to which the variance of the observed values about the corresponding predicted values will be less than that of the

observed values about the mean. It was concluded that to make a substantial reduction in σ_ρ relative to σ, say one-half, ρ must be greater than 0.86. However, it was stated that predictions should be considered "useful" for values of ρ down to about 0.5 since even though σ is not much reduced, the predicted value itself is adjusted from the long-term mean by one-half the presently observed difference.

3.4.2 Updating with Fourier Coefficients

In a later article, Ames, Egan, and MacGinitie, [20], use Fourier coefficients to update the data to eliminate the random variability in the input data. The random variability caused unavoidable growth of irregularities in the diurnal (daily) curves of the long-term function. Thus, instead of using the technique of running averages (equation 3.4.2) to update the hourly averages when a new measurement is realized, the long-term data is converted to a limited number of Fourier coefficients from which the desired values are found as needed. For the mean values, eight harmonics were used; for the standard deviations, four harmonics were used.

The following equation was used to derive the Fourier coefficients from the set of data with a 24-hour period of 144 10-minute intervals:

$$a_n(\text{NEW}) = a_n(\text{OLD}) + \varepsilon \frac{2}{T} [x(t) - \bar{x}(t)] \cos \left(\frac{2\pi nt}{T}\right) , \qquad (3.4.6)$$

where $\varepsilon = 0.0944$ and $T = 144$. The value of ε was chosen so as to allow the Fourier coefficient to follow long-term ionospheric changes with a time constant of approximately 11 days.

Ames, Egan, and MacGinitie comment that this conversion to Fourier coefficients not only improves the prediction quality, but also substantially reduces the required amount of computer memory capacity. Also, the data storage requirement is reduced by the approximation of the autocorrelation function by a decaying exponential.

3.4.3 The Autocorrelation Function

Ames and Egan throughout their paper take the position that the autocorrelation that they have calculated is the true state of nature, that is, that they have the true parameter value, not just an estimate of it. This

is most clearly shown in their constant reference to the calculated autocorrelation as ρ, not $\hat{\rho}$, or r, which has become the widely-accepted symbol for the sample autocorrelation function in time series analysis. This can also be seen later in section 3.4.5 when the expected error in predictions is discussed; Ames and Egan's expected error depends solely on the autocorrelation they have calculated. They also take this position when, after using a negative exponential function to approximate the autocorrelation, they then compare it to their estimate of ρ concluding that the approximation is only a few percent larger than the observed values of the autocorrelation. They simply compare two different estimates of the true state of nature.

In the appendix of their paper, Ames and Egan, [1], give the following equation to compute the autocorrelation:

$$\rho(t,T) = \frac{\sum_{i=1}^{N} [x_i(t) - \bar{x}(t)]\,[x_i(t-T) - \bar{x}(t-T)]}{\sqrt{\sum_{i=1}^{N} [x_i(t) - \bar{x}(t)]^2 \quad \sum_{i=1}^{N} [x_i(t-T) - \bar{x}(t-T)]^2}} \qquad (3.4.7)$$

Of course, they do not obtain $\rho(t,T)$ the true state of nature, but just an estimate of it, say $r(t,T)$. The estimate (3.4.7) is a function of the time t and the prediction lead time T.

The above estimate of $\rho(t,T)$ is essentially equivalent to the estimate given by the following expression:

$$r_{xx}(k) = \frac{\sum_{t=1}^{N-k} (x_t - \bar{x}_1)\,(x_{t+k} - \bar{x}_2)}{\left[\sum_{t=1}^{N-k} (x_t - \bar{x}_1)^2 \quad \sum_{t=1}^{N-k} (x_{t+k} - \bar{x}_2)\right]^{1/2}} , \qquad (3.4.8)$$

where $\bar{x}_1$ and $\bar{x}_2$ are the means of the first and the last (N-K) observations, respectively. Equation (3.4.8) expresses the lead time in terms of lag k where $r_{xx}(k)$ is a function only of the lag k. The estimates (3.4.8) and (3.4.7) are not recommended [3] in estimating the autocorrelation of the grounds that, although it gives a reasonable estimate of ρ when considered

in isolation from other values of the autocorrelation function, it does not give a satisfactory estimate when a set of estimates is required. The main disadvantage of (3.4.8), and hence (3.4.7), is that two means are used for the mean correction and that these change with lag; in addition, the normalizing factor changes with lag k. The net result of these modifications is that these estimates are not positive definite which violates the property of the autocorrelation function.

We suggest the following estimate, [3], [6], which gives the most satisfactory estimate of the sample autocorrelation function:

$$r_{xx}(k) = \frac{c_{xx}(k)}{c_{xx}(0)} \quad , \tag{3.4.9}$$

where

$$c_{xx}(k) = \frac{1}{N} \sum_{t=1}^{N-k} (x_t - \bar{x})\,(x_{t+k} - \bar{x}),\ k = 0, 1, \ldots, N-1 \quad . \tag{3.4.10}$$

($c_{xx}(k)$ is the autocovariance function). Equations (3.4.9) and (3.4.10) are functions only of the lag k and are independent of time.

3.4.4 On the Prediction Process

Recall that Ames and Egan use the following equation to forecast future value of the ionospheric data:

$$\hat{x}(t+T) = \bar{x}(t+T) + [x(t) - \bar{x}(t)]\,\rho(t,T) \quad . \tag{3.4.11}$$

Further, recall how the ionospheric data is collected. This is essentially what occurs: first a day is divided into 144 10-minute increments; then ionospheric soundings are transmitted, then received and recorded for each 10-minute increment throughout the day; this is repeated for several days. The ionospheric series, unlike the series usually encountered in practice, have several realizations for each time slot. Initially, to begin the prediction process using (3.4.11), it is necessary to speculate or reckon the predictions for the first four or five days until sufficient information becomes available. Once four or five days of data have been collected,

"fairly" smooth estimates of $\bar{x}(t+T)$, $\bar{x}(t)$, and $\hat{\rho}(t,T)$ can be obtained and the prediction process (3.4.11) really begins. We question how good the estimates of $\bar{x}(t+T)$, $\bar{x}(t)$, and $\hat{\rho}(t,T)$ are from samples of only four or five points. In view of this, we are lead to the statement by Yaglom, [4], "If the number of observed values of a series is small (< 10 say), then the entire formulation of the problem is clearly quite unrealistic, since we would not be able to make a *sufficiently reliable* determination of the autocorrelation function."

Also, we feel that the prediction model (3.4.11) is quite unrealistic with respect to the expression $\bar{x}(t+T)$. It would appear that Ames and Egan use the value they are trying to predict in calculating the mean of the t+T time slot. The paper was extremely vague in how this mean was calculated.

We question the use of Fourier coefficients in converting and, hence, in reducing the data for computer memory capacity for two reasons. First, we fail to see how the required means, autocorrelation, etc., can be removed so easily from the Fourier coefficients as needed. Secondly, the ionospheric data appears to exhibit non-stationary properties (this has been verified by the examination of other ionospheric data), and Fourier analysis breaks down when applied to data which exhibit *random* changes of frequencies, amplitudes, and phases, since Fourier analysis is based on the assumption of *fixed* frequencies, amplitudes, and phases.

We feel that the prediction process of Ames and Egan is quite limited in several respects due in part to the criticisms presented above. First, very few practical problems (in time series) arise such that we would have more than one realization for a specific time slot. Ames and Egan's prediction process (3.4.11) is developed solely from the viewpoint of having several realizations for each time slot. Secondly, as we mentioned in the previous paragraphs, it is quite unrealistic to estimate the parameters in the prediction model with so small a sample. (Ames and Egan make no reference as to how much previous data is necessary when utilizing their approach). Finally, it seems very expensive to require so many previous days of data (at least 10) in order to properly employ the model.

3.4.5 Expected Error in Predictions

Ames and Egan state that the expected error depends on the autocorrelation and is given by:

$$\hat{\sigma}_{\rho}(t+T) = \hat{\sigma}(t+T)\sqrt{1 - \rho^2(t,T)} \quad . \tag{3.4.12}$$

$\hat{\sigma}(t+T)$ is the sample standard deviation computed for the t+T time slot. Under the premise that the expected error depends on the autocorrelation, they are able to conclude that the expected reduction of variance is achieved when $\hat{\rho}$ is greater than 0.86.

Then, to measure the performance of the prediction model (3.4.11), they used the following expression:

$$\sqrt{\frac{\Sigma^{N}[MOF(t) - \hat{MOF}(t)]^2}{N}} \Big/ \sigma_{MOF}(t) \tag{3.4.13}$$

and compared the results to (3.4.12). From this comparison, Ames and Egan were able to conclude that the prediction process performed nearly as well as was theoretically expected. To have the theorectically expected error, it would have been necessary to have the true states of nature in equation (3.4.12). It is apparent that Ames and Egan have again assumed the erroneous position that they have the true states of nature, whereas, they have only estimates.

It appears that the expected error would depend to a certain extent on the autocorrelation function due to its presence in the prediction model (3.4.11). However, Ames and Egan are quite vague on this point and give no derivation of the dependence of the expected error on the autocorrelation, equation (3.4.12).

It seems that a better criterion to determine the goodness-of-fit of a fitted model or a prediction process would be given by the squared error loss; that is,

$$M.S.E. = \sum_{t=1}^{N} [x(t) - \hat{x}(t)]^2 \quad , \tag{3.4.14}$$

where $x(t)$ is the observed series and $\hat{x}(t)$ is the predicted (modeled) series.

Regardless of the criticisms that we have made in this section, some interesting ionospheric predictions were obtained using Ames and Egan's prediction process. In table 3.13, a comparison is made between the best predictions obtained from the use of Ames and Egan's model, made for the 13th day of the experiment, for lead times of 1, 2 and 3 steps ahead against the time-series approach without updating.

Table 3.13 A Comparison of Forecasts for the 13th Day OI Observations at Origin t = 72 Between the Ames-Egan and Time Series Approaches

TIME	OBSERVED VALUE	LEAD TIME	AMES-EGAN FORECAST	DIFFERENCE	TIME SERIES FORECAST	DIFFER-ENCE
1150	9.30	1	9.12	-.18	9.17	-.13
1200	9.60	2	9.14	-.46	9.13	-.47
1210	9.60	3	10.09	+.49	9.17	-.43

The t = 72 origin occurs at the most stable time of day for the ionosphere. Therefore, from the Ames-Egan point of view, these forecasts are among the best possible over the 24-hour period. Other times of day yield much poorer forecasts with their method. Clearly, the time-series approach is better not only from the theoretical point of view, as we have shown, but also from the actual excercising of the models.

3.5 SUMMARY AND CONCLUSIONS

In this section, the procedural approach developed in Section 2.4 was followed precisely in characterizing actual data. Namely, ionospheric data obtained by sounding the ionosphere in the HF range was modeled and analyzed. Specifically, the experimental design and acquisition of data over the 500 Km path between Ft. Monmouth, N. J., and Ft. Drum, N. Y., was discussed. The resulting information, which was time dependent, consisted of collecting VI and OI soundings every ten minutes throughout a 24-hour period. We justified that the data were indeed non-stationary stochastic realizations, and then proceeded to perform a time series analysis. The thrust of this section was towards analyzing four stochastic realizations, two of which were randomly selected VI and OI diurnal series, and two of which were the 18-day averaged

VI and OI series. The random selection process yielded the 13^{th} day ionospheric observations for analysis along with the averaged information.

Following the procedural approach recommended in Section 2.4, the following stochastic processes were formulated as the most appropriate characterizations of the given information:

i. $x_t = 1.289x_{t-1} + 0.106x_{t-2} - 0.395x_{t-3} + .007 + Z_t$ for the 13^{th} day observed VI,

ii. $x_t = 1.324x_{t-1} - 0.207x_{t-2} + 0.184x_{t-3} - 0.043x_{t-4} - 0.258x_{t-5} + .001 + Z_t$ for the 18-day averaged VI.

iii. $x_t = 1.484x_{t-1} - 0.586x_{t-2} + 0.368x_{t-3} - 0.266x_{t-4} + Z_t$ for the 13^{th} day observed OI,

iv. $x_t = 1.426x_{t-1} - 0.204x_{t-2} - 0.060x_{t-3} - 0.212x_{t-4} - 0.070x_{t-5} + .0016 + Z_t$ for the 18-day averaged OI.

In selecting these models, we utilized the criterion of minimum residual variance because, as indicated in Section 2, we believe this to be the most appropriate criterion for decision with respect to identifying the actual difference equations which characterize the ionospheric information. Furthermore, we have structured tables that show the short and long-term forecasts of VI and OI soundings along with their confidence limits. These models, in addition to being useful for prediction purposes, can be utilized in formulating the theoretical spectrum. Such a spectrum would be extremely useful in comparing the smoothed spectral density of the raw information with respect to identifying the *most* useful spectral density estimate which will convey information concerning the distribution of variance as a function of time. Such information will be useful in designing more efficient HF communications systems.

In addition, we have discussed the Ames-Egan model for predicting ionospheric conditions. The shortcomings concerning the relevance of this model were discussed in some detail in section 3.4.

4. SPECTRAL ANALYSIS OF VERTICAL INCIDENCE and SHORT-PATH OBLIQUE INCIDENCE IONOSPHERIC SOUNDINGS

4.1 INTRODUCTION

In Section 3.3, a detailed modeling procedure was illustrated that yielded appropriate time series models for the ionospheric data described in section 3.2. It was concluded that the models obtained did characterize the true underlying stochastic processes to a high degree. However, additional analysis of this information is necessary to utilize the ionospheric media more efficiently. Additional information, therefore, will be sought with regard to the distribution of the variance of the filtered data with respect to frequency. Thus, we will utilize the *power spectra* to describe in detail how the variance of the non-stationary realizations are distributed with frequency of occurrence (not the observed critical frequencies).

Ionospheric information is usually collected at individual stations as VI data, and, for the benefit of communicators operating over specified paths, is usually translated into equivalent OI information through the classical *Secant ϕ Law*, [2]. Since there are an infinite number of oblique paths that can be utilized by communicators, one can see the importance of converting the VI information. Also, consider that the number of VI sounder stations is limited throughout the world. This means that any such data acquired at one station may also be translated into VI information suitable for interpretation at other geographical locations within reason. Relationships for various translations that have been developed in the United States by the National Bureau of Standards, [2], and used by communicators throughout the world, can be traced back to at least 1941.

The classical *Secant ϕ Law* is a widely used *linear* relationship between OI and VI data. With Secant ϕ used as the obliquity factor, the law simply stated is:

$$X_{OI} = X_{VI} \cdot \text{Secant } \phi,$$

where X_{VI} is the observed vertical incidence information, ϕ is the angle of incidence of the radio wave path at its entrance into the ionosphere, and

X_{OI} is the equivalent information over an oblique path. The linear relationship certainly cannot be expected to yield suitable *equivalent OI* information in view of the highly stochastic nature of the ionosphere. The Secant ϕ Law relies on the assumptions of a *spectral reflection* of energy from the ionosphere (actually, reflections are dispersive in nature) and on the concept of stratified ionospheric layers. This implies homogeneous ionospheric layers, where boundaries between layers of electron density are always definable. This, of course, is not the case since the ionosphere is random and inhomogeneous, and it is affected by a variety of anomalous activity, i.e., sunspots, magnetic storms, diurnal and seasonal changes in structure. The Secant ϕ Law, [2], also implies that as path distance increases, the oblique information becomes more uncorrelated with the vertical incidence information. At the 500 Km path distance, over the specified Fort Monmouth - Fort Drum path, the difference between OI and VI became significant with respect to forecasting ionospheric conditions over the path using VI data alone.

Thus, one can see that additional information as to the distribution of the variance of the filtered OI and VI information is extremely important, and that information on the bivariate behavior of the two is essential in order to gain a more realistic view of the relationship between VI and OI. In the succeeding sections, a detailed spectral analysis of the 13^{th} day observed OI and VI information will be performed. In section 4.2, the basic concept of "aliasing" will be presented. The univariate spectral analysis will be addressed in section 4.3. The bivariate analysis, which consists of co-spectral, quadrature spectral, cross-amplitude spectral, phase, and coherency spectral estimates, will be presented in section 4.4. A summary and conclusions are given in section 4.5.

4.2 BASIC CONCEPTS OF "ALIASING"

With regard to the three windows described in detail in section 2.9, the concept of *aliasing* is predicated on the suppositions that:

i) the *window* should not be too wide, exposing a significant amount of disturbances (peaks and valleys of the power spectra), and,

ii) at the same time, the window should not be closed too far so as to avoid seeing the disturbances.

A significant point is that one should utilize ingenuity to detect the appropriate window length, L, so that irrelevant information is not exposed and relevant information is not eliminated. One can, by visually inspecting the power spectra as L is varied, determine the optimum L that will play the critical role in interpretation of the final, smoothed spectral estimates.

As L increases, the associated confidence intervals decrease. Since we wish to minimize the confidence interval, so as to more closely approach the true state of nature, a precise analysis is done for each window with respect to L. This is done by using the *theoretical spectrum* as a guide to the relevant peaks and valleys. Having analyzed each of the lag windows, i.e., those of Bartlett, Tukey, and Parzen (refer to section 2.9), the decision is then made as to the most appropriate L to be used for the filtered data. As a result of our analysis, the most appropriate L (each window may have a different optimal L) is the one that identifies itself with the *optimal* window.

In the following sections, we will utilize this philosophy and the detailed procedure of sections 2.5 through 2.9 to obtain the univariate and bivariate spectral estimates.

4.3 UNIVARIATE SPECTRAL ANALYSIS OF IONOSPHERIC INFORMATION

In this section, an analysis of two univariate time series will be presented. Specifically, the series corresponding to the 13^{th} day VI and OI information (refer to section 3.2) will be analyzed by the method of power spectra, described in sections 2.5 through 2.9. The ionospheric data was obtained every 10 minutes throughout the day (24 hours) for a total of 144 recordings. Estimates of the *spectral density function* are obtained from the filtered data using the Bartlett, Tukey, and Parzen lag windows described in section 2.9.

4.3.1 Estimate of the Spectral Density Function Using Bartlett's Lag Window

The values of the estimate of the spectral density function using Bartlett's lag window, equation (2.9.4), were calculated and plotted versus frequency for L = 8, 12, 16, 24, and 32 units. As a basis of comparison, the estimates were plotted on the same set of axes. For these values of L, and for L = 20, we calculated the bandwidth, the confidence intervals, and the degrees of freedom which are shown in table 4.1.

Table 4.1 Truncation Point, Bandwidth, Degrees of Freedom, and Confidence Intervals for Bartlett's Lag Window

L	Bandwidth	d.f.	95% C.I. for Log $\Gamma xx(f)$	
8	.188	54	-.154	.176
12	.125	36	-.179	.226
16	.094	27	-.204	.267
20	.075	22	-.223	.301
24	.063	18	-.243	.340
32	.047	13	-.279	.414

The formula used for the bandwidth of the estimate of the spectral density function is given by:

$$b = \frac{b_1}{L\Delta} = \frac{1.5}{L} \quad ,$$

and the equation for the degrees of freedom is given by:

$$\nu = 2\,\frac{T}{L}\,b_1 = 2Tb = 2(144)b = 288b \ .$$

Note that since we have chosen $\Delta = 1$, we have $L = M$.

Figures 4.1 and 4.2 give a comparison of the *theoretical* spectral density functions of the AR processes which characterize the VI and OI series, respectively (equations 3.3.1 and 3.3.3), and the smoothed estimates for the various truncation points, along with the 95% confidence intervals.

It is a known fact that increasing the bandwidth of the estimate of the spectral density involves increasing the amount of bias and decreasing the variance; thus, a compromise has to be reached as to which is the best value of L. In making such a decision, one should take into consideration the confidence interval, the degrees of freedom, and the visual appearance of the plot of the estimates. For L = 8, the plots are very smooth and have a shape which follows the trend of the theoretical spectrum with the bandwidth being wide enough to conceal any peaks that may be present. In both cases, by increasing L to 12, we obtain an indication of other peaks appearing at f = .20 and .44 cycles per second for the OI spectrum and at f = .20, .30, and .39 cycles per second for the VI spectrum. These are in addition to the major peaks in the

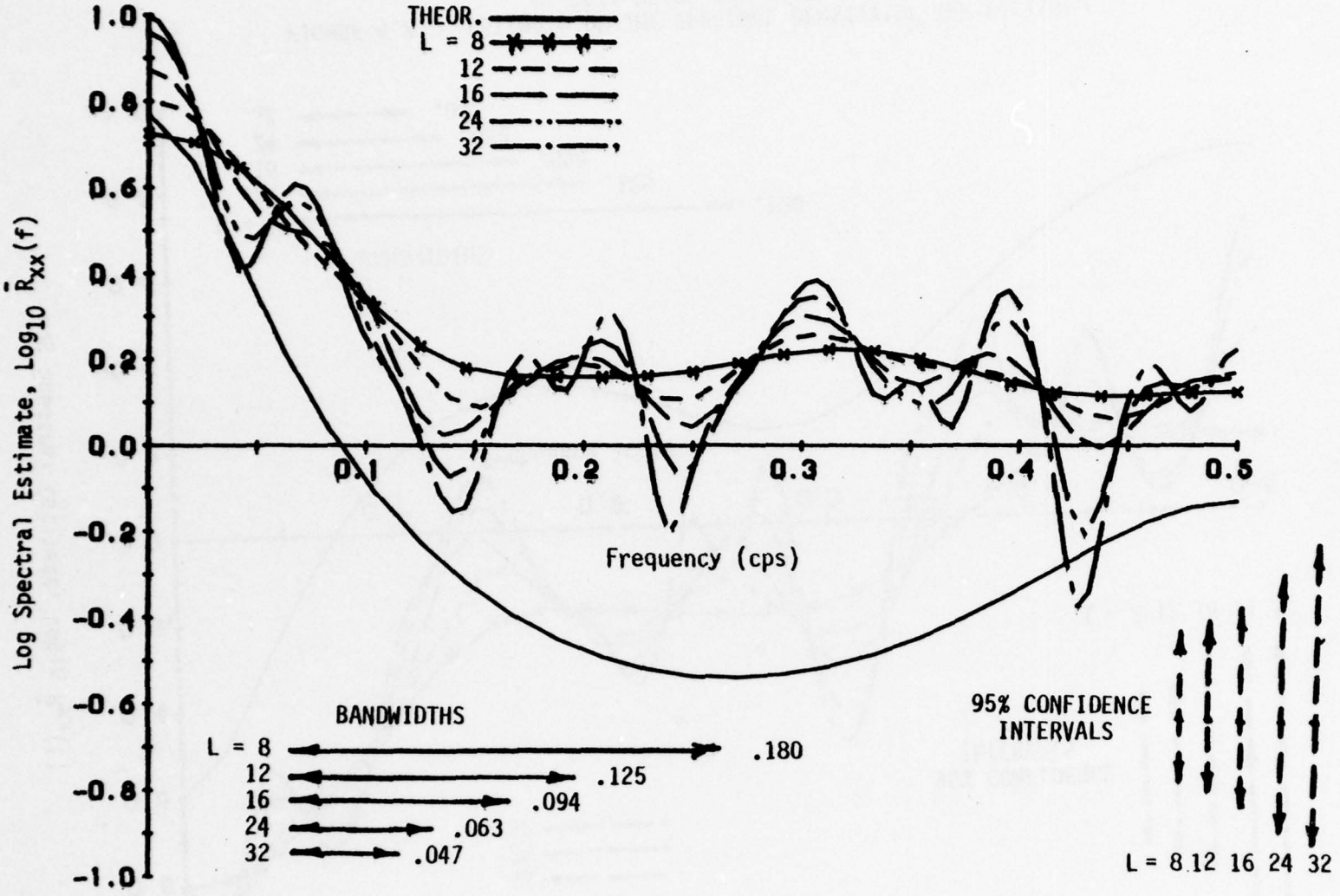

FIGURE 4.1 ESTIMATE OF THE SPECTRAL DENSITY OF THE FILTERED VI DATA USING THE BARTLETT LAG WINDOW

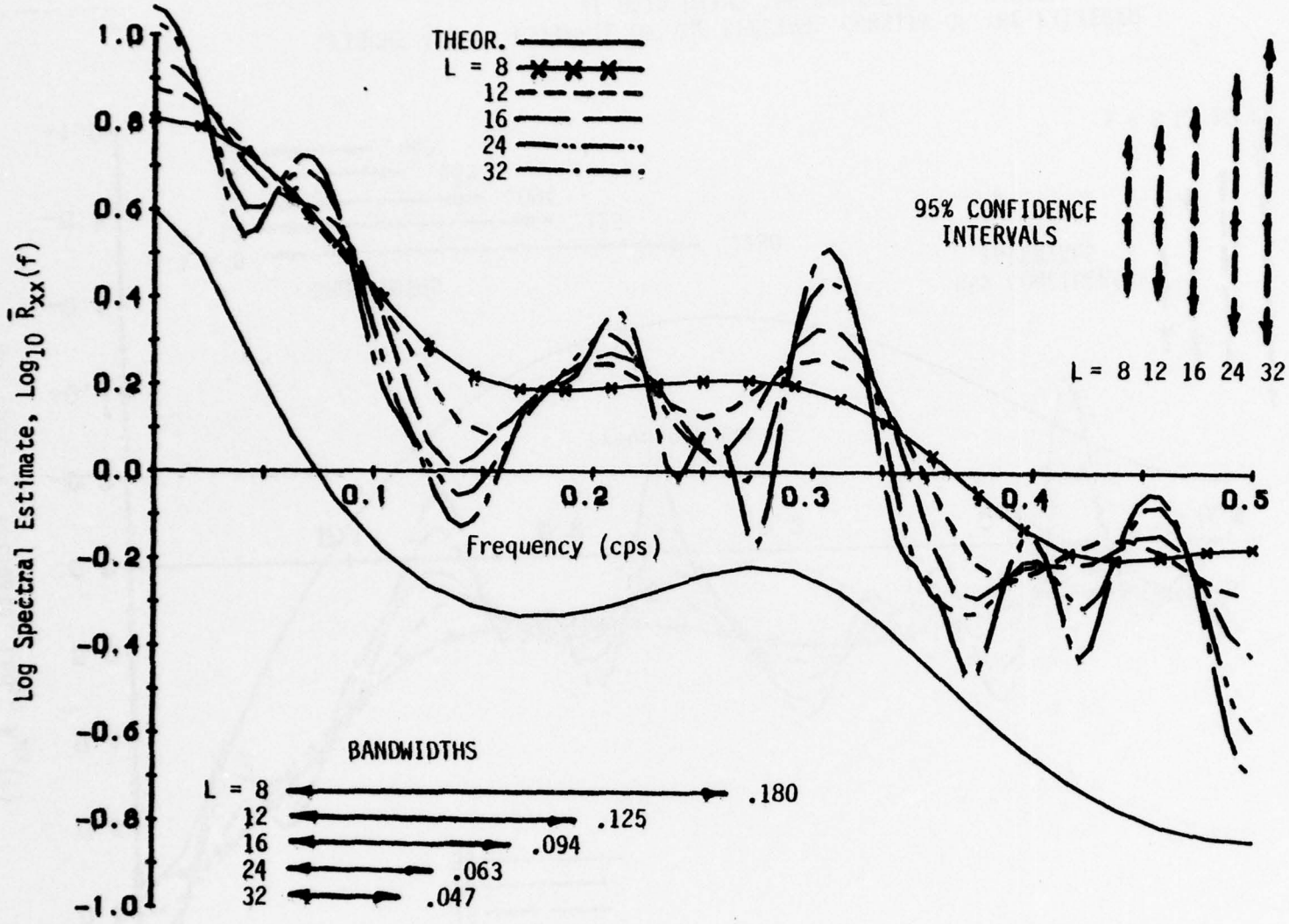

FIGURE 4.2 ESTIMATE OF THE SPECTRAL DENSITY OF THE FILTERED OI DATA USING THE BARTLETT LAG WINDOW

theoretical spectral densities. The plots are still quite smooth and the bandwidth is wide enough to give a great deal of faith to the estimates. By increasing L to 16, the bandwidth seems to be in a very shakey range. In this case, both spectra display the peaks of the theoretical spectral densities and also those of the L = 12 spectra. However, the curves have changed very little from those for which L = 12. Since larger values of L produce many small erratic peaks, we chose L = 16 to estimate the spectral densities of the VI and OI filtered data using Bartlett's lag window.

4.3.2 Estimate of the Spectral Density Function Using Tukey's Lag Window

Using Tukey's lag window given by equation (2.9.6) the smooth spectral density estimates $\bar{R}_{xx}(f)$ for the VI and OI filtered data were calculated for L = 8, 12, 14, 16, and 24 units. Figures 4.3 and 4.4 show the spectral density estimates and the theoretical spectra for the filtered data using the Tukey lag window for the various truncation lengths along with the 95% confidence intervals and the various bandwidths associated with these truncation points. It is clear that for L = 8, the sample spectra have the same general shape as the theoretical spectra and the curves are very smooth. By increasing the truncation value to 12, the plots are still fairly smooth, but peaks appear in both estimates at about f = .19, .31, and .39 cycles per second, and at f = .21 and .45 cycles per second, respectively. At L = 16, the peaks are slightly more pronounced, and as L is increased above 16, more peaks appear at higher frequencies. This indicates that the variances are increasing and, thus, the sample spectra are becoming more erratic for L > 16. On this basis, it was decided to try to obtain better estimates than those calculated by computing additional spectral density estimates for L = 14 units.

Table 4.2 shows, for the various truncation points, the bandwidth, degrees of freedom, and confidence intervals using Tukey's lag window. The bandwidth b = 1.33/L.

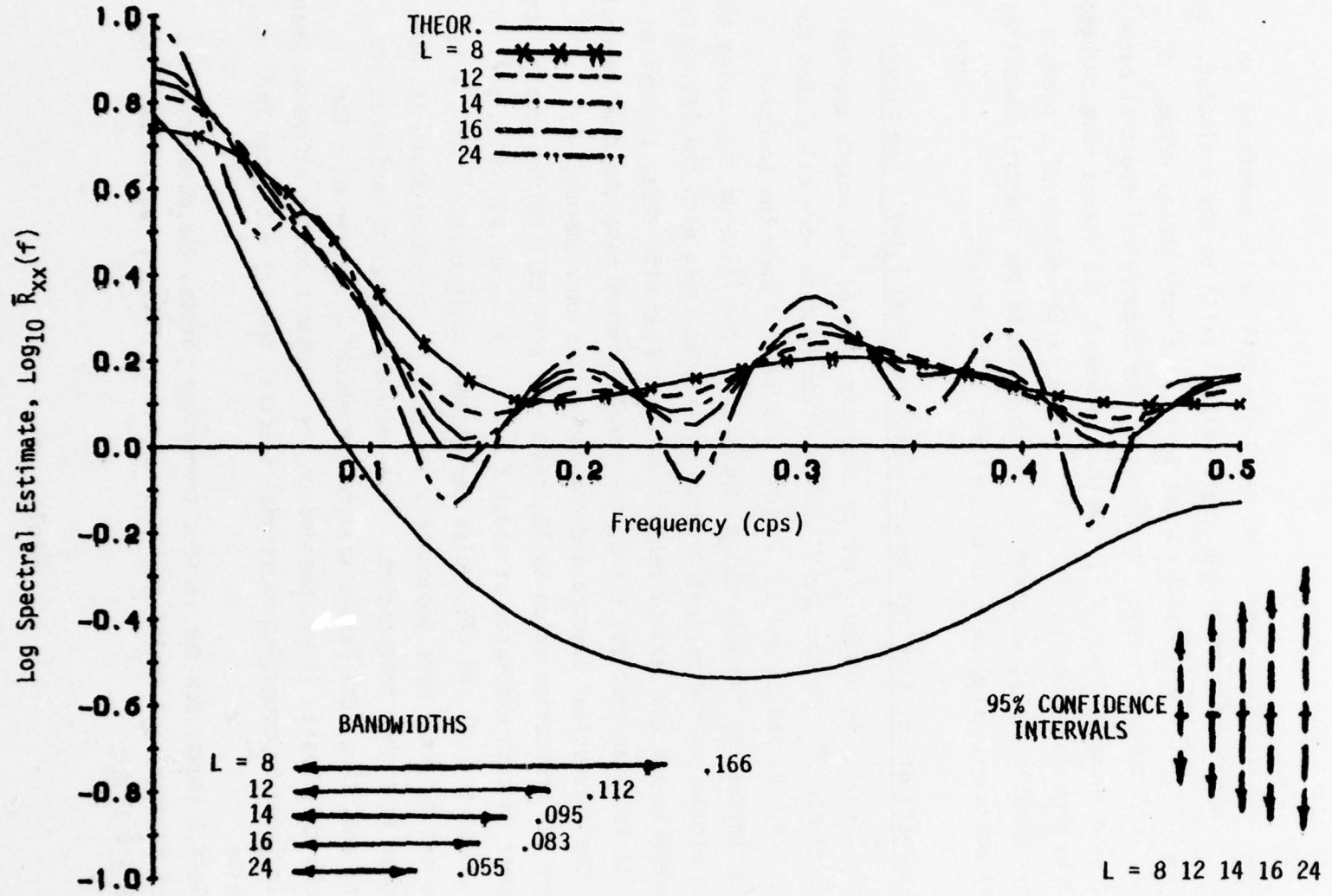

FIGURE 4.3 ESTIMATE OF THE SPECTRAL DENSITY OF THE FILTERED VI DATA USING THE TUKEY LAG WINDOW

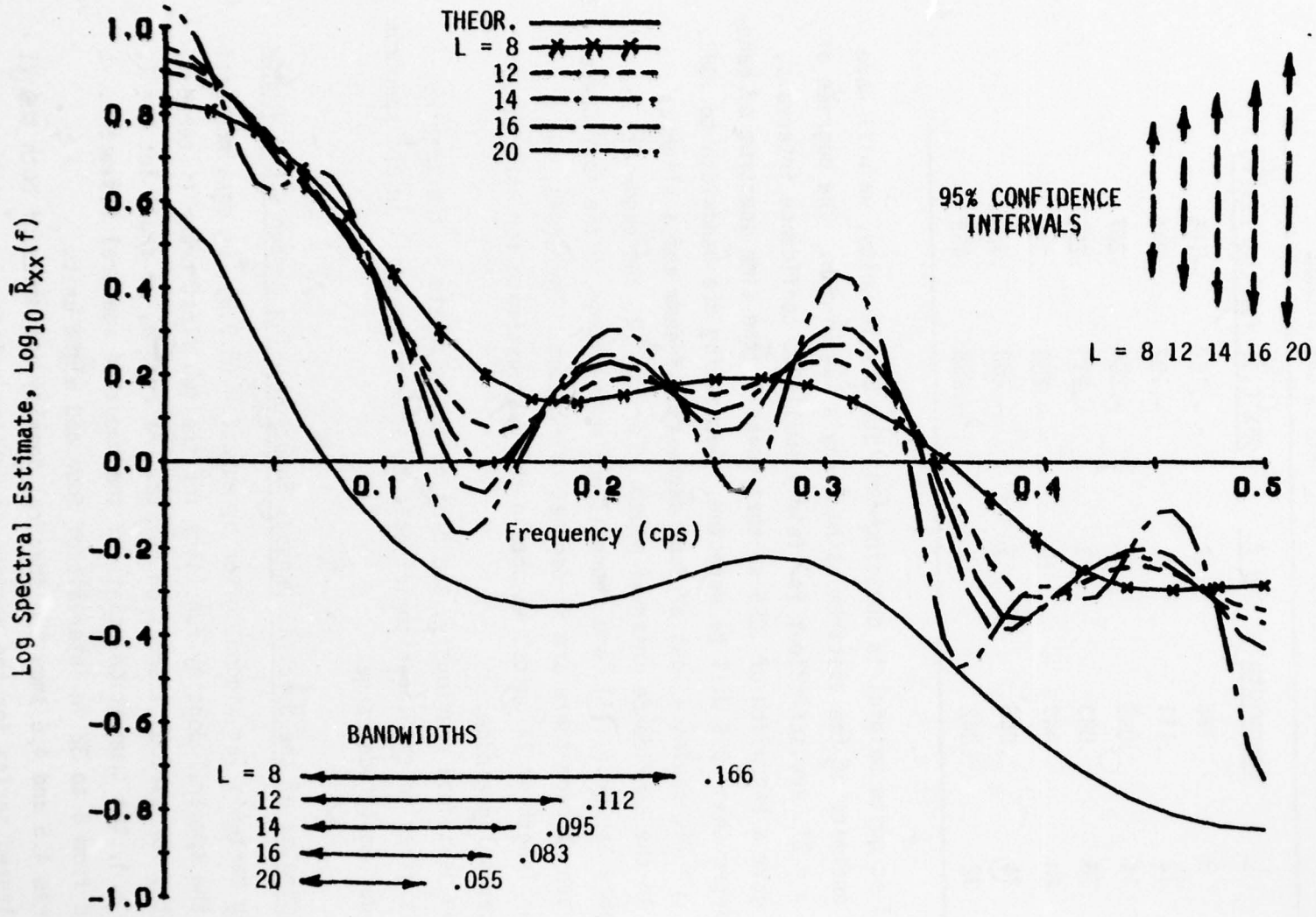

FIGURE 4.4 ESTIMATE OF THE SPECTRAL DENSITY OF THE FILTERED OI DATA USING THE TUKEY LAG WINDOW

Table 4.2 Truncation Point, Bandwidth, Degrees of Freedom, and Confidence Intervals for Tukey's Lag Window

L	Bandwidth	d.f.	95% C.I. for Log $\Gamma_{xx}(f)$	
8	.166	47	-.159	.195
12	.111	31	-.192	.246
14	.095	27	-.204	.267
16	.083	23	-.219	.294
20	.067	19	-.238	.329
24	.055	15	-.263	.380
32	.042	12	-.288	.436

Table 4.2 is quite helpful in deciding that for L = 14 units, we will have the best estimate of the spectrum using Tukey's lag window. The degrees of freedom, $\nu = 27$, are sufficient for fairly small 95% confidence intervals, and this gave a bandwidth of .095 so that peaks in the time spectrum of bandwidths larger than .095 will be detected. Decreasing the bandwidth to .083, that is, L = 16, causes a loss of four degrees of freeom and a slight increase in the confidence interval width. For L = 12, the bandwidth is considerably larger (.111), and there is not much change in the confidence interval even though there are 31 degrees of freedom. Therefore, for a truncation length of 14 units, we obtain the best estimate for both spectra using Tukey's lag window.

As we mentioned previously, the plot of the estimate of the spectral density is given in the logarithmic scale to show more detail in the spectrum over a wider amplitude range.

4.3.3 Estimates of the Spectral Density Function Using Parzen's Lag Window

Using Parzen's lag window, given by equation (2.9.8), we obtained estimates of the spectral density functions for the two first order filtered VI and OI data, for various truncation points. As before, we shall let $\Delta = 1$, so that L = M, the truncation points of the smoothed spectral estimator. L was varied from 8 to 32 in intervals of four and eight units.

Figures 4.5 and 4.6 show the spectral density estimates of both the VI and OI filtered series for the various truncation points along with the

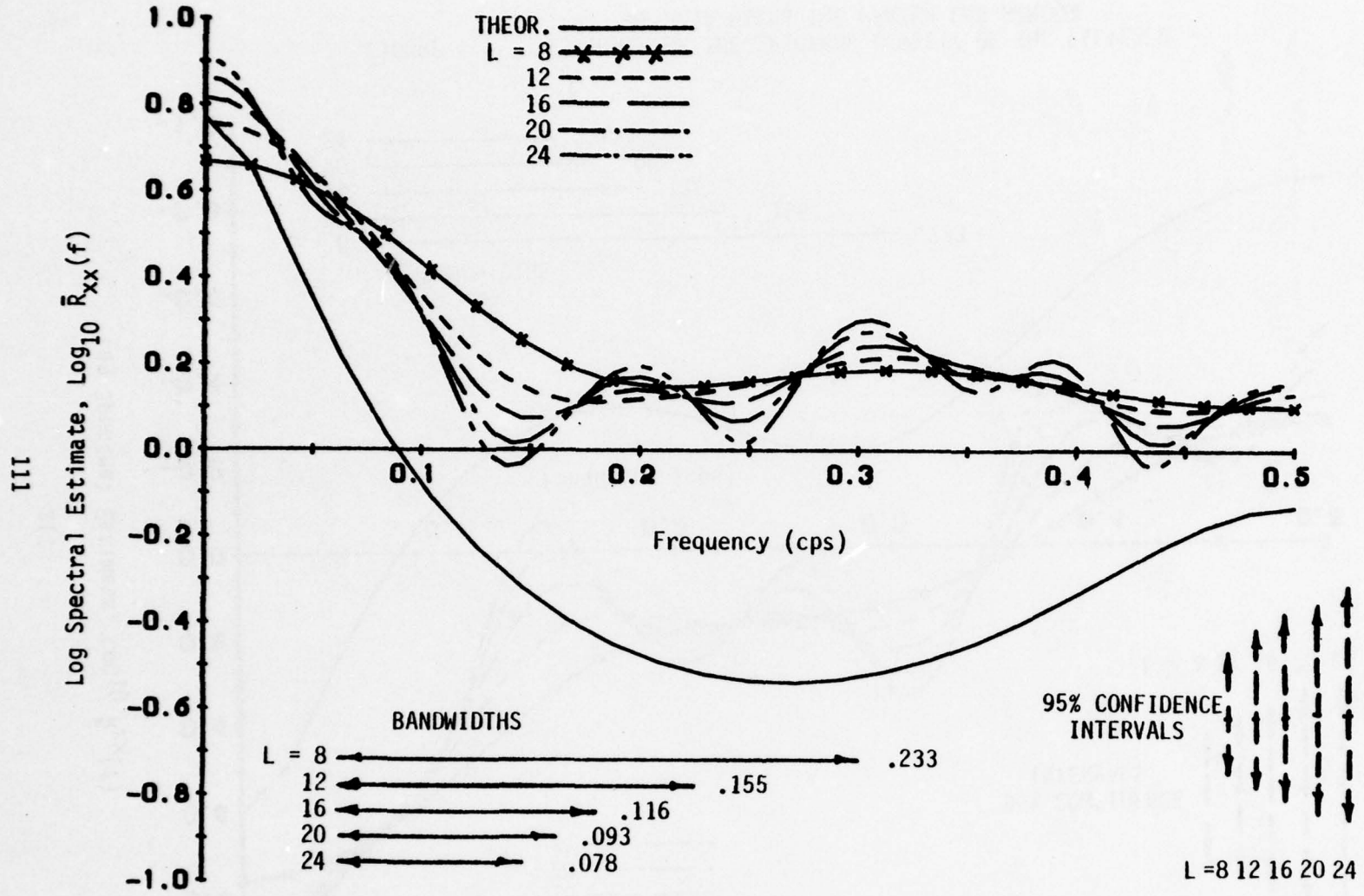

FIGURE 4.5 ESTIMATE OF THE SPECTRAL DENSITY OF THE FILTERED VI DATA USING THE PARZEN LAG WINDOW

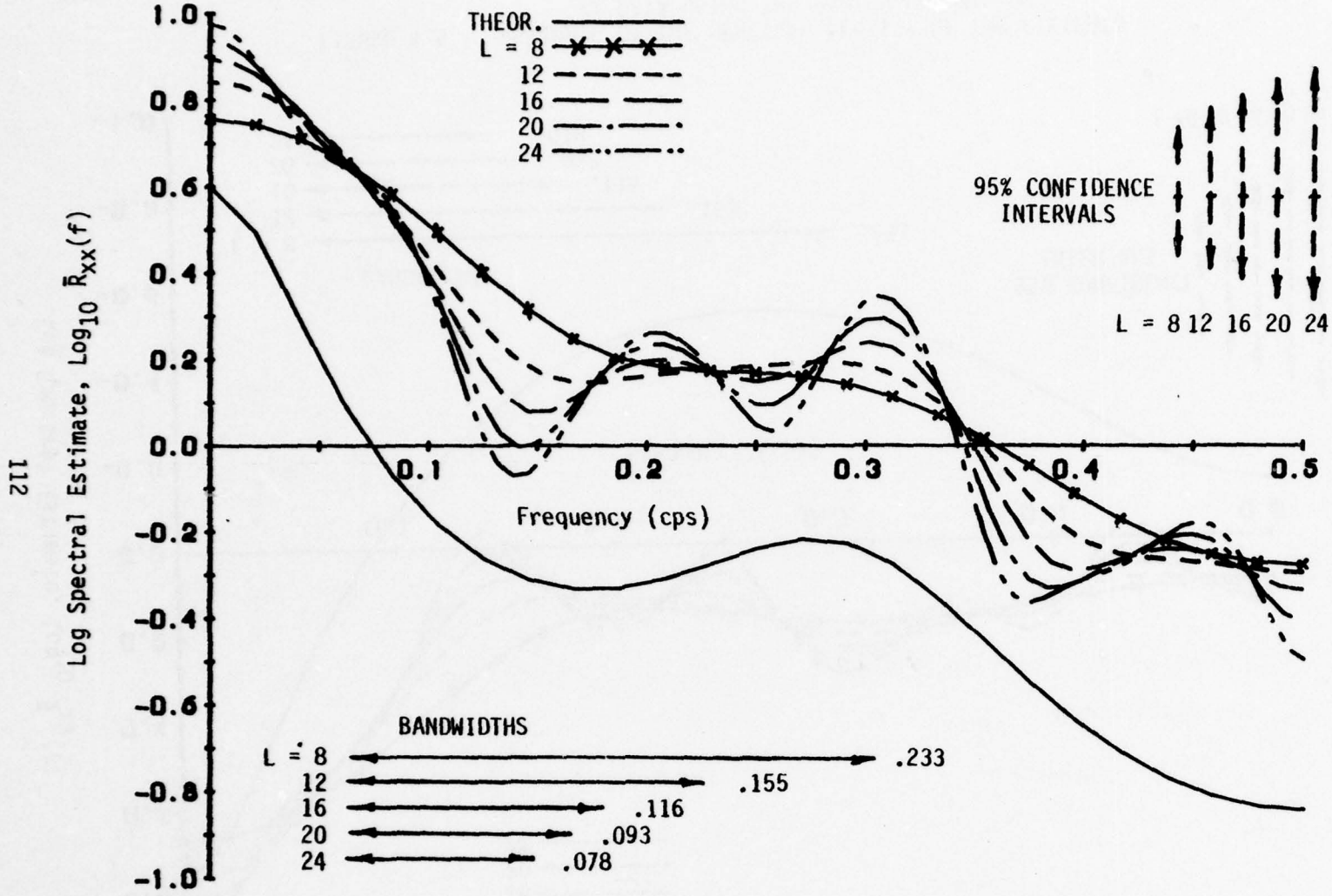

FIGURE 4.6 ESTIMATE OF THE SPECTRAL DENSITY OF THE FILTERED OI DATA USING THE PARZEN LAG WINDOW

theoretical spectral density of the respective autoregressive processes. In addition, 95% confidence intervals and the corresponding bandwidths are displayed. The bandwidth using Parzen's lag window is given by:

$$b = \frac{1.86}{L\Delta} = \frac{1.86}{L} \quad .$$

The degrees of freedom for the confidence intervals were found using the following relationship:

$$\nu = 2 \frac{T}{M} b_1 = 288b \quad ,$$

where $b_1 = 1.86$ for the Parzen window and T = total of observations, which in these cases is 144 soundings. Table 4.3 gives, for the various truncation points, the corresponding bandwidths, degrees of freedom, and a 95% confidence interval for the theoretical spectrum, $\Gamma xx(f)$, for the Parzen lag window.

Table 4.3 Bandwidth, Degrees of Freedom, and 95% Confidence Intervals for Selected Values of L for Parzen's Window

L	Bandwidth	d.f.	95% C.I. for Log $\Gamma xx(f)$	
8	.233	67	-.135	.160
12	.155	44	-.164	.203
16	.116	33	-.186	.235
20	.093	27	-.204	.267
24	.078	22	-.223	.301
32	.058	16	-.255	.365

In selecting a proper value for L for the spectral densities, one should be able to detect peaks in the spectra, have reasonable confidence intervals, and a bandwidth that provides a reasonable bias. For an L value of 8 units, the spectral densities were much too smooth, and we were unable to detect peaks less than .233 wide. Increasing the L values from 16 to 20 units gave a fairly reasonable display of both spectral densities. At L = 20, two major peaks occur that are quite similar to those of the respective theoretical densities. For a truncation point of 24 units, very small peaks began to

appear which indicate that the variances may be influencing each of the densities. This was also evident at L = 32, where the peaks became very erratic and very noticeable. Thus, the choice was narrowed very quickly to choosing either L = 16 or 20 units. The confidence intervals for L = 16 and 20 are .421 and .471, respectively. The bandwidth for L = 20, however, is smaller by about 20% from that of L = 16. Therefore, the spectral densities corresponding to L = 20 units were selected as the most reasonable. The spectral density estimates clearly show, for both the VI and OI filtered series, that most of the power is concentrated at low frequencies. For example, a major peak for the OI spectrum is located at f = .15 cycles per second with smaller peaks located at f = .30 and .41 cycles per second. The bandwidth for L = 20 units is .093, which means that we can detect peaks with a width of this value or greater. The above remarks are graphically verified in figures 4.5 and 4.6 where the theoretical spectral density for the respective autoregressive models are compared with the spectral estimate for L = 8, 12, 16, 20, and 24 units. In addition, the 95% confidence intervals and the corresponding bandwidths for the truncation points are given.

4.4 BIVARIATE SPECTRAL ANALYSIS OF THE IONOSPHERIC INFORMATION

In this section, we shall be concerned with analyzing the *bivariate* behavior of the 13^{th} day observed vertical and oblique incidence ionospheric soundings for the 500 Km experiment. More specifically, estimates of the smoothed *quadrature*, *phase*, and *cross-amplitude* spectra will be obtained using the three lag windows discussed in section 2.9. In addition, estimates of the *coherency spectrum* will be obtained.

Having calculated and plotted the cross-amplitude spectrum, one can detect whether or not frequency components in the vertical incidence soundings are associated with large or small amplitudes at the same frequency in the OI series. The estimate of the phase spectrum of the two stochastic realizations helps us in determining whether or not frequency components in the VI series are in phase or out of phase (lag or lead) with components at the same frequency in the OI series. The cross-amplitude spectrum, $A_{yz}(f)$, is a measure of the covariance that exists between the OI and VI soundings at frequency f, and is the square root of the sum of the squares of the co-spectral and coquadrature spectral estimates. An estimate of the

cross-amplitude spectrum and the *phase* spectrum would suffice to provide a complete description of the behavior of the two series.

In general, the squared *coherency* spectrum plays the role of a correlation coefficient with respect to frequency. Its usefulness lies in the fact that dimensions do not enter the picture when the correlation is measured with respect to frequency. Unlike the squared coherency spectrum, the cross-amplitude spectrum depends upon the dimensions of the OI and VI soundings. This is the reason the squared coherency spectrum is sometimes preferred over the cross-amplitude spectrum and, together with the phase spectrum, will give a complete picture of the cross correlation behavior of the OI and VI soundings.

With respect to the aims of the present study, we will only give the equations (estimates) that characterize the above concepts, and we will not discuss the theoretical implications. For complete details of these concepts, refer to sections 2.5 through 2.9.

4.4.1 Co-Spectrum Estimates Using the Bartlett, Tukey, and Parzen Lag Windows

We shall, in what follows, obtain estimates for the co-spectral, quadrature, phase, and cross-amplitude spectral estimates using Bartlett's lag window. These smoothed estimates were obtained using the truncation points L = M = 8, 12, 16, 24, and 32 units. These truncation points correspond to decreasing the bandwidth to $b = b_1/L = 1.5/L$.

Figure 4.7 shows the smoothed co-spectral estimates. Similarly, figure 4.8 shows the various smoothed quadrature spectral estimates. It is clear that for $L \geq 24$ units, the estimates in both cases become very erratic. As we mentioned previously, compromising between bias and variance, it appears that for L = 16 units, we have the best estimate using Bartlett's lag window with b = .094 and $\nu = 27$ degrees of freedom. The smoothed cross-amplitude spectral estimate and the smoothed phase spectral estimate, plotted for L = 16, each on separate sets of axes to enhance the details of the series, are shown in figures 4.9 and 4.10, respectively.

The smoothed co-spectral, quadrature, phase, and cross-amplitude spectral estimates were similarly obtained using Tukey's lag window. The truncation points used for the co-spectral and quadrature spectral estimates

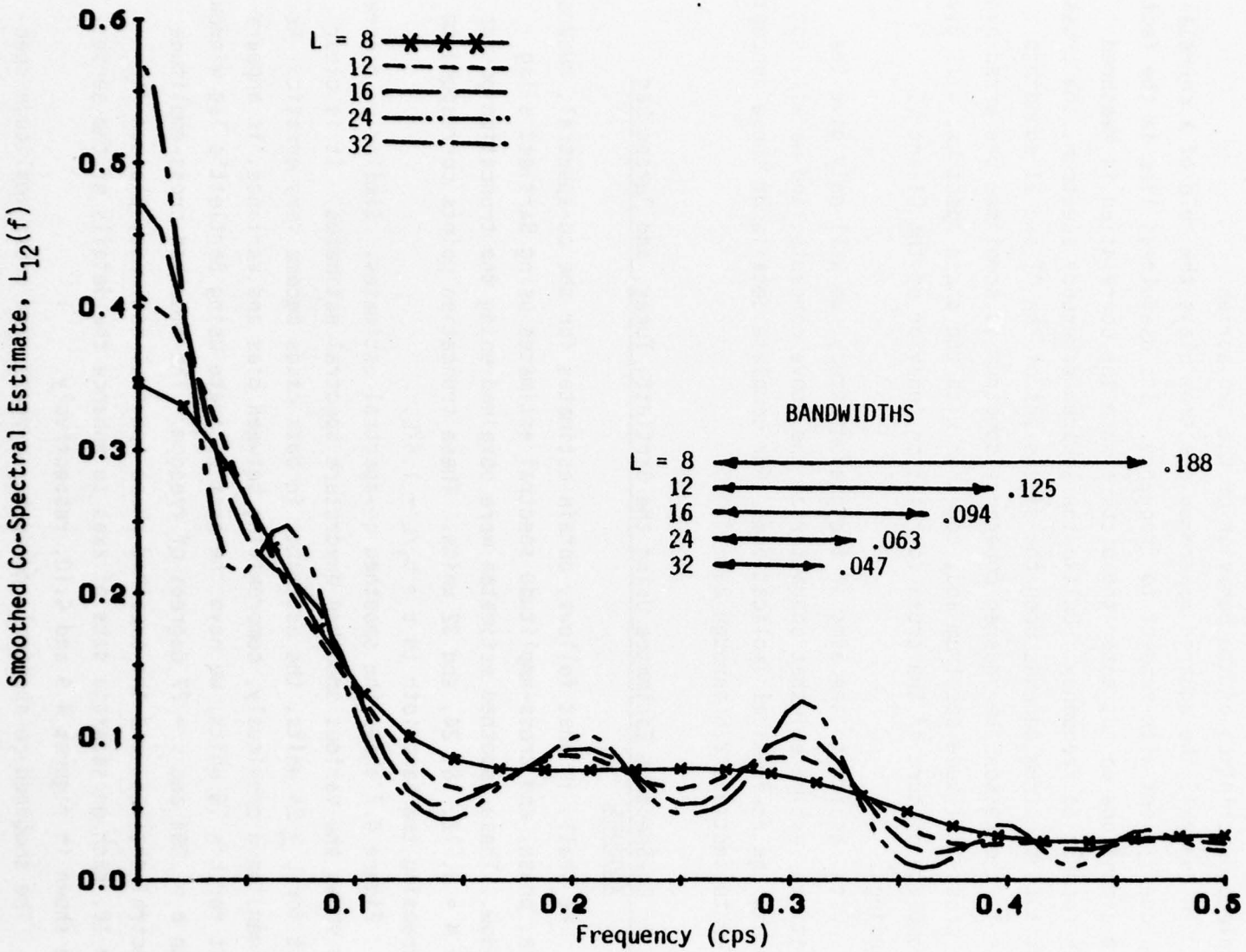

FIGURE 4.7 SMOOTHED CO-SPECTRAL ESTIMATES USING THE BARTLETT LAG WINDOW

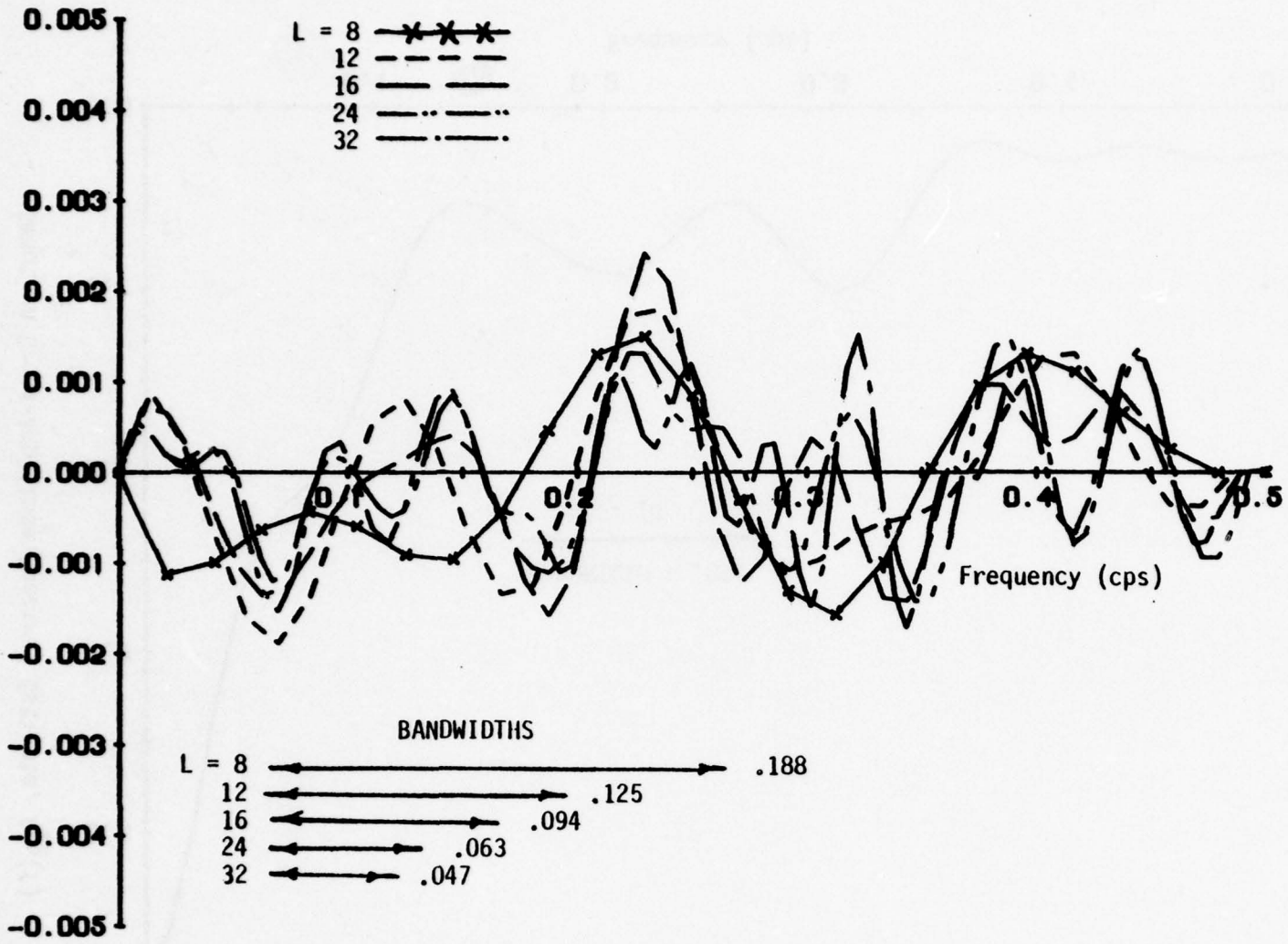

FIGURE 4.8 SMOOTHED QUADRATURE SPECTRAL ESTIMATES USING THE BARTLETT LAG WINDOW

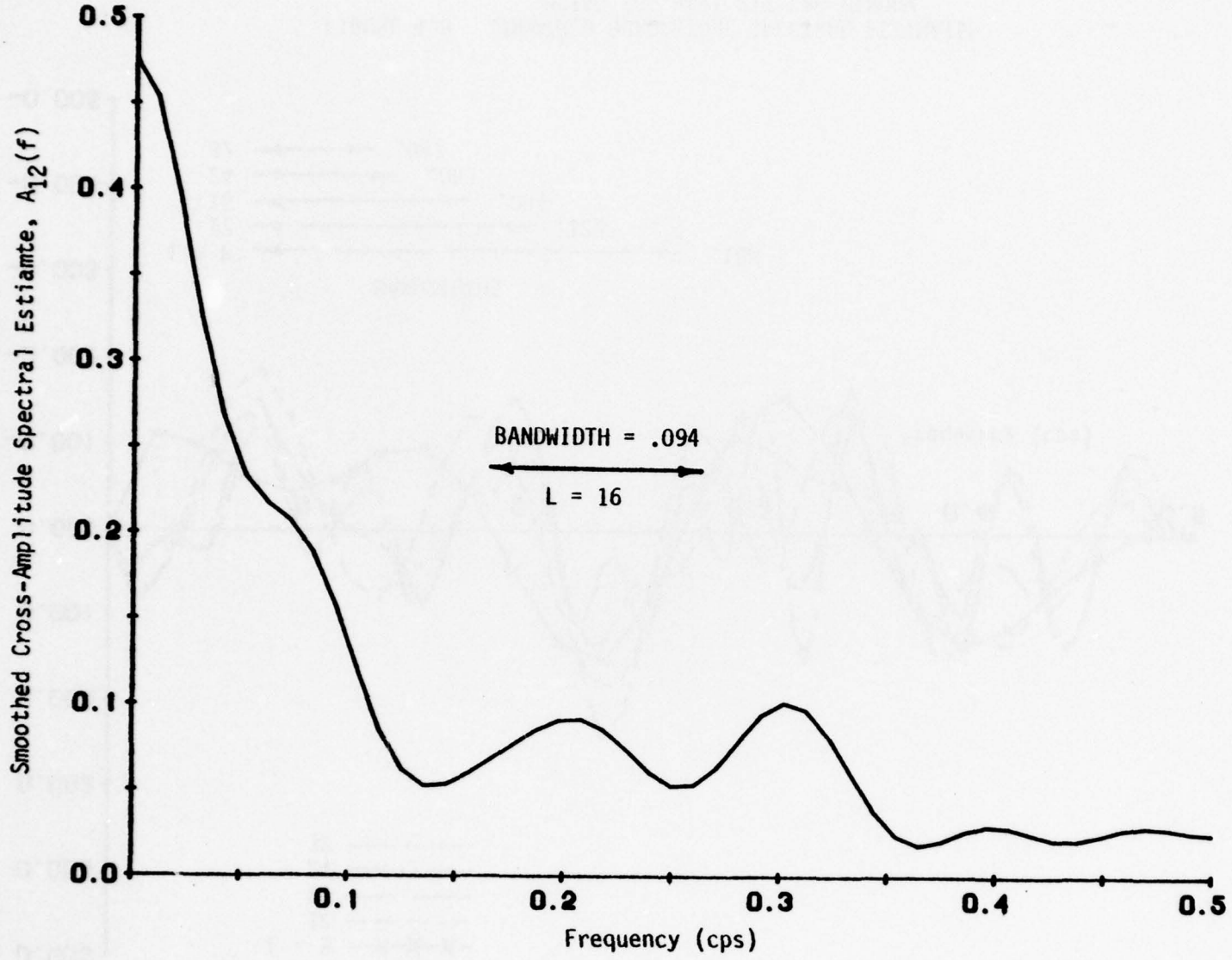

FIGURE 4.9 SMOOTHED CROSS-AMPLITUDE SPECTRAL ESTIMATE USING THE BARTLETT LAG WINDOW FOR L = 16

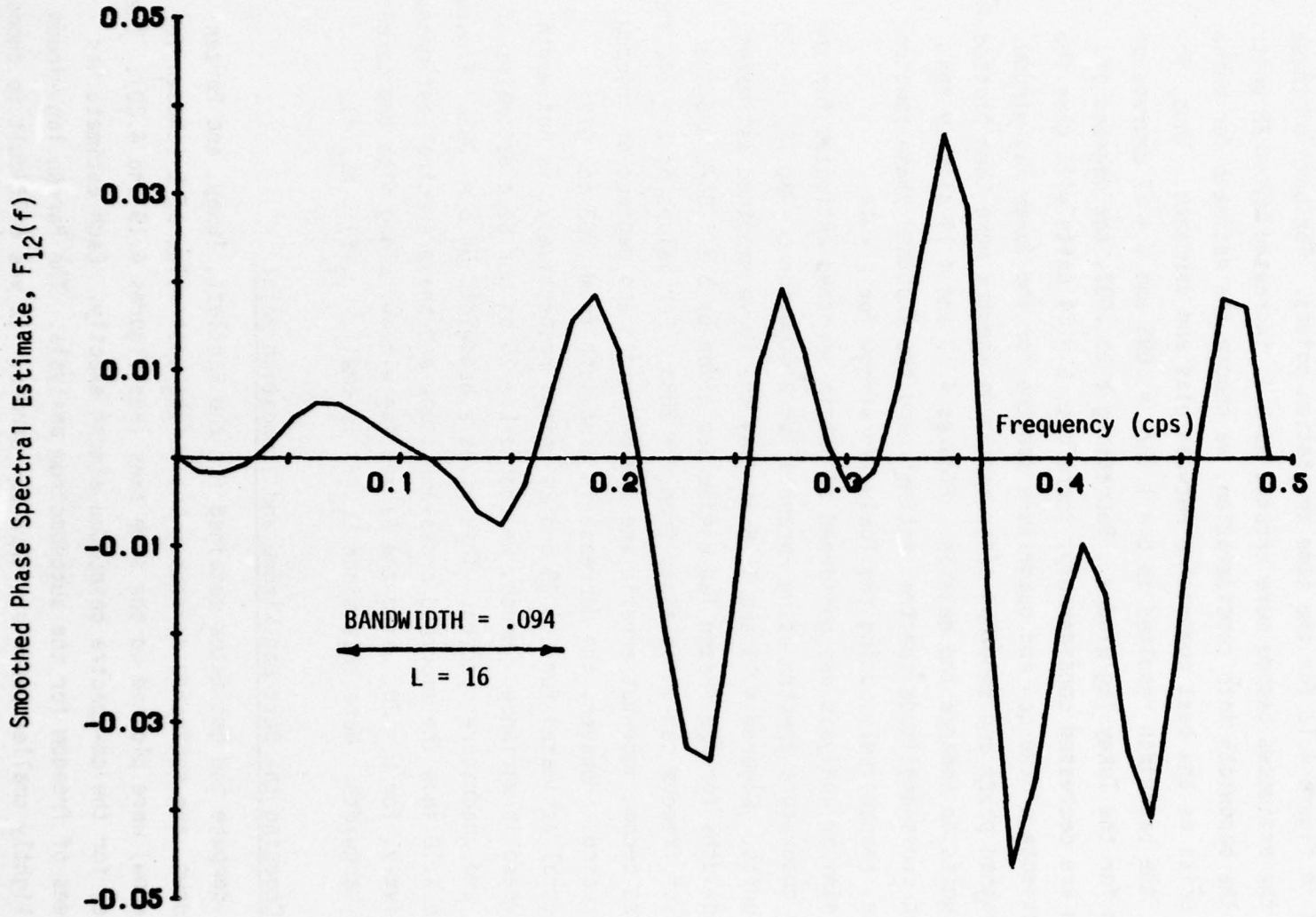

FIGURE 4.10 SMOOTHED PHASE SPECTRAL ESTIMATE USING THE BARTLETT LAG WINDOW FOR L = 16

were L = 8, 12, 14, 16, 20 and 24 units. Figure 4.11 displays the smoothed co-spectral estimates. The smoothed quadrature spectral estimates are plotted in figure 4.12 for the same truncation points. For both of these cases, the estimates become more erratic as L is increased beyond 20 units. Taking the bandwidth into consideration, we choose the estimate for which L = 14 units as the best compromise between bias and variance. Thus, for L = 14, the bandwidth resulted in b = 1.33/L = .095 and ν = 27 degrees of freedom for the Tukey lag window. Decreasing b to .083, the degrees of freedom are decreased considerably; therefore, L = 14 units will give the best estimate of the co- and quadrature spectra for the Tukey lag window. The smoothed phase and smoothed cross-amplitude spectra were then plotted for L = 14 units to enhance the details. Figures 4.13 and 4.14 display the smoothed cross-amplitude spectral estimate and the smoothed phase spectral estimate, respectively, using the Tukey lag window for L = 14.

A similar analysis was performed to obtain smoothed estimates for the co- and quadrature spectra using Parzen's lag window for L = 8, 12, 16, 20 and 24 units. Figures 4.15 and 4.16 display the above smoothed estimates. The bandwidths for the Parzen lag window are given by b = 1.86/L and the degrees of freedom can be obtained from ν = 288b. For values of $L \geq 24$, the estimates become somewhat erratic and the bandwidth and degrees of freedom are decreased. However, the decrease in bandwidth from .093 to .078 (co-spectral estimate) for L = 20 and 24 units, respectively, is not worth the decrease in variance. Hence, we choose L = 20 as our best estimates of the co- and quadrature spectra. This gives a bandwidth of b = .093. Figures 4.17 and 4.18 show the smoothed cross-amplitude and phase spectral estimates, respectively, for L = 20, using the Parzen lag window, along with the corresponding bandwidth. Note that since $F_{12}(f)$ is small, $L_{12}(f) \simeq A_{12}(f)$.

4.4.2 Choosing the Best Lag Window and Truncation Point

To compare the estimates obtained for the Bartlett, Tukey, and Parzen lag windows, the estimates corresponding to the best value of L (chosen for each window) were plotted on the same axes (see figures 4.19 and 4.20). The estimates for the co-spectra coincided almost exactly. Each estimate has 27 degrees of freedom for the autospectrum analysis. The Parzen lag window has a slightly smaller bandwidth than the others. It was difficult to choose

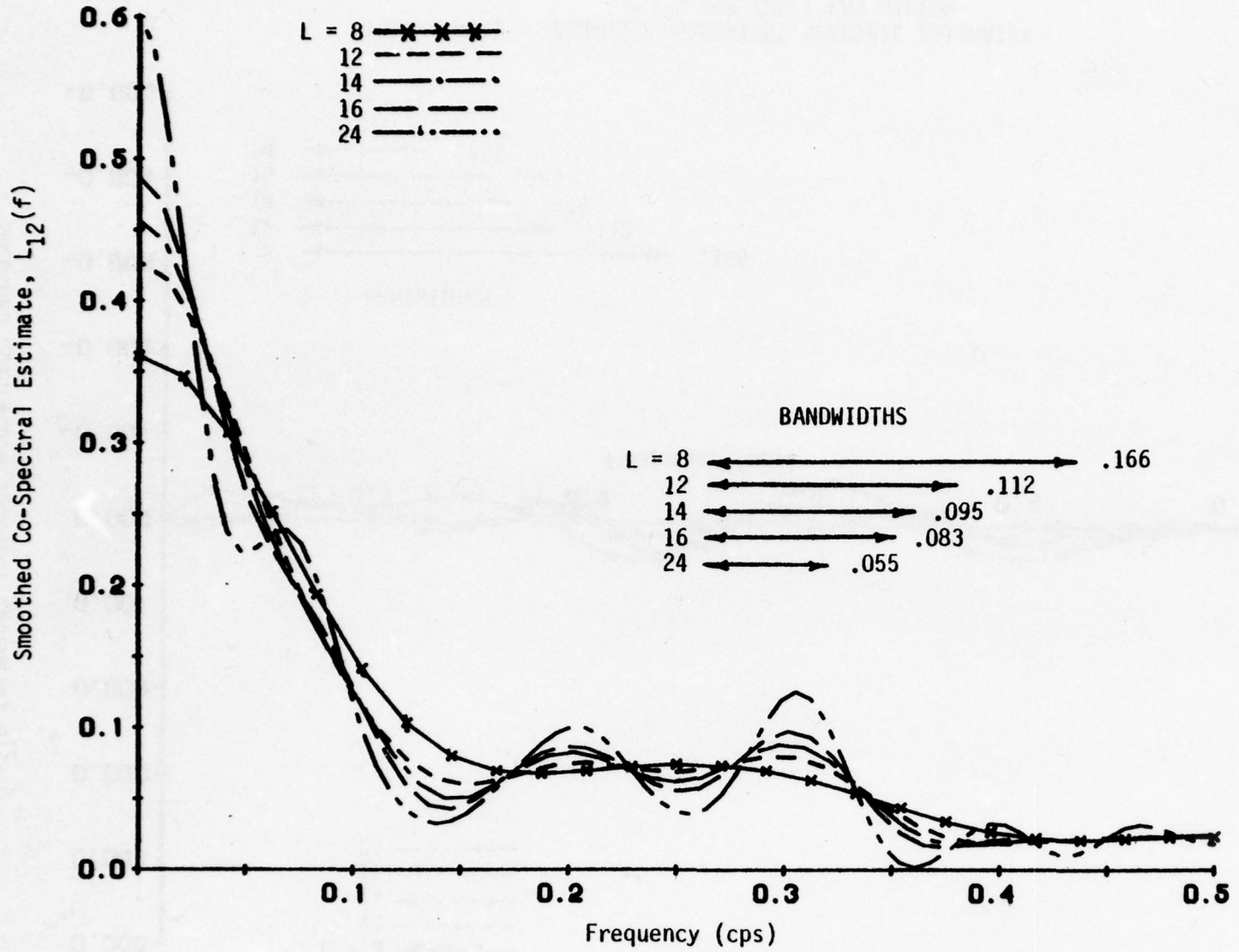

FIGURE 4.11 SMOOTHED CO-SPECTRAL ESTIMATES USING THE TUKEY LAG WINDOW

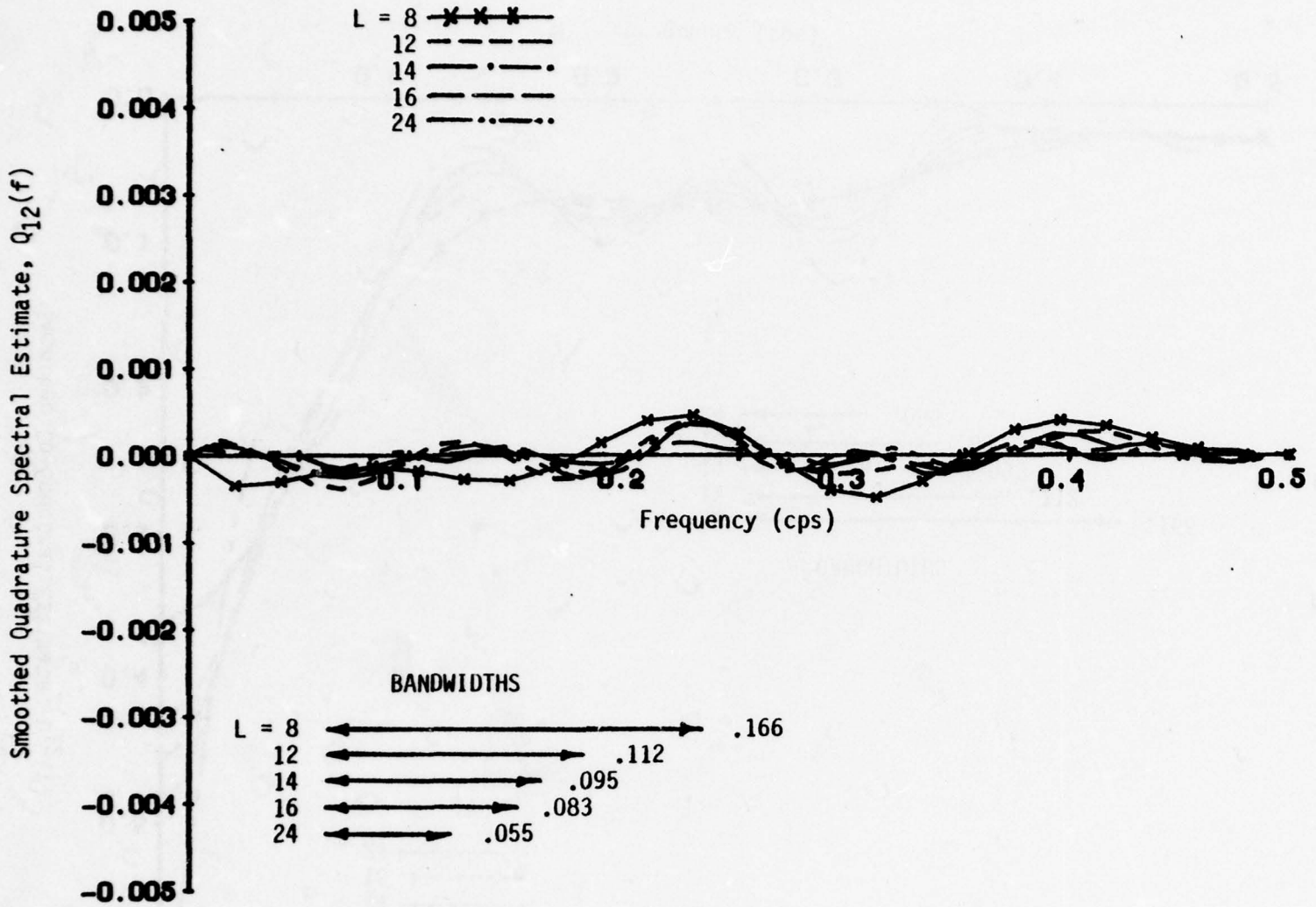

FIGURE 4.12 SMOOTHED QUADRATURE SPECTRAL ESTIMATES USING THE TUKEY LAG WINDOW

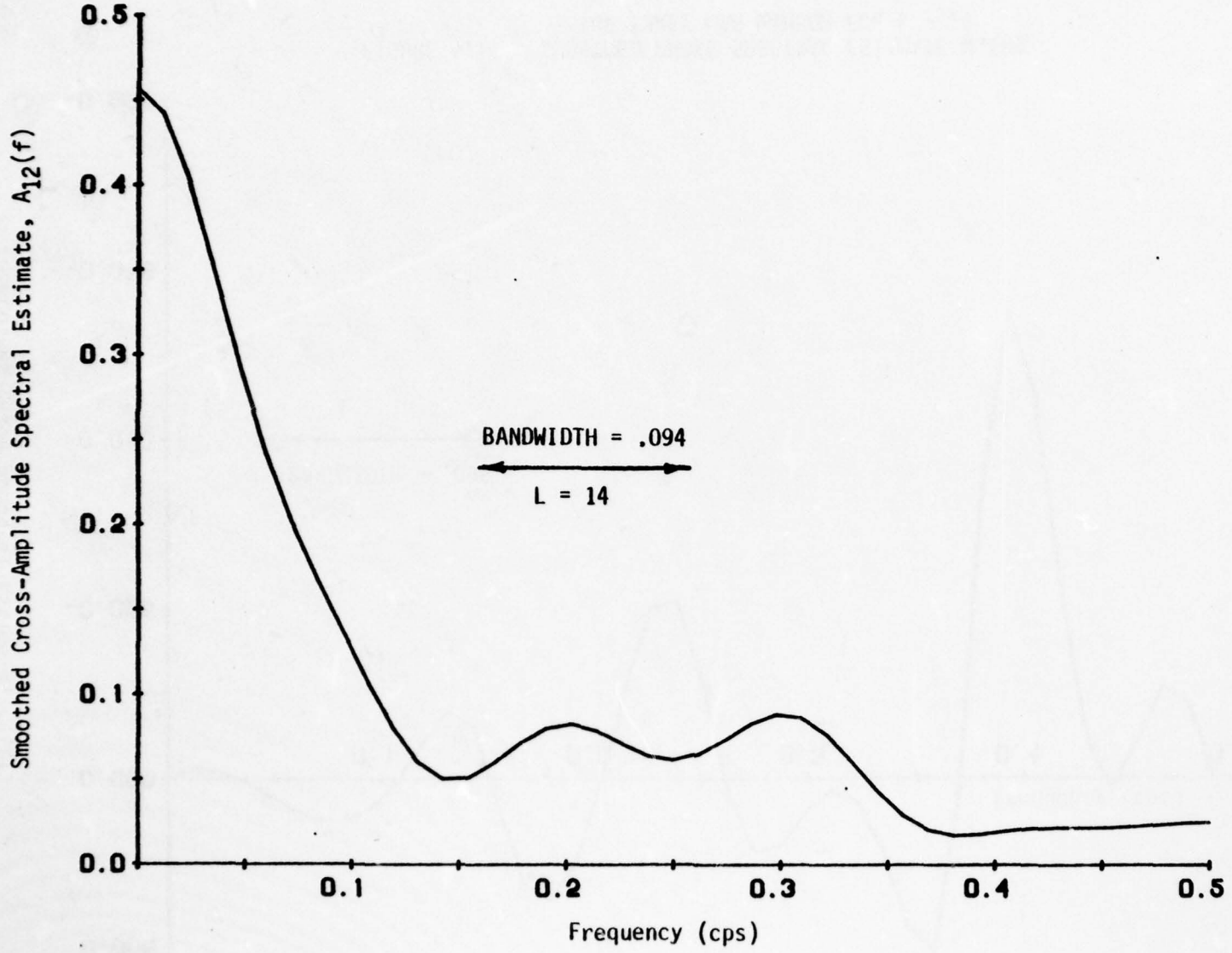

FIGURE 4.13 SMOOTHED CROSS-AMPLITUDE SPECTRAL ESTIMATE USING THE TUKEY LAG WINDOW FOR L = 14

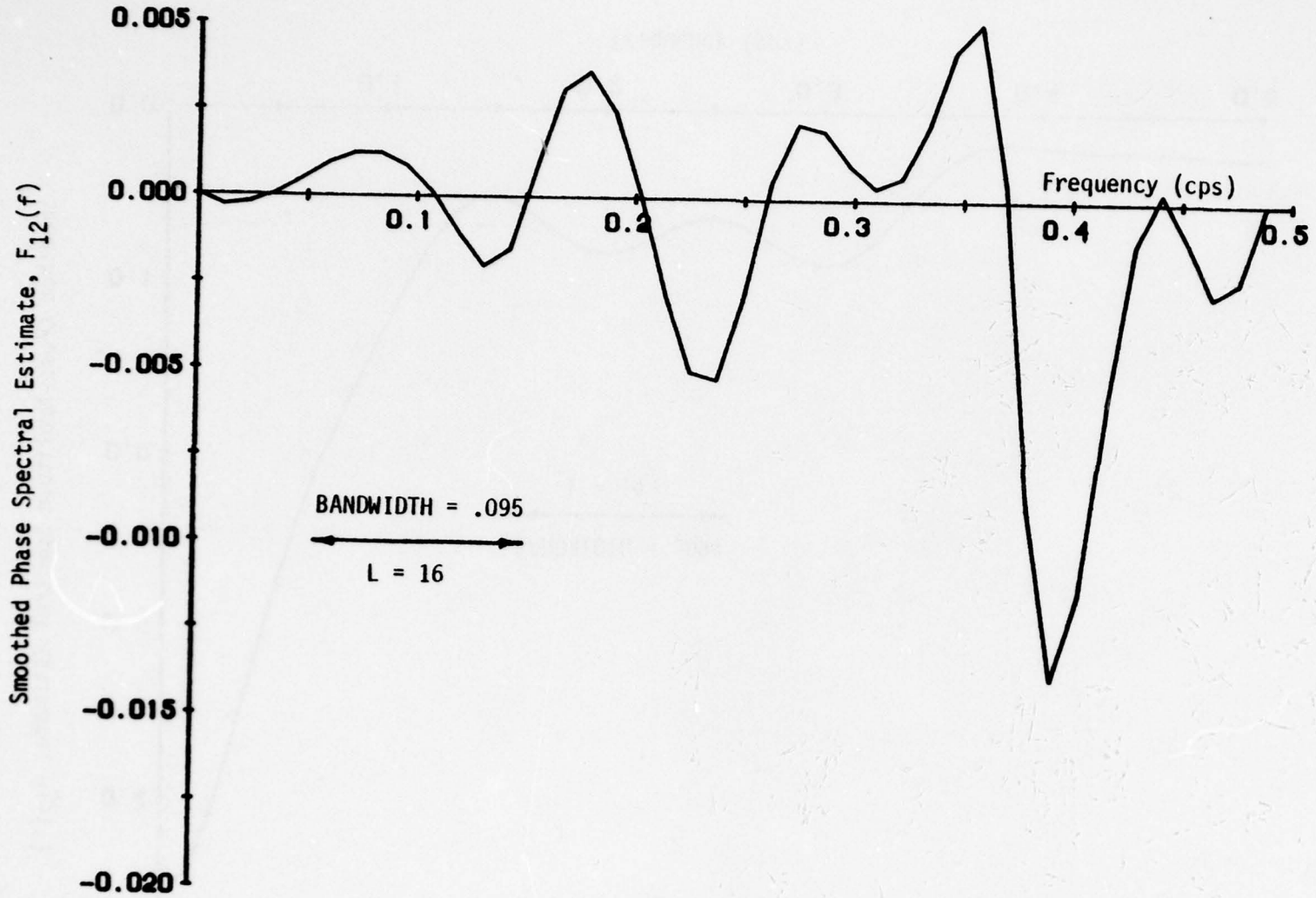

FIGURE 4.14 SMOOTHED PHASE SPECTRAL ESTIMATE USING THE TUKEY LAG WINDOW FOR L = 14

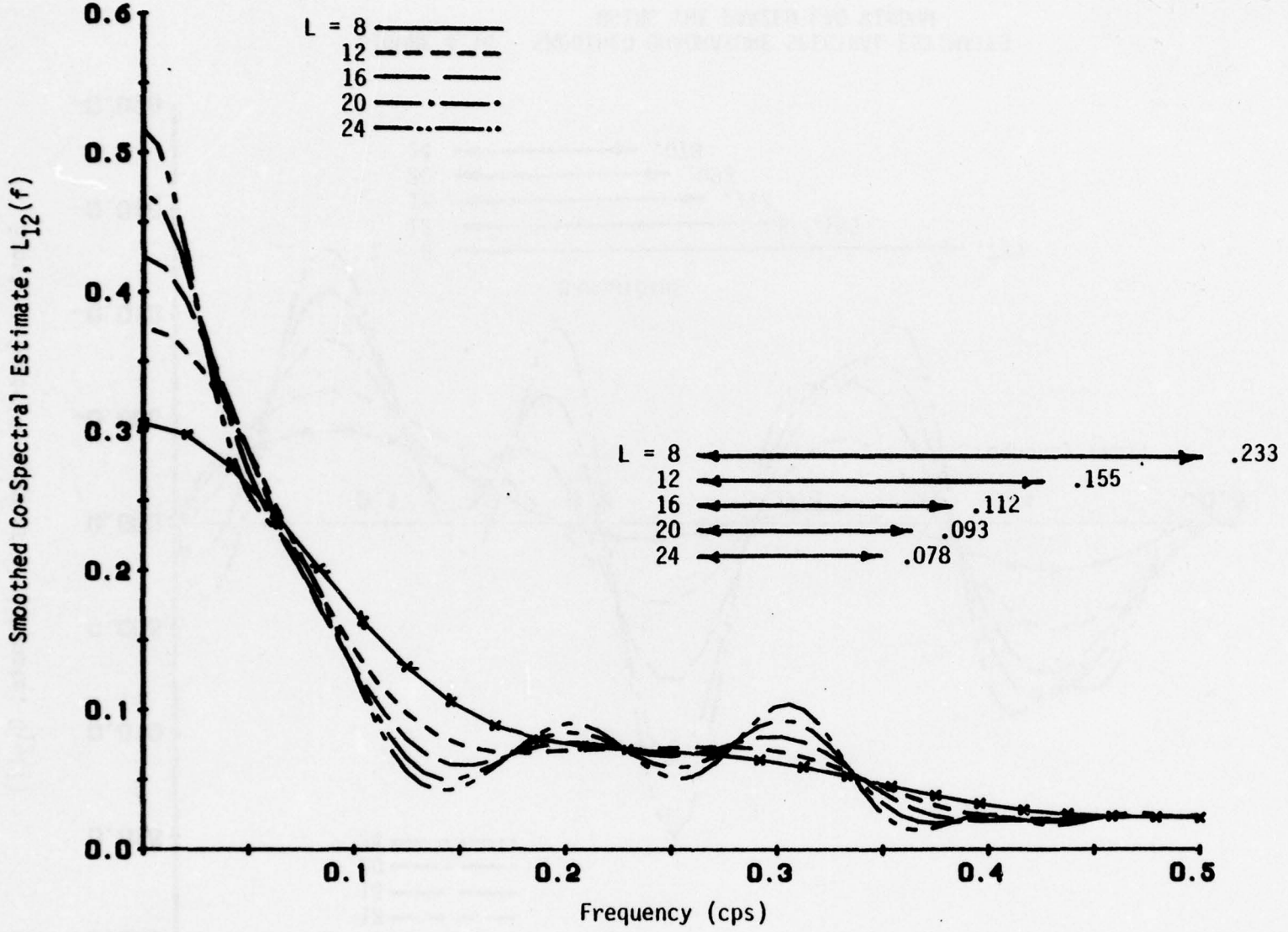

FIGURE 4.15 SMOOTHED CO-SPECTRAL ESTIMATES USING THE PARZEN LAG WINDOW

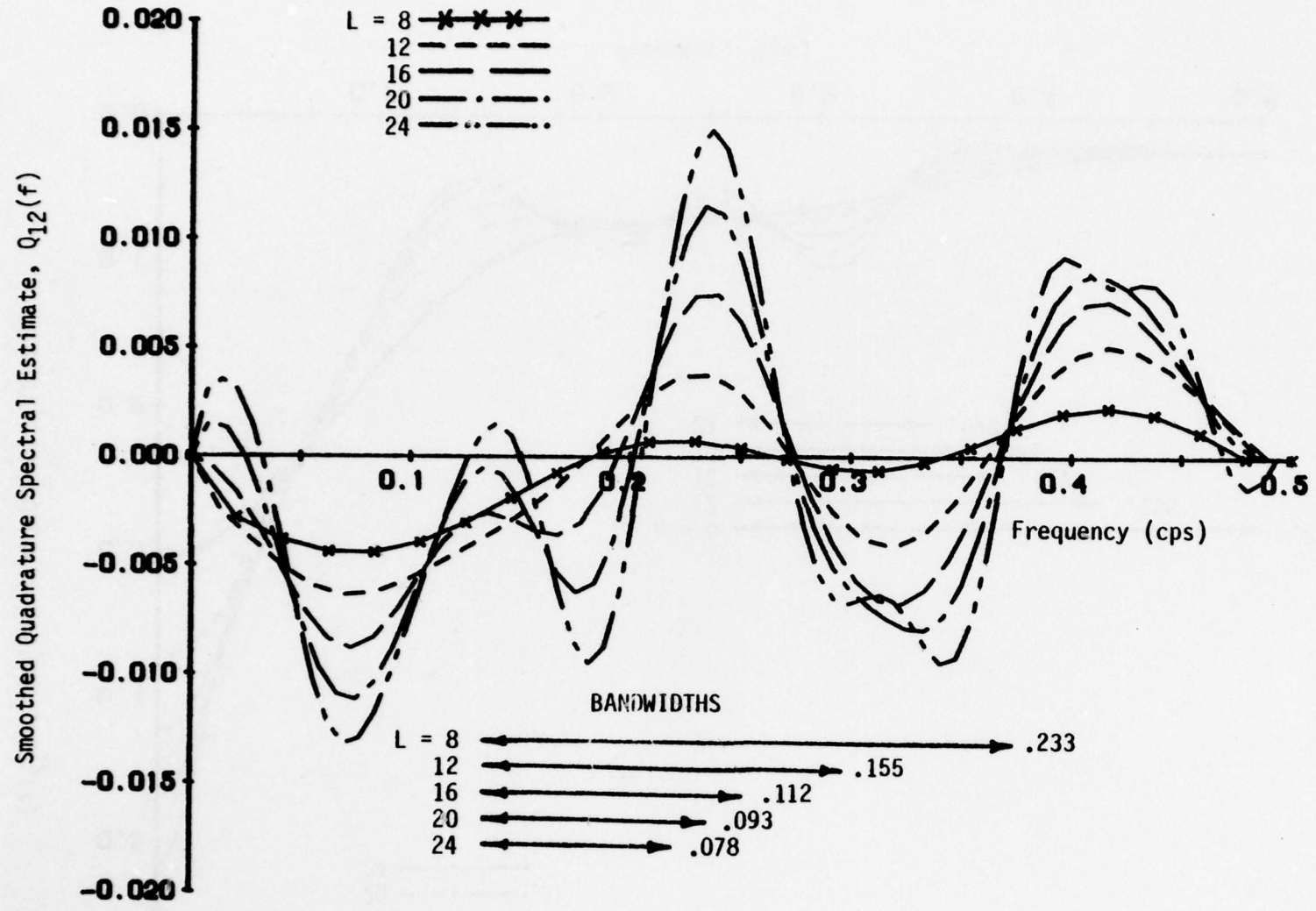

FIGURE 4.16 SMOOTHED QUADRATURE SPECTRAL ESTIMATES USING THE PARZEN LAG WINDOW

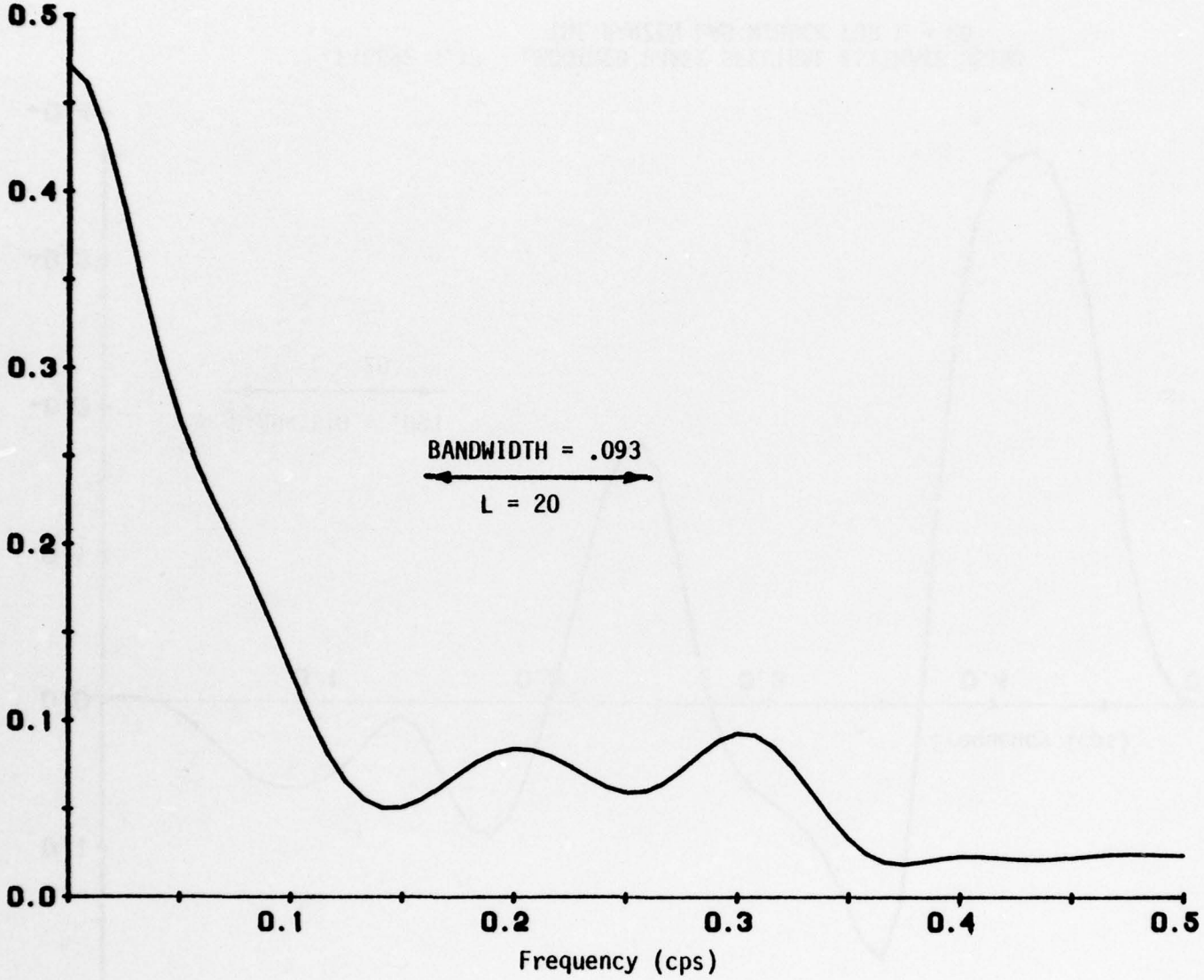

FIGURE 4.17 SMOOTHED CROSS-AMPLITUDE SPECTRAL ESTIMATE USING THE PARZEN LAG WINDOW FOR L = 20

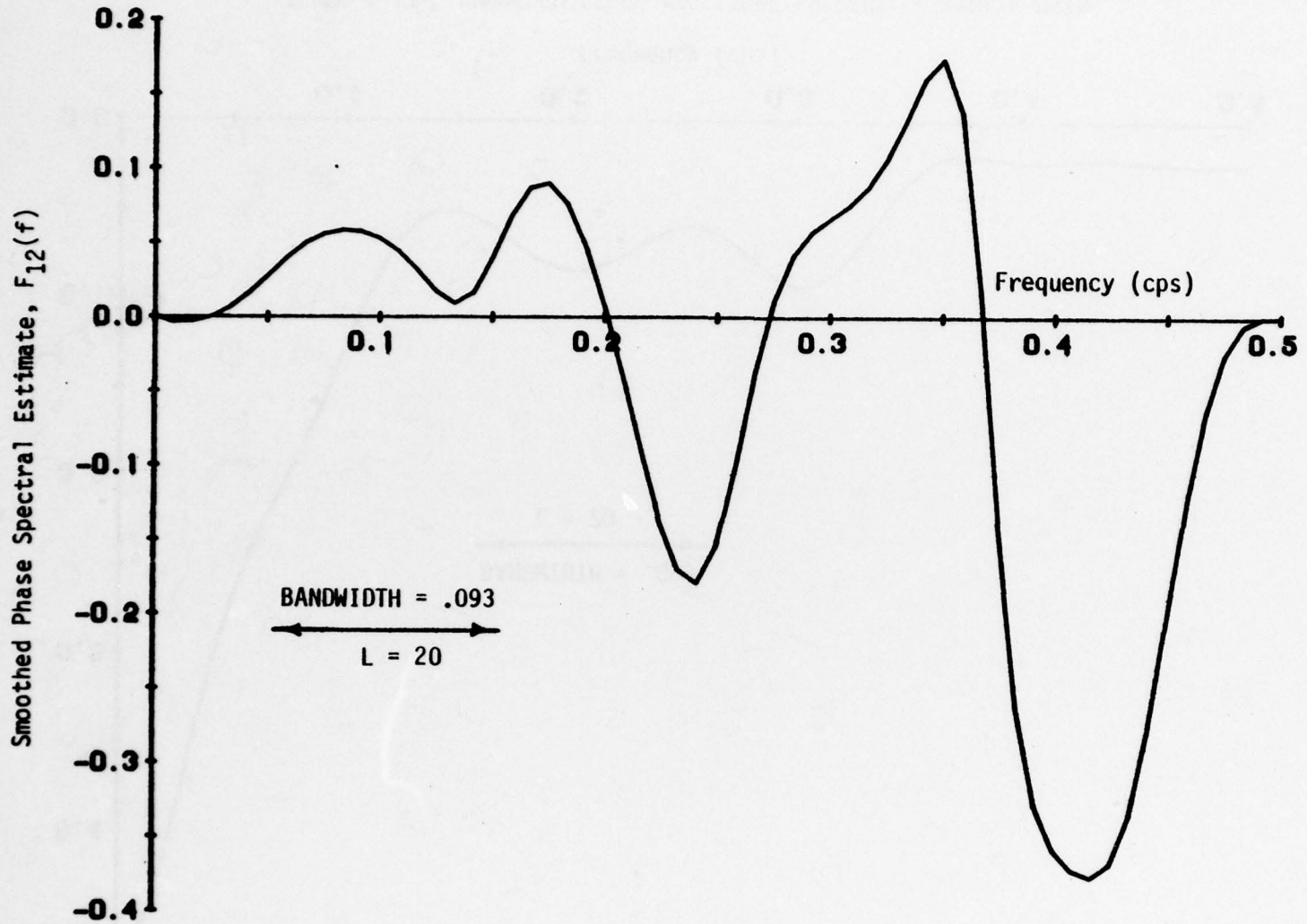

FIGURE 4.18 SMOOTHED PHASE SPECTRAL ESTIMATE USING THE PARZEN LAG WINDOW FOR L = 20

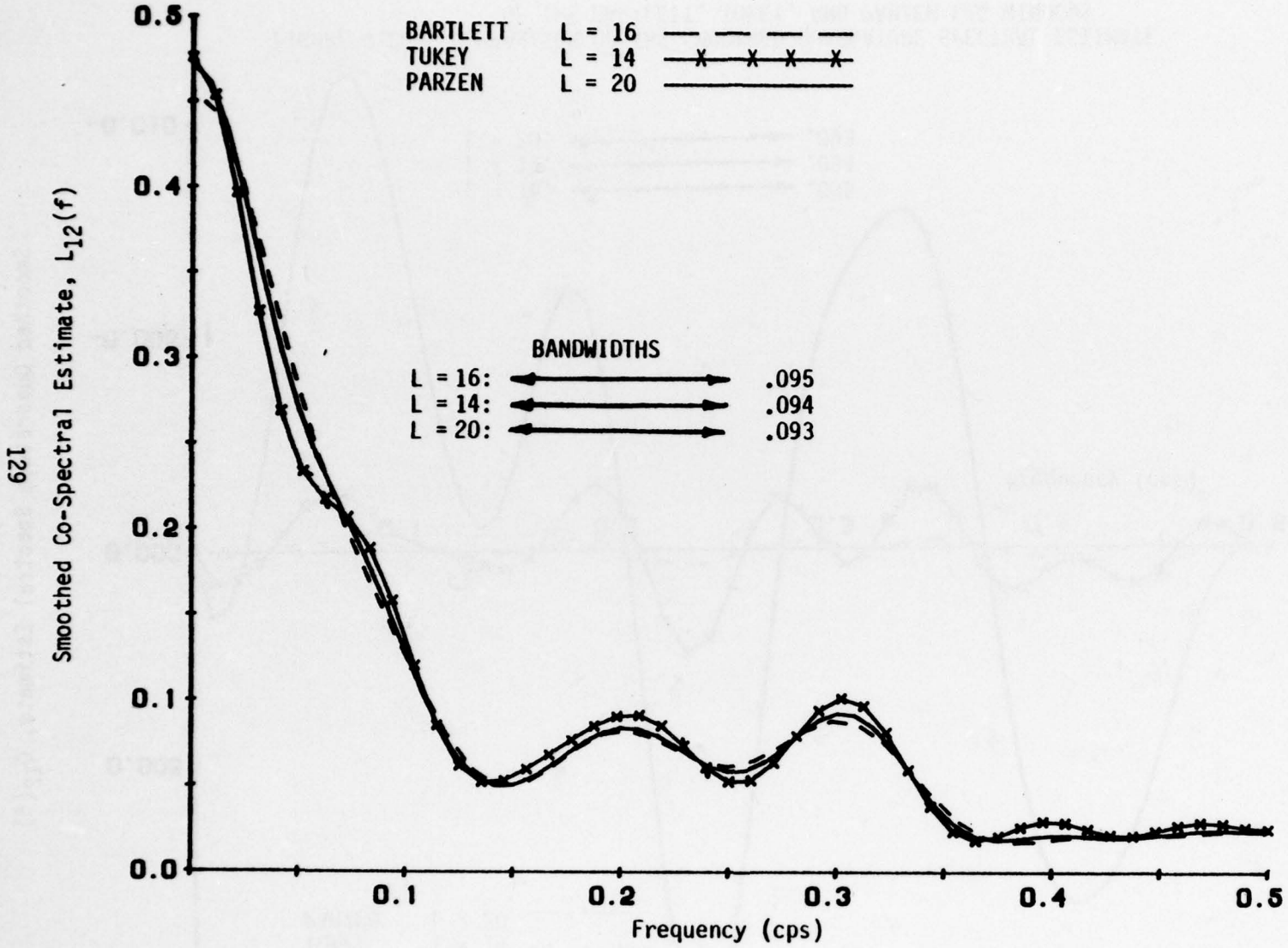

FIGURE 4.19 COMPARISON OF THE SMOOTHED CO-SPECTRAL ESTIMATE OF THE BARTLETT, TUKEY, AND PARZEN LAG WINDOWS

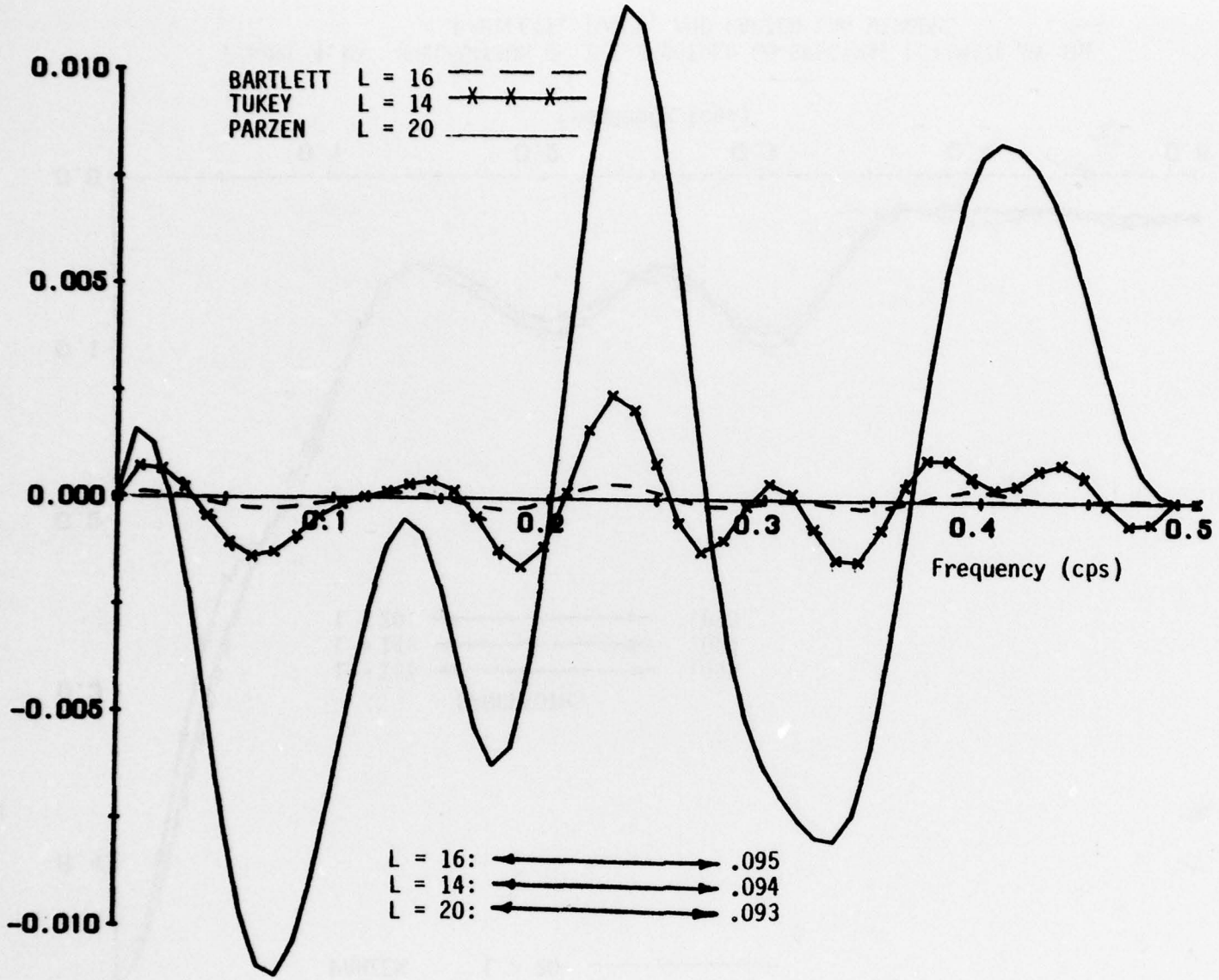

FIGURE 4.20 COMPARISON OF THE SMOOTHED QUADRATURE SPECTRAL ESTIMATE OF THE BARTLETT, TUKEY, AND PARZEN LAG WINDOWS

the best window, but since Parzen's lag window for L = 20 units gave a bandwidth of .093, it was chosen as the best smoothed estimate of the co- and quadrature spectra. The smoothed estimates for the phase and cross-amplitude spectra are also best represented by the lag window of L = 20 units. The smoothed sample co-spectral estimate estimates the covariance due to the in-phase components. There are peaks at about .20 and .31 cycles per second which correspond to the peaks in the autospectra due to the fact that the variance is a special case of the covariance (see figure 4.21). At frequencies less than .15 cycles per second, the covariance between the VI and OI realizations is fairly large and constant over the frequency range 0 to .15 cycles per second. The variance at most frequencies in the autospectra is fairly large. However, the covariance distribution of the in-phase components of the filtered ionospheric series is small, and therefore, the series in-phase components are not very dependent. The larger value of the sample cospectrum is near 0 cycles per second corresponding to variance values of autospectra of about 10 at the same frequency for the Parzen lag window. However, L = 20 units, and hence, the correlation is small as will be verified by the squared coherency spectral estimate.

The smoothed quadrature spectral estimate estimates the covariance of the out-of-phase components of the two filtered time series. This also shows that there is small covariance between the out-of-phase components of the two filtered series and, hence, that they are not very correlated. The largest value of the estimate is .012 for the chosen lag window (Parzen, L = 20), and the smallest value is -.011 (see figure 4.22). One can conclude, therefore, that there is little covariance exhibited throughout the range 0 to .50 cps., but the out-of-phase components vary in a sinusoidal manner at all frequencies.

The smoothed phase spectral estimate estimates the phase angle in radians by which the VI filtered time series leads or lags the filtered OI series (see figure 4.18). At frequencies 0 to .05 cps., the phases are approximately the same (phase spectral estimate near 0). At frequencies between .05 cps. and .20 cps., the *in-phase components* of the two time series *lag* the out-of-phase components very slightly. From .20 cps. to approximately .27 cps., the *out-of-phase components lag* the in-phase components. From .27 cps. to .37 cps., the *in-phase is lagging,* and from .37 cps. to

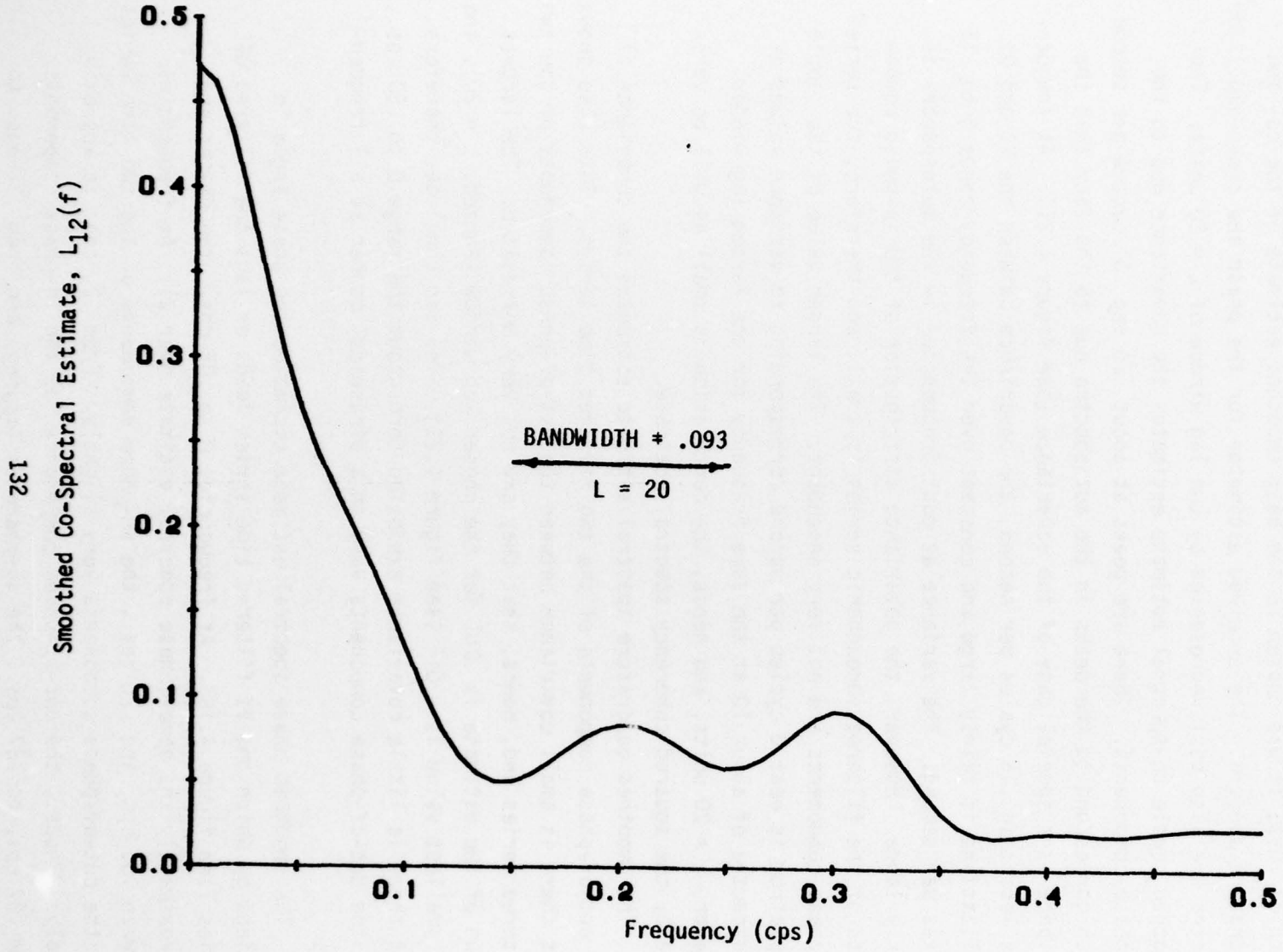

FIGURE 4.21 SMOOTHED CO-SPECTRAL ESTIMATE USING THE PARZEN LAG WINDOW FOR L = 20

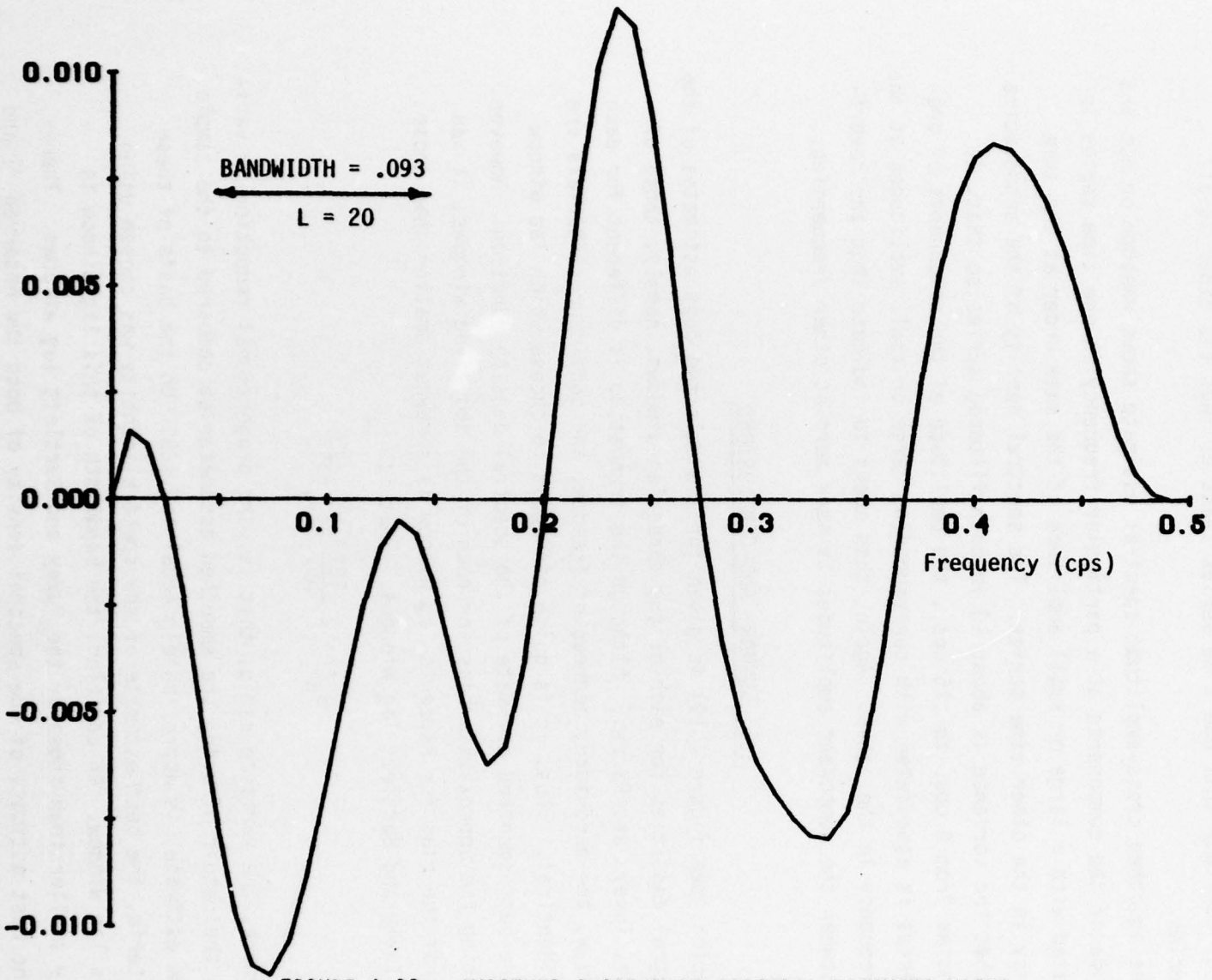

FIGURE 4.22 SMOOTHED QUADRATURE SPECTRAL ESTIMATE USING THE PARZEN LAG WINDOW FOR L = 20

.5 cps., the *out-of-phase components lag* the in-phase components of the two time series. Since the phases alternate leading, there is no reason to assume or conclude that one time series leads or lags the other at all frequencies.

The smoothed cross-amplitude spectral estimate shows whether or not the amplitude of the components at a particular frequency in one time series is associated with a large or small amplitude of the same order at the same frequency in the other time series. The spectral density of the autospectra shows that the variance is about 10 in both filtered series so that, at frequencies from 0 cps. to .15 cps., the amplitude of the components of one time series is associated with corresponding large or small amplitudes at the same frequency in the other. Again, this seems to indicate that the covariance between the component amplitudes is near zero at other frequencies.

4.5 SUMMARY AND CONCLUSIONS

A plot (see figure 4.19) is given for the selected best estimates of the co-spectral densities for each of the three lag windows, namely, those of Bartlett, Tukey, and Parzen. Although the truncation is different for each lag window, the bandwidth, degrees of freedom, and confidence intervals are almost identical. Thus, it is quite difficult to choose which lag window gives the best smoothed estimate of the spectral density function. However, calculating the approximate bias for each of the above lag windows, it was found that the bias for Parzen's lag window is somewhat smaller than those of the Tukey and Bartlett lag windows. That is:

$$B_p(f) = \frac{.152}{400} \Gamma^2_{yy}(f) \quad .$$

Furthermore, the variance ratio, that is, the proportional reduction in variance as the result of using the smoothed estimator as compared to the sample spectrum estimate, is approximately equal to .128. On the basis of these two criteria, the best estimate of the spectral density was chosen using Parzen's lag window. In addition, the bandwidth of this lag window is slightly smaller than those of the Tukey and Bartlett lag windows. Therefore, the best estimate of the spectral density of both the observed VI and OI soundings was obtained using Parzen's lag window for L = 20 units. This value of L resulted in a 95% confidence interval width of .471 with 27 degrees

of freedom, and a bandwidth of b = .093. The bandwidth is less than 1/5 of the total frequency range over which the spectral density function is estimated. Since we are detecting peaks with widths of .093 or more, the peaks appearing in the estimated spectral density of the OI spectrum at frequencies f = .15, .30, and .40 cps., are valid peaks and they should be taken into consideration in interpreting the behavior of the observed OI soundings (see figure 4.6). The process generating the soundings exhibits a large variance around these three frequencies for the filtered data. These frequencies approximately coincide with the most critical times of day for ionospheric support of HF communications. They are: the pre-dawn dip (ionosphere stratifies into D, E, F_1 and F_2 layers due to the sun's energy); mid-day (where stability is a function of various natural and man-made anomalies); and twilight (where the ionosphere recombines into *one* F layer). Such information should be taken into account in the design and operation of an HF communications system. Frequencies above f = .200 cps. on the spectral estimates gives the lowest power, that is, the least variance.

The Parzen lag window for L = 20 units and b = .093 was used to obtain smoothed estimates of the co- and quadrature spectra. The smoothed estimates of the phase and cross-amplitude spectra were also obtained using the same lag window and L = 20 units.

The smoothed sample co-spectral estimate estimates the covariance due to the in-phase components. There is a peak at about .20 cps. and one at .31 cps. which correspond to the peaks in the autospectra. At frequencies above .150 cps., the covariance is reasonably small and approximately constant over the frequency range of .15 to .50 cps. The variance at most frequencies in the autospectra is fairly large. However, the covariance distribution of the in-phase components of the two filtered series is small and has, due to the ionospheric series, in-phase components that are not very dependent. The larger value of the sample spectra is near 0 cps., corresponding to variance values of the autospectra of about 10, at the same frequency, using the Parzen lag window for L = 20 units. Hence, the correlation between the OI and VI soundings is small as was verified by the squared coherency spectral estimate (figure 4.23).

The smoothed quadrature spectral estimate estimates the covariance of the out-of-phase components of the filtered VI and OI soundings. It showed

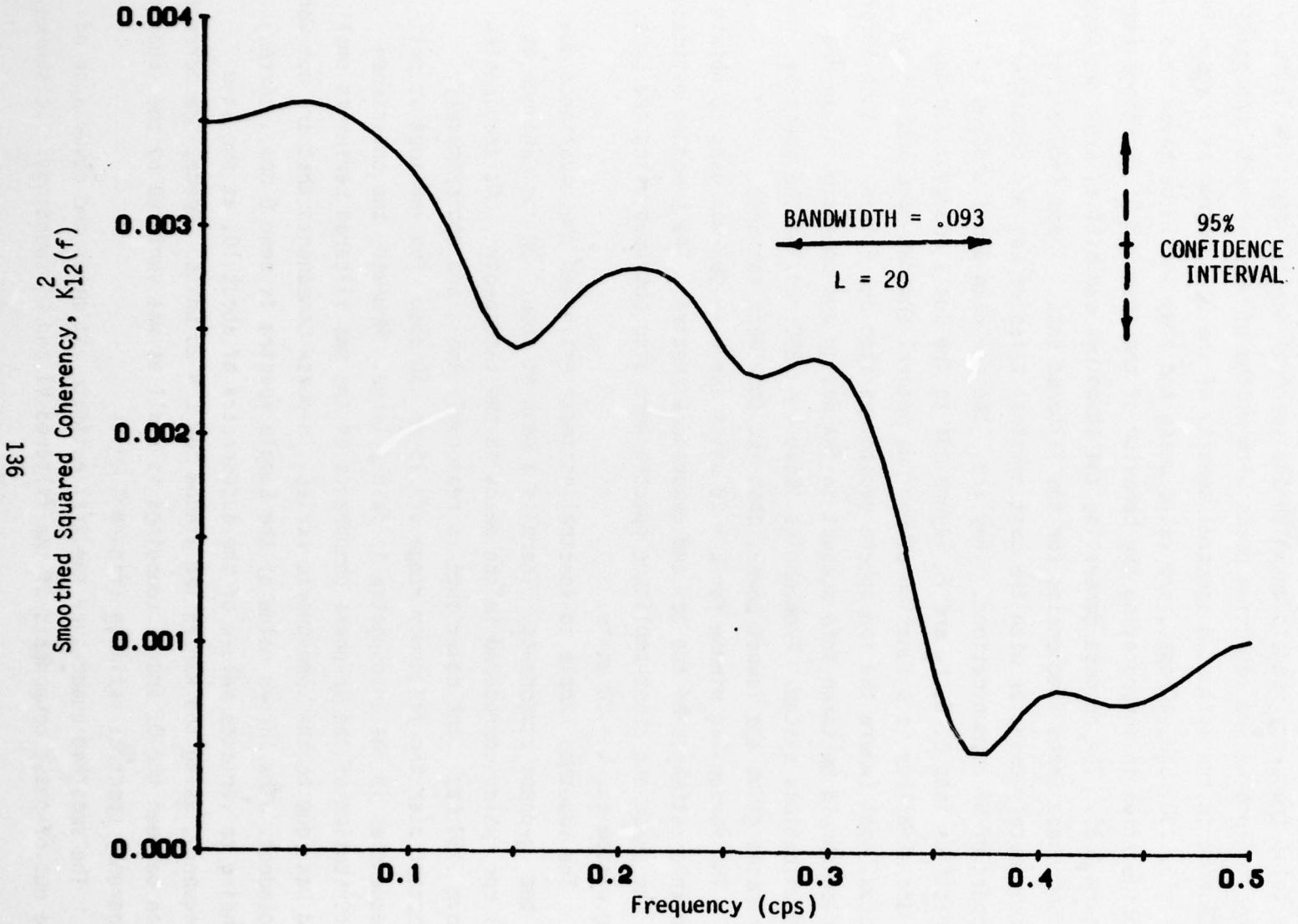

FIGURE 4.23 SMOOTHED SQUARED COHERENCY FOR THE PARZEN LAG WINDOW FOR L = 20

that the covariance between the out-of-phase components of the two filtered series is small, and hence, that they are not very correlated. The largest value is .012 for the chosen lag window, and the smallest value is -.011. There is little or no covariance exhibited throughout the range from 0 to .50 cps., but the out-of-phase components vary in a sinusoidal manner at all frequencies.

The smoothed phase spectral estimate estimates the phase angle in radians by which one filtered time series leads or lags another. At frequencies 0 to .05 cps., the phases are approximately the same; that is, the phase spectral estimate is near zero. At frequencies between .05 cps. and .20 cps., the in-phase components of the two time series lag the out-of-phase components very slightly. From .20 cps. to approximately .27 cps., the out-of-phase components lag the in-phase components. From .27 cps. to .37 cps., the in-phase components are lagging, and from .37 cps. to .50 cps., the out-of-phase components lag the in-phase components of the two ionospheric time series. Since the phase is alternately leading, there is no reason to assume or conclude that one time series leads or lags the other at all frequencies.

The smoothed cross-amplitude spectral estimate shows whether or not the amplitude of the components at a particular frequency in one time series is associated with a large or small amplitude of the same order at the same frequency in another time series. The spectral density of the autospectra shows that the variance is about 10 in both the filtered VI and OI soundings, so that, at frequencies from 0 cps. to .15 cps., the amplitude of the components of one time series is associated with corresponding large or small amplitudes (at the same frequency) of the other. Again, this indicates that the covariance between the component amplitudes is near zero at other frequencies.

In order to obtain a better representation of the important peaks and a confidence interval, the squared coherency was calculated and plotted (see figure 4.23).

A 95% confidence interval was obtained using the following expression:

$$y_{yx}(f) = \pm 1.96 \sqrt{L/2b_1N}$$

$$= \pm 1.96 \sqrt{20/2(1.86)144} = \pm .379 \ ,$$

and is shown on the graph of the smoothed squared coherency spectrum. This squared coherency spectral estimate gives the correlation between the observed VI soundings and the observed OI soundings for the 500 Km experiment. At low frequencies, we have very little correlation between the two filtered series (maximum of $\sim$ .004) as shown by the expanded scale. One can conclude that there is virtually no correlation. The fact that, at all frequencies, the squared coherency approaches zero indicates that the noise level is high in the filtered series for all components at all frequencies. This indicates high variance in the autospectra for the corresponding frequencies. Therefore, we conclude that the OI and VI filtered series are not correlated within the 0 to .50 cps. range.

BIBLIOGRAPHY

1. Ames, J. W., and R. D. Egan, "Digital Recording and Short Term Prediction of Oblique Ionospheric Propagation," IEEE Transcript, Vol. AP-15, pp. 382-389, (May 1967).

2. Davies, K., Ionospheric Radio Propagation. US Dept. of Commerce National Bureau of Standards, NBS Monograph #80, 1965.

3. Jenkins, G. M., and D. G. Watts. Spectral Analysis and its Application. San Francisco, California: Holden-Day, 1968.

4. Yaglom, A. M. An Introduction to the Theory of Stationary Random Functions. New York, N. Y.: Dover, 1962.

5. Jury, E. I. Theory and Application of the Z Transform Method. New York, N. Y.: J. Wiley, 1964.

6. Box, G. E. P., and G. M. Jenkins, Time Series Analysis, Forecasting, and Control. San Francisco, California: Holden-Day, 1970.

7. Fisher, R. A., "Statistical Methods and Scientific Inference," New York: Hafner, 1956.

8. Whittle, P., "Estimation and Information on Stationary Time Series," ARKIV FUR MATHEMATIK, Vol. II, p. 423, (1953).

9. Anderson, R. L., "Distribution of the Serial Correlation Coefficient," Annals of Mathematical Statistics, Vol. 13.1, 1942.

10. Kendall, M. G., and A. Stuart. The Advanced Theory of Statistics, Vol. 3. London, England: Griffen, 1966.

11. Bartlett, M. S., An Introduction to Stochastic Processes with Special Reference to Methods and Applications, Cambridge, England: Cambridge University Press, 1953.

12. Tukey, J. W. "Discussion Emphasizing the Connection Between Analysis of Variance and Spectral Analysis," Technometrica, Vol. 3, p. 191, (1961).

13. Blackman, R. B. and J. W. Tukey. Measurement of Power Spectra From the Point of View of Communications Engineering. Dover Publications, 1958, (ISBN 0-486-60507-8).

14. Shinners, S. M., and C. R. Berger, "Investigation and Identification of Human Operator Performance Models Using the Theory of Time-Series Analysis," Aerospace Medical Research Laboratory Technical Report No. AMRL-TR-72-88, Air Force Systems Command, (February 1973).

15. Akaike, H., "Fitting Autoregressive Models for Prediction," Annals of the Institute of Statistical Mathematics, Vol. 21, p. 243, (1969).

16. Jones, R. H., "Fitting Autoregressions," Journal of the American Statistical Association, Vol. 70, No. 351, (September 1975).

17. Akaike, H., "Low Pass Filter Design," Annals of the Institute of Statistical Mathematics, Vol. 23, p. 163, (1971).

18. Jones,R. H., "Identification and Autoregressive Spectrum Estimation," IEEE Transactions on Automatic Control, Vol. AC-19, No. 6, (1974).

19. Conover, W. J., Practical Nonparametric Statistics. New York: J. Wiley, 1971.

20. Ames, J. W., R. D. Egan, and J. MacGinitie, "Short-Term Prediction of HF Communication Circuit Performance," Granger Associates Technical Report, Palo Alto, California, 1967.